THE UNIVERSITY OF ALBERTA

LEVELS IN ^{26}Al BELOW 4 MeV EXCITATION

by

© DAVID ALEXANDER HUTCHEON

A THESIS

SUBMITTED TO THE FACULTY OF GRADUATE STUDIES

IN PARTIAL FULFILMENT OF THE REQUIREMENTS FOR THE

DEGREE OF DOCTOR OF PHILOSOPHY

DEPARTMENT OF PHYSICS

EDMONTON, ALBERTA

SPRING, 1969

UNIVERSITY OF ALBERTA

FACULTY OF GRADUATE STUDIES

The undersigned certify that they have read, and recommend to the Faculty of Graduate Studies for acceptance, a thesis entitled LEVELS IN ^{26}Al BELOW 4 MeV EXCITATION, submitted by David Alexander Hutcheon in partial fulfilment of the requirements for the degree of Doctor of Philosophy.

ABSTRACT

States in ^{26}Al below 4 MeV excitation were studied by detection in coincidence of protons and gamma rays from the reaction $^{24}Mg(^{3}He,p\gamma)^{26}Al$ (Q = 5.92 MeV). Gamma-ray angular distributions were measured for bombarding energies of 5.3 and 6.0 MeV. Branching ratios generally were in good agreement with other particle-gamma coincidence measurements and did not agree well with results of proton-capture studies.

Spin values J=1 were obtained for an excited state at 1.852 MeV, one of the states at 2.07 MeV and the state at 2.740 MeV. J=2 was found for the level at 3.159 MeV.

The Nilsson model for odd-odd nuclei and a mixed configuration shell model were used to predict energy levels of ^{26}Al. Both models were able to give fair agreement with experiment for the ground and first few excited states. Some electromagnetic transition probabilities were calculated using the shell model wave functions.

ACKNOWLEDGEMENTS

I would like to thank my supervisor, Dr. W.C. Olsen, for his encouragement and support in the course of this work.

I am especially grateful to my two colleagues, Dwain Sykes and Cliff Vermette, for their assistance in collecting data and the innumerable helpful discussions on all aspects of the work.

Other people who assisted in doing the coincidence runs include R.G. Humphries, T.P.G. Carola, Dr. D.M. Sheppard and Dr. B.D. Sowerby.

I wish to thank Dr. S.S.M.Wong, who made available the shell model computer program and who made helpful suggestions concerning the use of it.

The cooperation of J.B. Elliott, L. Holm and the other members of the Nuclear Research Center technical staff is deeply appreciated.

I would like also to thank Mrs. L. Medford for her expeditious typing of this thesis.

Finally, I wish to acknowledge the financial assistance of the National Research Council and an I.W. Killam Fellowship.

TABLE OF CONTENTS

Table of Contents, continued

LIST OF TABLES

LIST OF FIGURES

List of Figures, continued

I. BACKGROUND

Measurement of electromagnetic properties of bound states in nuclei is a useful, if indirect, method for studying nuclear forces. From such measurement it is possible to determine spins, parities and excitation energies of nuclear levels, as well as electric or magnetic moments and electromagnetic transition rates, without reference to a particular theory of nuclear interactions. The link with nuclear theory is through comparison of these measurements with predictions of some model for the nucleus.

In this work electromagnetic decay properties of levels in ^{26}Al were studied. ^{26}Al, an odd-odd nucleus near the middle of the sd shell, is a difficult case to treat with either the shell model or a collective model. Model calculations applied to ^{26}Al have tended to be parts of more general surveys, with no consideration of electromagnetic properties. It is of interest to compare models which apply to ^{26}Al to try to decide, for instance, whether the nucleus is permanently deformed, as its even-even and odd-A neighbors appear to be.

The first extensive studies of excited states in ^{26}Al were by charged particle spectrometry or by the gamma rays resulting from proton capture. More than twenty excited states of less than 4 MeV excitation were found by reactions ^{24}Mg(τ,p)^{26}Al (Hi59), ^{27}Al(τ,α)^{26}Al (Ta60a) and ^{28}Si(d,α)^{26}Al (Br59). Gamma ray studies used the capture reaction

$^{25}Mg(p,\gamma)^{26}Al$ (Gr56,Mu60,Ne62,Ho63,Bi64). Because of the complexity of the gamma-ray decay scheme and the relatively poor resolution of the NaI(Tl) detectors, gamma ray spectra obtained in the proton capture experiments were difficult to interpret. Gamma-ray branching ratios assigned to levels above 2 MeV excitation in various proton capture studies differed from one another and from more recent coincidence measurements. Spins of the ground state and first and third excited states were deduced from observation of beta decay to and from these levels. A list of references and summary of information gained by such measurements may be found in the compilation by Endt and Van der Leun (En67).

In the past two years much information has come from three additional types of experiment. The first type involves transfer of a proton to a ^{25}Mg target by either a (d,n) reaction (Fu68) or a (τ,d) reaction (We68). Whenever the angular distribution of outgoing particles shows a stripping pattern characteristic of a certain angular momentum transfer, it is possible to deduce the parity and limit possible spin values for the corresponding state of ^{26}Al. In particular, if there is present an $l_p=0$ component in the angular distribution, the spin is restricted to 2 or 3 and the parity is positive. A second recent development has been the use of high-resolution lithium drifted germanium detectors to study the ^{26}Al gamma-ray spectra produced by (p,γ) and (p,n) reactions (Wi67, Ha68a, Ha68b). Several lifetimes were determined by the Doppler shift attenuation method and decay modes of a triplet of states at 2.07 MeV found from the Ge(Li) detector spectra. Finally,

gamma rays have been detected in coincidence with protons in the reaction $^{24}Mg(\tau,p\gamma)^{26}Al$ (Bi68, Si68 and this work). Analysis of the gamma-ray spectra is simplified because each gamma ray can be associated with an excited state through the energy of the coincident proton. Further simplification results if the proton detector can be placed in a special geometry.

Applications of nuclear models to ^{26}Al have tended to be as part of more general surveys, either of sd shell nuclei or of odd-odd nuclei. In the work of Bouten et al. (Bo67) ^{26}Al was treated in an intermediate-coupling shell model calculation of nuclei with masses 18 to 38. They considered only the configuration with 10 nucleons in the $1d_{5/2}$ shell. Fair agreement with the observed spectrum was obtained in the case of four out of five excited states, although the value of spin-orbit coupling was very large. More consideration has been given to models with two particles outside a deformed core. The Nilsson model for odd-odd nuclei was used by Weidinger et al. (We68) with no residual particle interaction or rotational-particle coupling. They found that the model was not particularly successful in giving spectroscopic factors for excited states in ^{26}Al, as measured by single-nucleon stripping reactions. Kelson (Ke64) considered the residual interaction as it affected the separation of the lowest T=0 and T=1 states of odd-odd nuclei in the sd shell. Picard and Pinho (Pi66) also have considered ^{26}Al in the study of residual interaction in deformed odd-odd nuclei.

II. ANALYSIS OF GAMMA-RAY ANGULAR DISTRIBUTIONS

In this study gamma rays were detected in coincidence with protons produced in the reaction $^{24}Mg(\tau,p\gamma)^{26}Al$. The proton detector had axial symmetry about the beam direction and detected particles emitted at close to 180° with respect to the beam direction (Method II of Litherland and Ferguson (Li61)). Through measurement of the energy of the coincident proton, each gamma ray could be associated with the gamma-ray decay of a particular excited state of residual nucleus. The theory of gamma-ray angular distributions obtained in such a way is described in the following section.

a. Gamma-ray decay of aligned nuclear states

Consider nuclei which are produced in an excited state by a process which has symmetry about some axis. For example, a system of nuclei formed by proton capture would have axial symmetry about the incident beam axis if neither target nor beam is polarized. In this study axial symmetry results from producing nuclei in states B* in which the reaction is A(a,b)B* and the detector of b particles has axial symmetry about the beam direction. The system of nuclei may be described by the relative number of nuclei, P(M), which are in the magnetic substates M, the quantization axis being along the symmetry axis. If the state B* has definite parity, there is symmetry under reflection through a plane normal to the beam direction (Fe65, page 77). A con-

sequence of reflection and axial symmetry is that the system is aligned, that is $P(M)=P(-M)$.

The decay of an aligned state is considered in the treatment by Rose and Brink (Ro67) of gamma-ray angular distributions. The following outline is based on the development given by Rose and Brink (Ro67) and follows their notation to a large extent.

The probability amplitude for a transition from state $|J_1M_1\rangle$ to state $|J_2M_2\rangle$ with emission of a gamma ray of circular polarization q ($q=\pm1$) in the direction $\vec{k}$ may be represented as $A_{M_1M_2}{}^{q}(\vec{k})$. If the spin projection M_2 is not observed, the probability of transition from the state $|J_1M_1\rangle$ to any substate of J_2 by emission of a gamma ray $(\vec{k},q)$ is $\sum_{M_2} |A_{M_1M_2}{}^{q}(\vec{k})|^2$. For a system of nuclei in various magnetic substates, with $P(M)$ being the population in substate M, the transition probability is

$$\sum_{M_1} P(M_1) \sum_{M_2} \left|A_{M_1M_2}{}^{q}(\vec{k})\right|^2 \qquad \text{(II.1)}$$

The amplitudes may be expressed in a multipole expansion as

$$A_{M_1M_2}{}^{q}(\vec{k}) = -\sqrt{\frac{k}{h}} \sum_{LM\pi} q^{\pi} \langle J_1M_1 | T_{LM}{}^{\pi} | J_2M_2\rangle \, \mathcal{D}^{L}_{Mq}(R) \qquad \text{(II.2)}$$

where $\mathcal{D}^{L}_{Mq}(R)$ is a rotation matrix element for the rotation R taking the beam axis into the direction $\vec{k}$. π represents the type of multipole

operator involved, being 0 for electric multipole operators and 1 for magnetic. When (II.2) is substituted into (II.1) the result is a sum of terms, each with a product of rotation matrices. Using the properties of rotation matrices, it is possible to replace each product by an expansion in Legendre polynomials, $P_K(\cos\theta)$. The sums may be reduced by standard techniques of vector coupling algebra to give an expression for the number of gamma rays emitted in the direction of $\vec{k}$,

$$W(J_1 \rightarrow J_2;\bar{k}q) = \frac{k}{h} \sum_{K,L,L',\pi,\pi'} B_K(J_1) P_K(\cos\theta)(-1)^{q+J_1-J_2+L'-L-K}$$

$$\times \sqrt{2J_1+1}\ (LqL'-q|K0)W(J_1J_1LL';KJ_2)q^{\pi+\pi'}$$

$$\langle J_1||T_L^{(\pi)}||J_2\rangle \langle J_1||T_{L'}^{(\pi')}||J_2\rangle^*, \qquad \text{(II.3)}$$

in which $(J_1M_1J_2M_2|JM)$ is a Clebsch-Gordan coefficient, $W(J_1J_1LL';KJ_2)$ is a Racah coefficient, $\langle J_1||T_L^{(\pi)}||J_2\rangle$ is a reduced matrix element for a multipole operator and $B_K(J_1) = \sum_{M_1} P_1(M_1)(-1)^{J_1-M_1}\sqrt{2J_1+1}\ (J_1M_1J_1-M_1|K0)$. There can be a contribution only from those multipoles satisfying the vector triangle relationship $|J_1-J_2| \leq L \leq (J_1+J_2)$ and $L\neq 0$. For a given L, parity conservation restricts π to electric or magnetic. In the usual case, the major contribution to a transition between nuclear states is from the lowest permitted multipole, with the importance of higher multipoles decreasing rapidly with increasing L. For all but rare occasions it

is sufficient to consider only the two lowest multipoles, $\bar{L}$ and L. The multipole mixing ration may be defined as

$$x = \frac{\langle J_1 \| T_L^{\langle \pi \rangle} \| J_2 \rangle}{\langle J_1 \| T_{\bar{L}}^{\langle \bar{\pi} \rangle} \| J_2 \rangle} \sqrt{\frac{2\bar{L}+1}{2L+1}} \qquad \text{(II.4)}$$

If polarization is not observed, the expression for the angular distribution becomes

$$W(\theta) = \sum_K B_K(J_1) P_K(\cos\theta) \; \frac{R_K(\bar{L}\bar{L}J_1J_2) + 2xR_K(\bar{L}LJ_1J_2) + x^2 R_K(LLJ_1J_2)}{1+x^2} \qquad \text{(II.5)}$$

in which $R_K(LL'J_1J_2) = (-1)^{1+J_1-J_2+L'-L-K} \sqrt{(2J_1+1)(2L+1)(2L'+1)}\ (L1L'-1\,|\,K0)$

$$\times W(J_1J_1LL';KJ_2)$$

has been introduced. In (II.5) the dependence upon substate population parameters is all contained in the $B_K(J_1)$, while nuclear properties appear only through the mixing ratio x. If the system is aligned, $B_K(J_1)=0$ for K odd, so the angular distribution may be expressed in even order Legendre polynomials--in other words, it is symmetric about $\theta = 90^\circ$.

If a transition from an aligned state J_1 to state J_2 is not observed, but the subsequent transition $J_2 \rightarrow J_3$ is observed, the angular distribution is

$$W(\theta) = \sum_K B_K(J_1)P_K(\cos\theta) \left\{ \frac{U_K(\bar{L}_{12}J_1J_2) + x_{12}^2 U_K(L_{12}J_1J_2)}{1+x_{12}^2} \right\} \qquad \text{(II.6)}$$

$$\times \left\{ \frac{R_K(\bar{L}_{23}\bar{L}_{23}J_2J_3) + 2x_{23}R_K(\bar{L}_{23}L_{23}J_2J_3) + x_{23}^2 R_K(L_{23}L_{23}J_2J_3)}{1+x_{23}^2} \right\}$$

where $U_K(LJ_1J_2) = (-1)^K W(J_1J_2J_1J_2;LK)/W(J_1J_2J_1J_2;L0)$.

Equation (II.6) can be generalized for further cascades by including a factor $\left\{ \frac{U_K(\bar{L}_{mn}J_mJ_n) + x_{mn}^2 U_K(L_{mn}J_mJ_n)}{1+x_{mn}^2} \right\}$ for each unobserved preceding transition $m \rightarrow n$.

b. Chi-squared fitting of angular distributions

An angular distribution calculated with equation (II.5) or (II.6) is to be compared with an observed angular distribution. Finite detector size tends to "wash out" the angular distribution, compared to the distribution that would be observed with an ideal point detector. For a cylindrical detector this attenuation may be corrected for by introducing coefficients, Q_K, for each order of Legendre polynomial. In equations (II.5) and II.6) each $P_K(\cos\theta)$ is to be replaced by $Q_K P_K(\cos\theta)$. A definition of the Q_K as well as a table of values for detectors in common use may be found in (Fe65).

Gamma-ray intensities measured at a series of angles $Y(\theta_i)$ are to be compared with the $W(\theta_i)$ calculated assuming certain spin J_1, mixing ratio x and population parameters, P(M). The goodness of fit is measured by the value of χ^2, defined by

$$\chi^2 = \sum_i \left(\frac{W(\theta_i) - Y(\theta_i)}{E(\theta_i)} \right)^2 \qquad \text{(II.7)}$$

where $E(\theta_i)^2$ is the variance in Y measured at θ_i. The problem of finding parameters which make χ^2 a minimum is simple if $W(\theta)$ is a linear function of the parameters (see, for example, Ma64, page 365). Spins and multipole mixing ratios do not appear linearly in the expression for $W(\theta)$, but the population parameters do. The usual method of analysis is to fix spins and mixing ratios and to vary population parameters so as to minimize χ^2. Different values of mixing ratio may be assumed with χ^2 minimized for each case. In order to span values of x over the range $-\infty$ to $+\infty$, it is customary to step through values of $\delta = \arctan x$.

Because of statistical fluctuations in counting rate, if an angular distribution measurement is repeated many times there will be a variation in calculated values of minimum χ^2. The distribution of χ^2 is tabulated (see, for example, Ab64, page 978) for various degrees of freedom, the number of degrees of freedom being the number of data points minus the number of free parameters. Tables of the confidence limit for a given χ^2 are available (Ab64). By confidence limit is meant

the probability that, for the correct theoretical expression, χ^2 will exceed a certain value. For example, with 5 degrees of freedom the 10% confidence limit is 9.24, meaning that if the correct theory is being used (in the present case, the correct spins and mixing ratios), χ^2 is expected to exceed 9.24 in 10% of the measurements.

In determining spins and mixing ratios the practice has been to reject solutions for which χ^2 is greater than the value at the 0.1% confidence limit. This criterion was applied in the present work. It is common, although not universal, in this type of work to normalize χ^2 by dividing by the number of degrees of freedom when giving results. Values of χ^2 obtained in this work are so normalized.

Two points should be mentioned regarding interpretation of χ^2 fits. First, E^2 in equation (II.7) should represent the variance in Y. If variation in Y is due solely to statistical fluctuations in counting rate, $Y(\theta_i)$ is a good estimate of $E(\theta_i)^2$ (unless $Y(\theta_i)$ is very small). If there is some other contribution to the variance of Y, it may be more difficult to make a proper estimate of E. Should values of minimum χ^2 consistently correspond to high or to low confidence limits, it may mean that the $E(\theta_i)$ are systematically over- or underestimated. Second, there may be cases for which it is not clear what is ν, the number of degrees of freedom. The number of data points should not be taken simply as the number of measurements if different measurements were made under identical conditions. For instance, two measurements at the same angle may be combined into one number without any loss of information, and so should not

be considered as independent data. (Cf. Fe65, page 103) In principle, measurements at angles of, say, 29° and 30° are independent, but in practice should not be taken as such because of the large angle subtended by a real detector. There may be circumstances under which the number of parameters is difficult to determine. As an example, consider the case in which population parameters are the free variables. It may be that some of the populations are known to be small (as in Method II, described in the next section). Treating them as free parameters will give a lower (unnormalized) χ^2 than if they are set to zero, but they will not be as effective in reducing χ^2 as the other population parameters are.

c. Restriction of magnetic substate populations

Analysis of gamma-ray angular distributions can be simplified if a special method is employed for doing particle-gamma coincidence studies, the so-called Method II of Litherland and Ferguson (Li61). In this method the detector of b particles from a reaction A(a,b)B* is placed at either 0° or 180° to the direction of the incident beam. For such a geometry, the projection of orbital angular momentum along the beam axis is zero for both particle a and particle b. Hence, the largest projection which can be produced in B* is $M_{max} = J_A + S_a + S_b$, where J_A, S_a and S_b are the intrinsic spins of the target and incoming and outgoing particles. For the reaction studied in this work, $^{24}Mg(\tau,p)^{26}Al$, $J_A=0$, $S_a=1/2$, $S_b=1/2$, so that $M_{max}=1$. The particle detector was an annular detector, permitting the beam to pass through its central hole to the target. Particles were detected at close to 180°. The axial symmetry of the system

assured alignment of the residual nuclei B*. With the alignment condition P(M) = P(-M) and the restriction $M_{max}=1$ the unknown parameters were P(0) and P(1).

Because of the finite size of the particle detector, there was some contribution from protons with $m_l \neq 0$, thereby populating states in ^{26}Al with M > 1. This problem has been considered by Litherland and Ferguson (Li61). The importance of the effect cannot be determined without a detailed knowledge of the reaction mechanism. If the populations P(0) and P(1) are the order of unity, P(2) should be the order of ξ^2, where ξ is the half-angle subtended by the annular detector.

III. MODELS APPLICABLE TO THE ^{26}Al NUCLEUS

a. Nilsson's model for odd-odd nuclei

The Nilsson model for deformed odd-A nuclei (Ni55) can be extended to odd-odd nuclei. This is a reasonable model to try for ^{26}Al because of the success of the Nilsson model in explaining the energy spectra of ^{25}Mg and ^{25}Al (Li58). The Hamiltonian may be expressed as a sum of particle and rotational energies. The particle energy is the sum of single particle energies and a residual interaction between the odd particles. The core rotational energy may be written in terms of total spin and particle spins in a manner analogous to the case of odd-A nuclei (Pr62, page 255). With such a substitution, there appear in the Hamiltonian terms which refer to both particle angular momenta $\vec{j}$ and total angular momentum $\vec{J}$. These terms may be called rotational-particle coupling terms (RPC). It is convenient to express the Hamiltonian as (Pi65)

$$H = H_p + H_{res} + H_{rot} + H_{rpc} \qquad \text{(III.1)}$$

where H_p is the sum of single particle energies for a deformed potential, H_{res} is the residual interaction between odd proton and odd neutron, H_{rot} is the core rotation contribution except for the rotational-particle coupling terms H_{rpc}.

The particle Hamiltonian is taken to be of the form

$$H_p = H_o + H_\delta + C\vec{l}\cdot\vec{s} + D\vec{l}^2 \qquad \text{(III.2)}$$

in which H_o is the Hamiltonian for a spherically symmetric harmonic oscillator with eigenvalues $N\hbar\omega_o$, $H_\delta = -\frac{4}{3}\hbar\omega_o\delta\sqrt{\frac{\pi}{5}}\,r^2Y_{20}$ represents a quadrupole distortion. Constants C and D are chosen to give shell model level spacings in the limit of zero deformation. Usually the parameters of the model are taken to be

$$\kappa = -\frac{1}{2}\frac{C}{\hbar\omega_o^o}, \quad \mu = \frac{2D}{C} \quad \text{and} \quad \eta = \frac{\delta}{\kappa}\frac{\omega_o(\delta)}{\omega_o^o}$$

The dependence of ω_o upon deformation arises from a requirement that nuclear volume remain constant. Its value at $\delta=0$, ω_o^o, is usually assumed to be related to nuclear mass through $\hbar\omega_o^o = 41A^{-1/3}$ MeV. Particle angular momentum, $\vec{j}$, is no longer a good quantum number, but its projection, Ω, along the symmetry axis is good. If coupling between oscillator shells N and N+2 is neglected, the eigenfunctions of H_p may be labelled by N, Ω and another label, say α. They may be expanded in terms of shell model eigenfunctions as

$$|\Omega\alpha\rangle = \sum_j C^\alpha_{j\Omega}|lj\Omega\rangle \qquad \text{(III.3a)}$$

$$|\Omega\alpha\rangle = \sum_{l\Lambda} a^\alpha_{l\Lambda}|l\Lambda\Sigma\rangle \qquad \text{(III.3b)}$$

where Λ is the projection of orbital angular momentum l, and Σ is the projection of intrinsic spin along the symmetry axis. Matrix elements of H_δ in $|l\Lambda\Sigma\rangle$ representation may be calculated from expressions given by Nilsson (Ni55).

The particle angular momenta $\vec{j}_n$ and $\vec{j}_p$ and the core rotational angular momentum $\vec{R}$, none of them constants of motion, combine to give total angular momentum $\vec{J}$ with projection M along a space-fixed axis. K is the projection of $\vec{J}$ along an axis fixed to the symmetry axis of the rotating core, and Ω the projection of total particle angular momentum along the same axis. Two coupling schemes are possible— $\Omega = \Omega_p + \Omega_n$ or $\Omega = |\Omega_p - \Omega_n|$. The eigenvalues of H_{rot} are (Pi65)

$$E_{rot} = \frac{\hbar^2}{2\mathcal{I}} \left\{ J(J+1) \pm 2\Omega_p\Omega_n - 2(\Omega_p \pm \Omega_n)^2 + \langle j_p^2 \rangle + \langle j_n^2 \rangle \right\} \qquad \text{(III.4)}$$

where $\mathcal{I}$ is the moment of inertia parameter and the plus or minus signs correspond to parallel or antiparallel combination of Ω_p and Ω_n. Expectation values $\langle j_n^2 \rangle$ and $\langle j_p^2 \rangle$ may readily be calculated from expansion (III.3a) of the single particle functions.

The RPC terms are

$$H_{rpc} = \frac{\hbar^2}{2\mathcal{I}} \left\{ (j_{p+}j_{n-} + j_{p-}j_{n+}) - (J_+ j_{p-} + J_- j_{p+}) - (J_+ j_{n-} + J_- j_{n+}) \right\} \qquad \text{(III.5)}$$

The first pair of terms couple the states with (Ω_n, Ω_p) to states (Ω_n+1, Ω_p-1) or (Ω_n-1, Ω_p+1). The remaining terms couple (K, Ω) to $(K-1, \Omega+1)$

and $(K+1,\Omega-1)$.

With neither H_{res} nor H_{rpc} the model is just the extreme single particle model, except that the potential is not spherically symmetric and rotational bands may be built on particle configurations. The states $|N\Omega\alpha\rangle$ can accomodate only two particles each, one of projection Ω and one of projection $-\Omega$. In the ground state the neutron and proton levels independently fill in order of increasing energy, leaving one of each type of nucleon unpaired. Higher energy states are produced by promotion of a particle or particles to higher energy states. Introduction of H_{res} and H_{rpc} mixes configurations which differ in the state of either one or two nucleons.

The operators for electromagnetic transitions are one-body operators, so that states connected by electromagnetic decay should have configurations differing by not more than one particle. If H_{res} and H_{rpc} are small, certain transitions may be strongly inhibited if the dominant configurations of the levels involved differ in two or more particle states. The possibility of such selection rules has been suggested by Gallagher (Ga60).

The effect of H_{res} has been considered by Picard and de Pinho (Pi65) and by Kelson (Ke64), mainly for its effect on the spacing of the 5^+ ground state and $0^+(T=1)$ first excited state.

b. The mixed configuration shell model

In the simplest shell model picture of ^{26}Al, 8 protons and 8 neutrons constitute an inert core and the remaining 10 nucleons are in the

$1d_{5/2}$ shell. Since this is equivalent to a full $1d_{5/2}$ shell plus one proton hole and one neutron hole, possible spins are those allowed a system of two $j=5/2$ particles. There are the $T=1$ states with $J=0,2,4$ and the $T=0$ states $J=1,3,5$. This is the only configuration allowed by Bouten et al. (Bo67) in their study of ^{26}Al as part of a broad survey in the sd shell. However, if a detailed study of ^{26}Al is to be made, it is necessary to have more than 6 states, which means that a mixture of single-particle configurations must be allowed.

Consider a nucleus with N nucleons distributed among a number of partially filled shells, with n_1 of them in shell 1, n_2 in shell 2, etc. Let the configuration be denoted by $(j_1)^{n_1}(j_2)^{n_2}\ldots$. For a given configuration there are many ways the particle angular momenta can be combined to give some total angular momentum J and isotopic spin T. A basis state might be represented by $\left|(j_1)^{n_1}\alpha_1 J_1 T_1;(j_2)^{n_2}\alpha_2 J_2 T_2;\ldots;JT\right\rangle$. The index α_1 distinguishes possible ways of combining n_1 particles in the j_1 shell to spin J_1 and isospin T_1. The combinations within a single shell may be classified by methods of group theory (F152). Seniority and reduced isotopic spin are useful quantum numbers in such classification. Seniority, s, is the number of nucleons left after removal of all pairs of particles coupled to $J=0$, $T=1$. Reduced isospin, t, is the isotopic spin of these remaining nucleons.

A state with n particles can be expressed as a sum of products of (n-2)-particle states and two-particle states. The coefficients in this expansion are called coefficients of fractional parentage. A matrix

element for a two-body operator, such as the one representing a residual two-body interaction may be reduced to sums of fractional parentage coefficients and matrix elements for two-particle states. The effect of any residual interaction is determined completely by the two-body matrix elements. In a similar manner matrix elements for one-body operators may be expressed in terms of one-body matrix elements and the fractional parentage coefficients from an expansion into (n-1)-particle and one-particle states.

A Hamiltonian of the form $H = \sum_i (T_i+V_i) + \sum_{i<j} V_{ij}$ may be evaluated if the single particle energies and two-body matrix elements are specified and if one is able to do the angular momentum coupling algebra.

IV. EXPERIMENTAL PROCEDURE

a. Apparatus

Protons and gamma rays from the bombardment of a ^{24}Mg target by ^{3}He ions were detected in coincidence using a system for analyzing gamma-ray angular distributions by Method II of Litherland and Ferguson (Li61). A detailed specification of apparatus described in this section may be found in Appendix A.

$^{3}He^{+}$ ions were accelerated by the University of Alberta 5.5 MV Van de Graaff generator. An analyzing magnet, which deflected the beam 90° into the horizontal plane, followed by a pair of slits provided energy selection and stabilization of the ^{3}He beam. Slight adjustments in the height of the beam at the target could be made by moving the energy-defining slits up or down. A switching magnet located two meters beyond the slits could deflect the beam in a horizontal plane. Immediately after the switching magnet was a double-focussing quadrupole pair which permitted focussing of the beam on target. Approximately 3 meters beyond the quadrupole magnet was the first of a series of 4 collimators. These collimators defined the position of the beam as it entered the target chamber and also prevented the beam from striking a carbon trap which was in the beam line before the target chamber. Each collimator consisted of tantalum sheet backed by a 1-1/2" long lead cylinder. The beam passed through circular holes in the center of

each collimator. The apertures in the tantalum sheets were 3/8", 1/4", 1/8" and 1/16".

Inside the 8" diameter cylindrical brass target chamber were a final collimator, an annular charged particle detector and a target holder. After passing through the target, the beam was stopped at the end of a 1-meter tube connected to the target chamber. The final collimator, tantalum foil with a 3/32" diameter hole mounted on a lead block, protected the annular detector.

Particles were counted using an annular silicon surface-barrier detector placed so as to count charged particles leaving the target at close to 180° with respect to the incoming beam. Initially the annular detector was placed 20 mm from the target and had a sensitive region of 5.5 mm inner diameter and 7.5 mm outer diameter. During a final measurement at 5.3 MeV bombarding energy a detector of inner diameter 8 mm, outer diameter 14 mm on the sensitive area and set 33 mm from the target was used. Thus, particles were detected at angles from 169° to 172° by the first detector and 168° to 173° by the second.

Experiments were carried out with a bias of +300 V on the target. If this was not done, secondary electrons from the target adversely affected detector resolution.

The gamma-ray detector was a 3" x 3" cylindrical NaI(Tl) crystal and photomultiplier assembly which was clamped to a rotatable arm. The frame on which this arm was mounted also supported the target chamber, ensuring that the axis of rotation of the detector passed through the

beam line. With the gamma-ray detector almost touching the chamber (approximately 10 cm from the target) the smallest angle to which it could be set was 31°. The restriction was due to interference of the beam-catching tube.

A schematic diagram of target chamber and detectors is presented in Figure 1.

Signals from the particle and gamma-ray detectors were fed into the coincidence system shown in Figure 2. Differences between times of arrival of signals from the particle detector and the gamma-ray detector were converted to voltage pulses by a time-to-amplitude converter (TAC). Timing signals were provided by passing bipolar signals from the amplifiers into fast zero crossing discriminators (FZCD). Output of the TAC consisted of a background due to random coincidences on which was a peak corresponding to true coincidence events. The full-width of the peak was approximately 30 nsec. Two windows were set on the TAC output, one containing the "trues" peak and associated "randoms" (T+R), the other set on an adjacent region of "randoms" (R). This provided two signals to be used for gating purposes. The linear signals, amplified and delayed, were fed into analog-to-digital converters (ADC's) which could be gated by either the T+R signal or the R signal. The output of the TAC was fed into a third ADC.

The outputs from the 3 ADC's together with the T+R signal were fed into an on-line computer. The computer could be programmed to

Fig. 1

Schematic diagram of target chamber, indicating positions of particle and gamma-ray detectors with respect to the target.

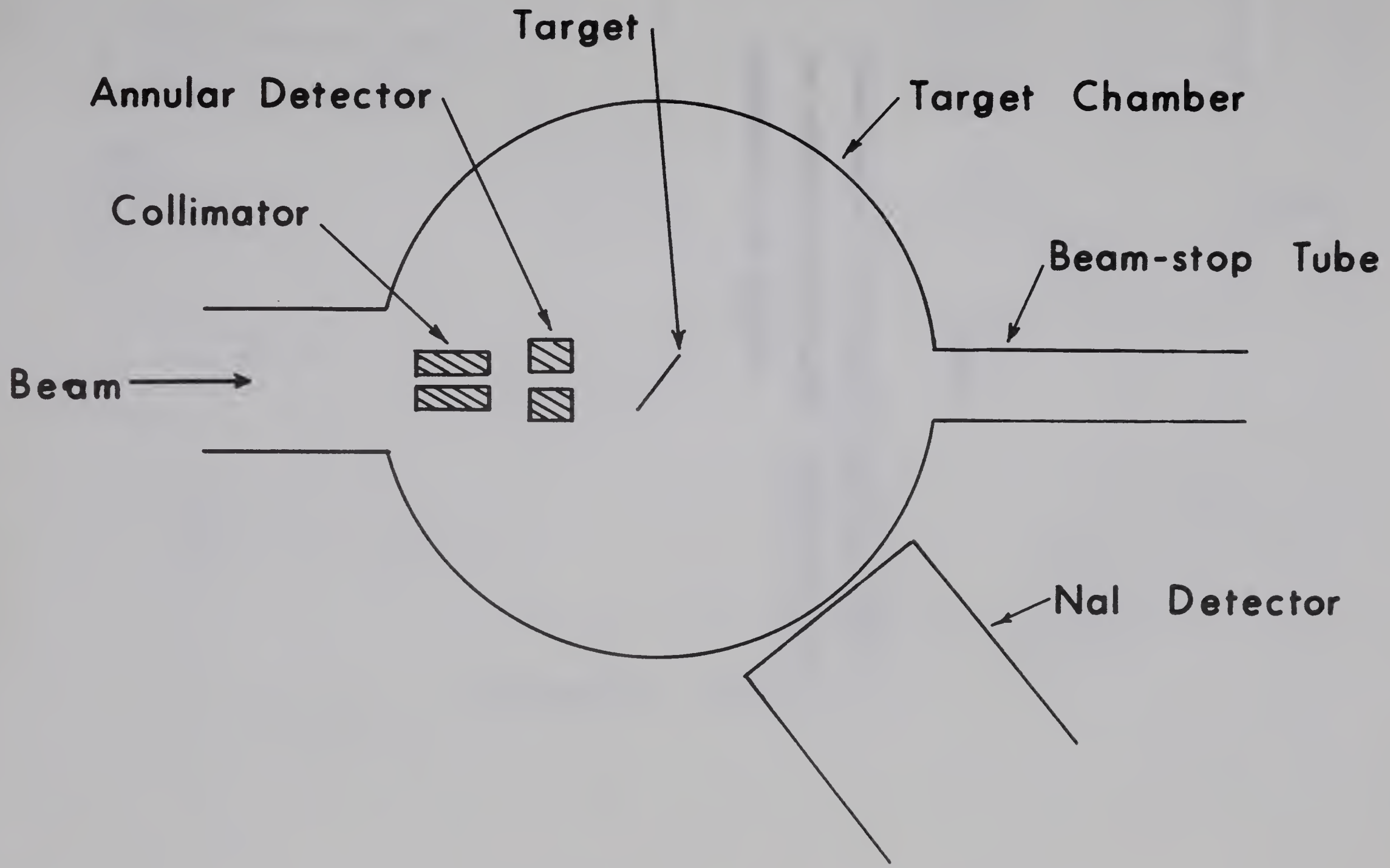
Target
Annular Detector
Target Chamber
Collimator
Beam-stop Tube
Beam
NaI Detector

WiFi Device
Beam-side port
Input/Output Channel
Target
Antenna Selection Network
Antenna
Beam

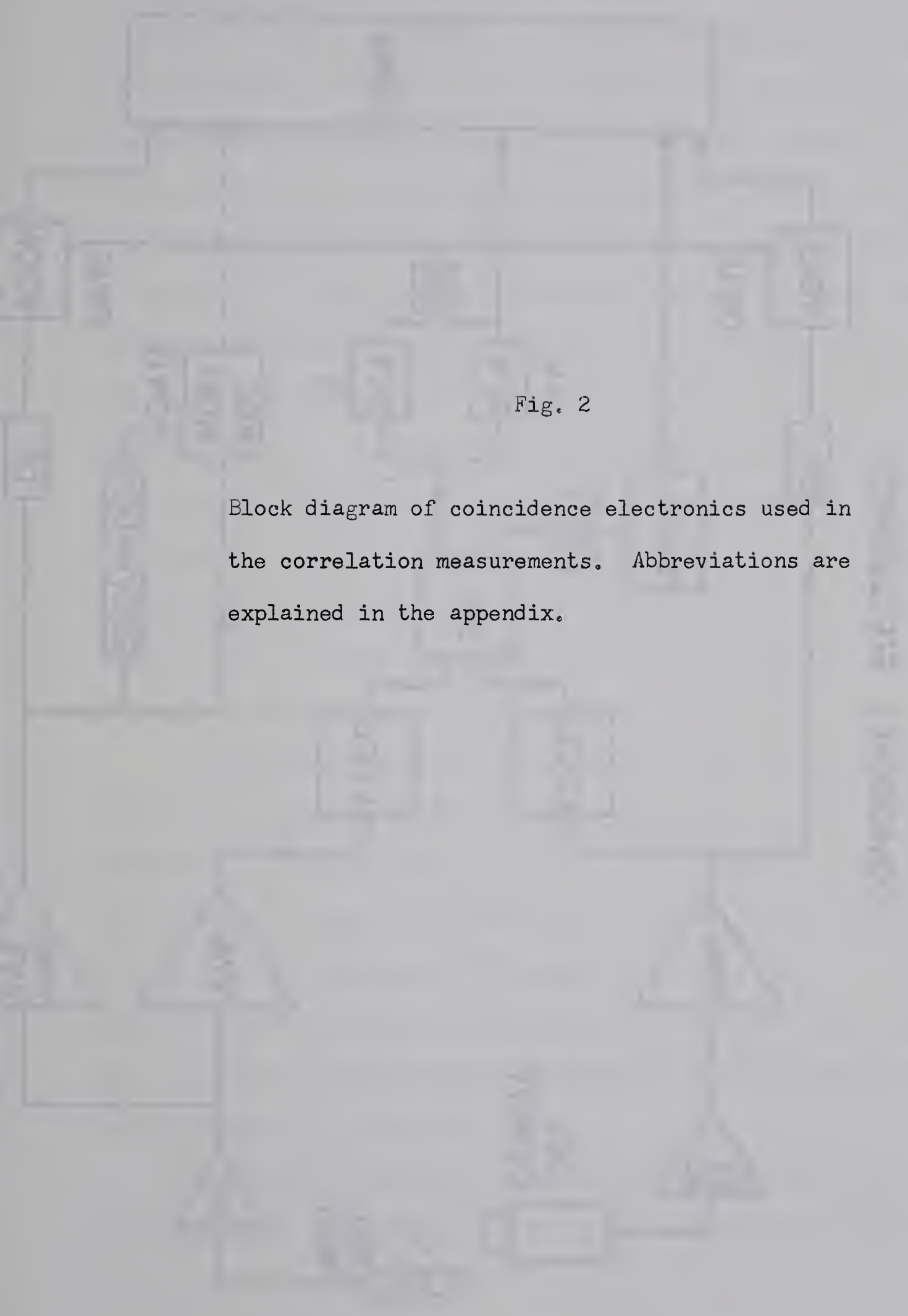

Fig. 2

Block diagram of coincidence electronics used in the correlation measurements. Abbreviations are explained in the appendix.

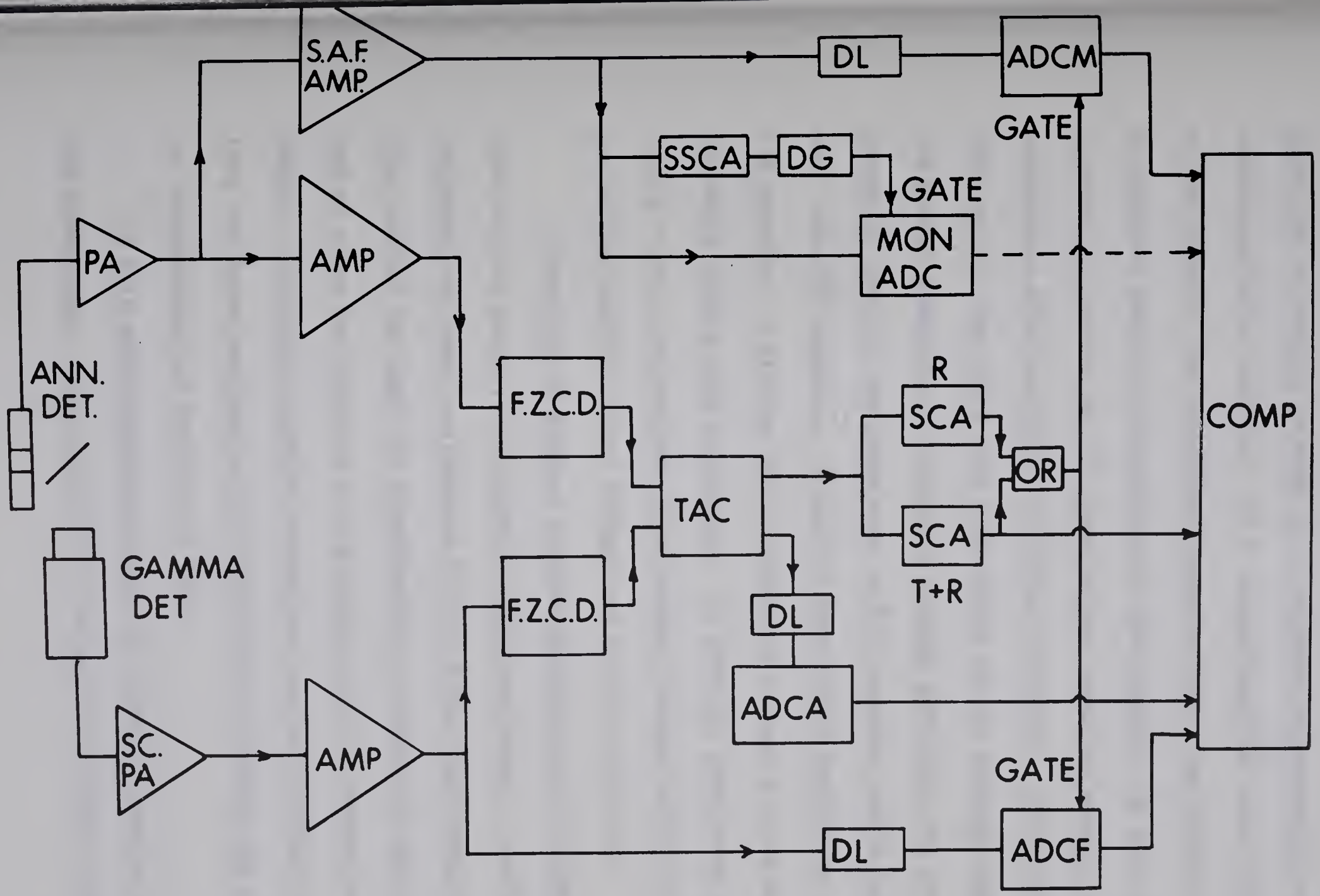

COINCIDENCE ELECTRONICS

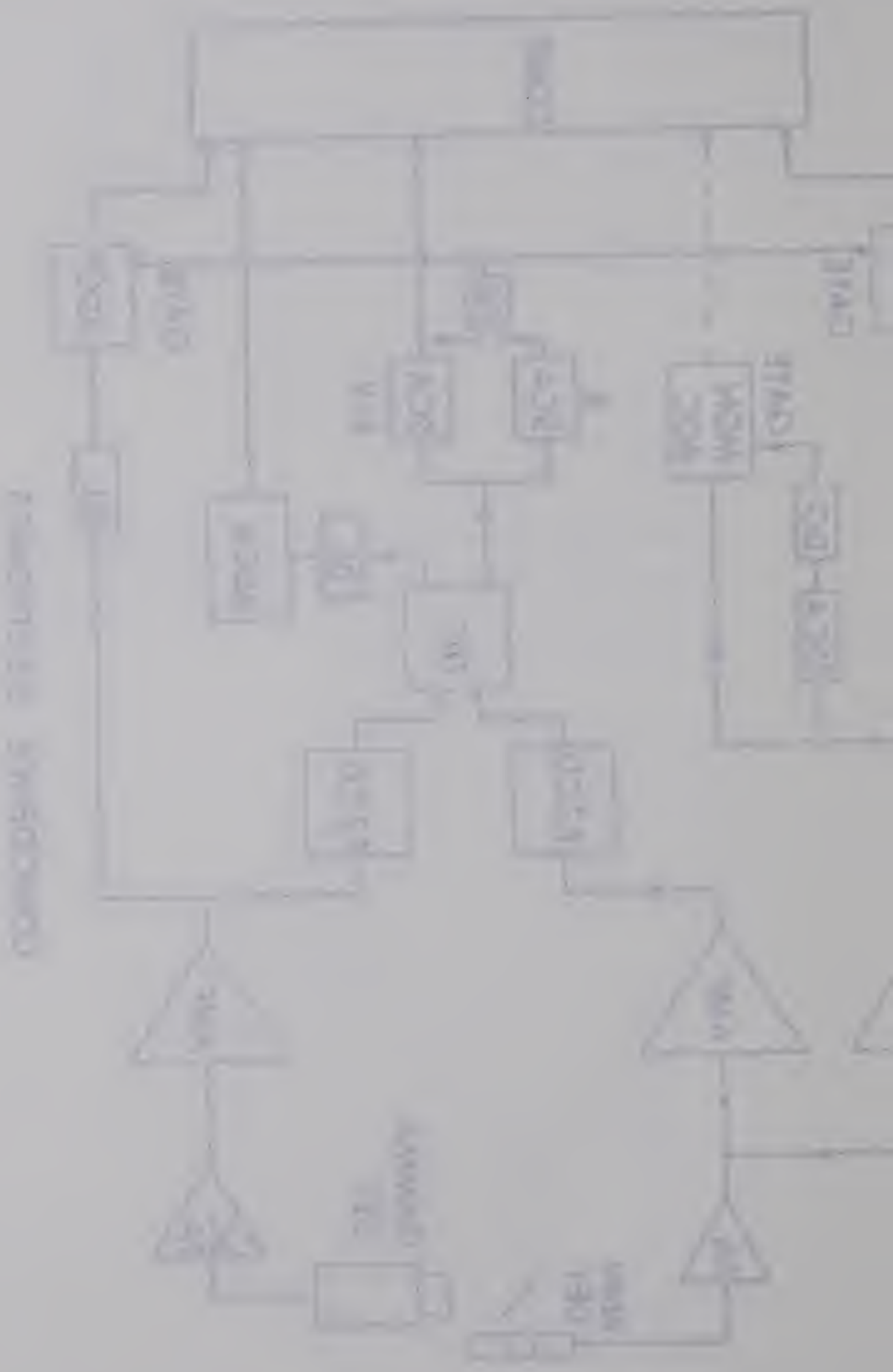

allow one to specify as many as 18 windows corresponding to peaks in the charged-particle spectrum. If a charged-particle count fell within one of the windows, the coincident gamma-ray count was stored in a region of computer memory corresponding to that window. As many as 18 T+R and R gamma-ray spectra of 256 channels each could be stored, each one in coincidence with one group of charged particles. All coincident counts from each of the ADC's were also stored in the computer memory. The T+R energy spectrum of coincident charged particles was stored in 1024 channels, that of the gamma rays in 256 channels, while the TAC output went into 128 channels. R spectra were stored beside the corresponding T+R spectra. A display unit permitted all spectra to be monitored continuously during data collection. If particle peaks were seen to shift during a run, the spectrum of coincident charged particles was recorded, new window positions were defined and the run continued.

A spectrum of singles charged particles was collected in a separate ADC and memory. To minimize dead-time losses, a self-gating arrangement was used to eliminate all but a few high-energy proton peaks. This monitor was used for normalization of gamma-ray peak areas. At the end of a run the contents of the memory could be dumped into computer memory. Coincident spectra and monitor data were stored on magnetic tape for later analysis on the University of Alberta IBM 360 computer.

b. Acquisition and analysis of data

A thin self-supporting target of natural magnesium was used in the experiment. From the width of the peak of elastic scattered ^{3}He

particles, its thickness was estimated to be slightly less than 50 $\mu g/cm^2$.

The yield of singles protons was measured at 170° (using the annular counter) for bombarding energies ranging from 4.8 MeV to 6.2 MeV varied in 100 keV steps. The resulting yields for a few of the groups corresponding to low-lying excited states in ^{26}Al are shown in Figure 3. On the basis of the yields, 6.0 MeV was chosen as the bombarding energy for the first angular correlation measurements. A bombarding energy of 5.3 MeV was chosen for a second correlation measurement because certain levels of interest had relatively high yield at that energy.

System isotropy was checked by measuring the angular distribution of gamma rays from decay of the J=0 state at 2.31 MeV in ^{14}N, excited by the $^{12}C(\tau,p\gamma)^{14}N$ reaction. Yields at 31°, 55° and 90° (with slightly over 2% statistical uncertainty at each point) when fitted to a constant gave $\chi^2/\nu=1.3$.

For angular correlation runs, gamma rays were detected at angles of 31°, 43°, 55°, 65° and 90°. For the runs at $E_\tau=6.0$ MeV two measurements were made at each angle, each measurement taking approximately 6 hours. Average beam on target was around 225 nA. During the correlation measurements at $E_\tau=5.3$ MeV the average current was 125 nA; 4 measurements were made at 90°, 3 at 55° and 2 at each of 31°, 43° and 65°.

Since the natural abundances of ^{25}Mg and ^{26}Mg are 10% and 11%, reactions involving these isotopes in the natural magnesium target could give charged particles of the same energy as the protons which correspond to low-lying levels in ^{26}Al. These are the $^{25}Mg(\tau,\alpha)^{24}Mg$

Fig. 3

Yield of some proton groups from the reaction $^{24}Mg(\tau,p)^{26}Al$ at an angle of 170° for bombarding energies from 4.8 to 6.2 MeV.

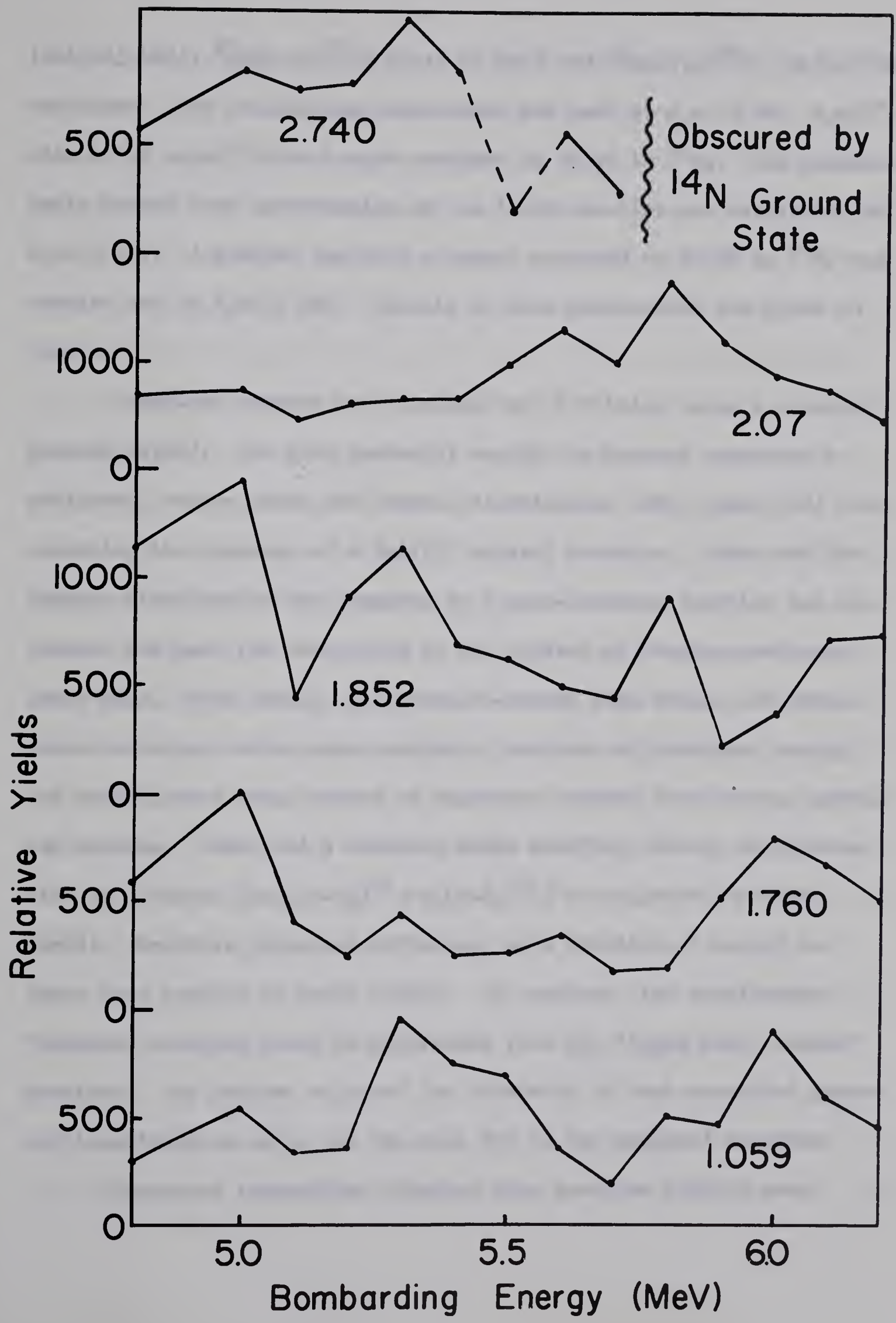
2.740
Obscured by
14N Ground
State
2.07
1.852
1.760
1.059
500
0
1000
0
1000
500
0
500
0
500
0
Relative Yields
5.0
5.5
6.0
Bombarding Energy (MeV)

2740
Observed by
M1 Ground
State
2027
1852
1750
1039
500
0
1000
0
1000
500
0
500
0
500
0
Relative Yields
50
55
60
Bombarding Energy (MeV)

(Q=13.25 MeV), $^{25}Mg(\tau,p)^{27}Al$ (Q=11.65 MeV) and $^{26}Mg(\tau,p)^{28}Al$ (Q=8.28 MeV) reactions. One coincidence measurement was made at E_τ=6.0 MeV, θ_γ=55° with a 175 $\mu g/cm^2$ thick target enriched to 99.4% in ^{26}Mg. The measurements showed that contribution of the third reaction was negligible at E_τ=6.0 MeV. A similar run with a target enriched to 99.7% in ^{24}Mg was carried out at E_τ=5.3 MeV. Results of this measurement are given in Chapter V.

Gamma-ray spectra were analyzed by χ^2 fitting using a computer program (Sy68). For each gamma-ray energy the program generated a photopeak, escape peaks and Compton distribution (Ev55, page 692) representing the response of a NaI(Tl) crystal detector. Peaks and the Compton distribution were smeared by a near-Gaussian function and allowance was made for absorption in the crystal of Compton-scattered gamma rays. Peak widths, photopeak-to-escape peak ratios and photopeak-to-Compton ratios were quadratic functions of photopeak energy, the coefficients being chosen to reproduce spectra from various gamma-ray sources. Peaks had a Gaussian shape modified through multiplication by a factor $[1+\alpha_1(E-E_o)^{n_1}+\alpha_2(E-E_o)^{n_2}]$ as suggested by Heath (He64). Relative photopeak efficiency as a function of energy was taken from results of Heath (He64). If required, the simultaneous "randoms" spectrum could be subtracted from the "trues plus randoms" spectrum. The program adjusted the intensity of each specified gamma-ray transition so as to get the best fit to the measured spectrum.

Gamma-ray intensities obtained from spectrum fitting were

normalized according to the area of the peak corresponding to the 1.059 MeV level in the monitor spectrum of singles protons. Monitor peak areas were determined using a peak-fitting routine of Tepel (Te66). This computer program automatically selected background points and fitted them to a straight line or parabola. Points above background then would be fitted to a reference peak shape supplied by the user.

A third computer program was used to fit the gamma-ray angular distributions according to the theory described in Chapter II. Angular distributions from several transitions involved in the decay of the initial state J_1 could be fitted simultaneously, using equation (II.5) and the generalized form of equation (II.6). The only transitions which could not be used were those from levels that were excited by more than one mode of decay from J_1. The Y_i and E_i for each transition were separately normalized to a_o for that transition. The program could also handle the angular distribution due to an unresolved pair of transitions, provided the relative intensities of the transitions were supplied. If some of the fitted population parameters had negative values, the one with the largest absolute value was set to zero and the fitting procedure repeated. The distributions were also fitted to

$$W(\theta) = a_o + a_2 P_2(\cos\theta) + a_4 P_4(\cos\theta) + \ldots a_{Kmax} P_{Kmax}(\cos\theta),$$

with the coefficients a_K of Legendre polynomials $P_K(\cos\theta)$ treated as parameters. The coefficients a_o were used in determining relative inten-

sities of different decay modes of a level (branching ratios). A further description of the program is given elsewhere (Hu68).

Fits were obtained with M=0 and M=1 substate populations of the initial state J_1 treated as the free parameters. Attenuation coefficients Q_2 and Q_4 were taken from a report by Rutledge (Ru59). Q_6 and Q_8 were estimated using the expression for a totally absorbing detector (Fe65, page 38). In determining χ^2 as a function of multipole mixing ratio, results from the run at E_γ =5.3 MeV were combined with those for E_γ=6.0 MeV. It was assumed that measurements at the two energies were statistically independent; for each mixing ratio the two values of (unnormalized) χ^2 were added and the results normalized to the total number of degrees of freedom.

For most cases the finite size of the proton detector was not considered because the importance of the effect could not be estimated. When definite spin assignments were made (for levels at 1.852, 2.740 and 3.159 MeV) calculations were repeated with P(2) fixed at 5% of the larger of P(0) or P(1). Slightly lower values of χ^2 were obtained, but no spin previously excluded gave χ^2 below the 0.1% confidence limit. In general it is expected that performing calculations with P(2) non-zero would give χ^2 below the 0.1% confidence limit for a slightly wider range of mixing ratios than those presented in Table 4.

V. EXPERIMENTAL RESULTS

Spectra of coincident charged particles at E_τ=5.3 MeV and E_τ=6.0 MeV are shown in Figures 5 and 6. The spectrum of protons associated with one level in ^{26}Al consisted of a narrow peak (approximately 50 keV full-width at half-maximum) and a long tail on the low-energy side of the peak. The tail possibly was due to energy loss by those ^{3}He particles which grazed the edge of a collimator but went on to cause a nuclear reaction at the target. The presence of tails meant that within a window in the spectrum of coincident protons there would be not only the peak of interest, but also the tails of all higher-energy peaks. The contribution due to this overlap could be 2 - 4% of the main peak area, depending on the width of window. A correction for estimated overlap was applied to the observed intensities.

A second problem was the presence of a photopeak at 1.35 MeV in many of the spectra. Photopeak energy could be determined only to within about 30 keV because the peak had few counts and sat on the Compton distributions of higher-energy gamma rays. While this might have been due in part to the transition 1.760→0.418 (labelling levels by their excitation energies in MeV), there were some cases for which this could not be the complete explanation. For instance, the gamma-ray spectrum associated with levels at 2.07 MeV (see Figure 9) had a larger 1.35 MeV photopeak than could be explained by overlap with the 1.760 MeV group.

Fig. 4

Branching ratios obtained in this work for levels in ^{26}Al below 4 MeV. Uncertainties in the branching ratios are ±10 except for numbers in parentheses for which uncertainties are ±20. References are (a) this work, (b) En67, (c) Bi68, (d) We68 and (e) Fu68.

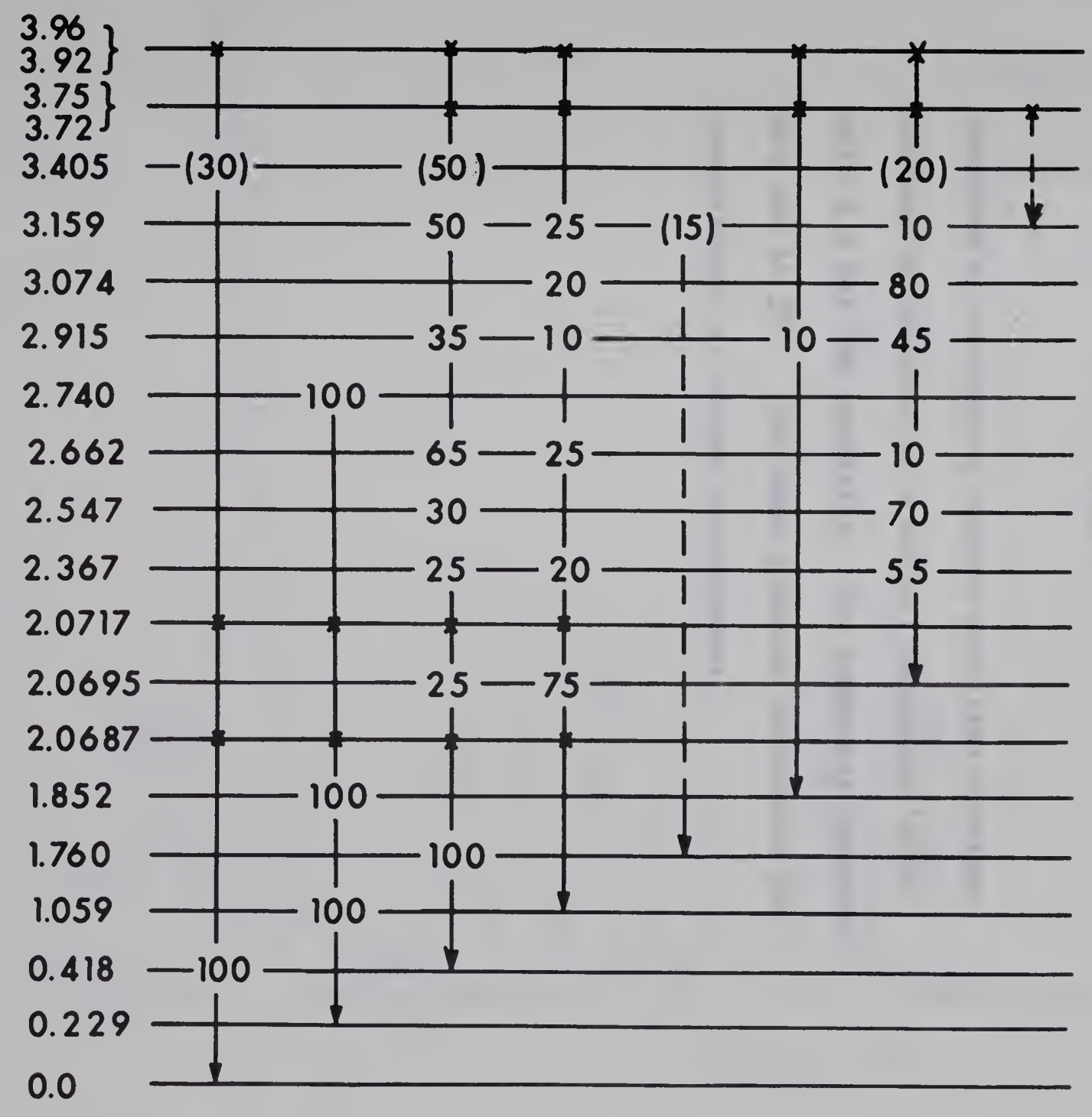
E_x (MeV)
3.96
3.92
3.75
3.72
3.405
3.159
3.074
2.915
2.740
2.662
2.547
2.367
2.0717
2.0695
2.0687
1.852
1.760
1.059
0.418
0.229
0.0
(30)
(50)
(20)
50
25
(15)
10
20
80
35
10
10
45
100
65
25
10
30
70
25
20
55
25
75
100
100
100
100
J^π
Reference for Spin Assignment
2^+ (T=1)
a
$(2,3)^+$
d,e
1
a,c
$(2,3)^+$
e
$(2,3)^+$
d,e
$(2,3)^+$
d,e
(1)
c
$(2^+$ T=1)
c
(3)
c
1
a,c
2^+
b
1^+
b
3^+
b
0^+ T=1
b
5^+
b

Fig. 4

Fig. 5

Spectrum of coincident charged particles obtained through bombardment of a natural magnesium target with 5.3 MeV ^{3}He particles. The gamma-ray detector was set at 55°. The lower spectrum represents the contribution of random coincidences.

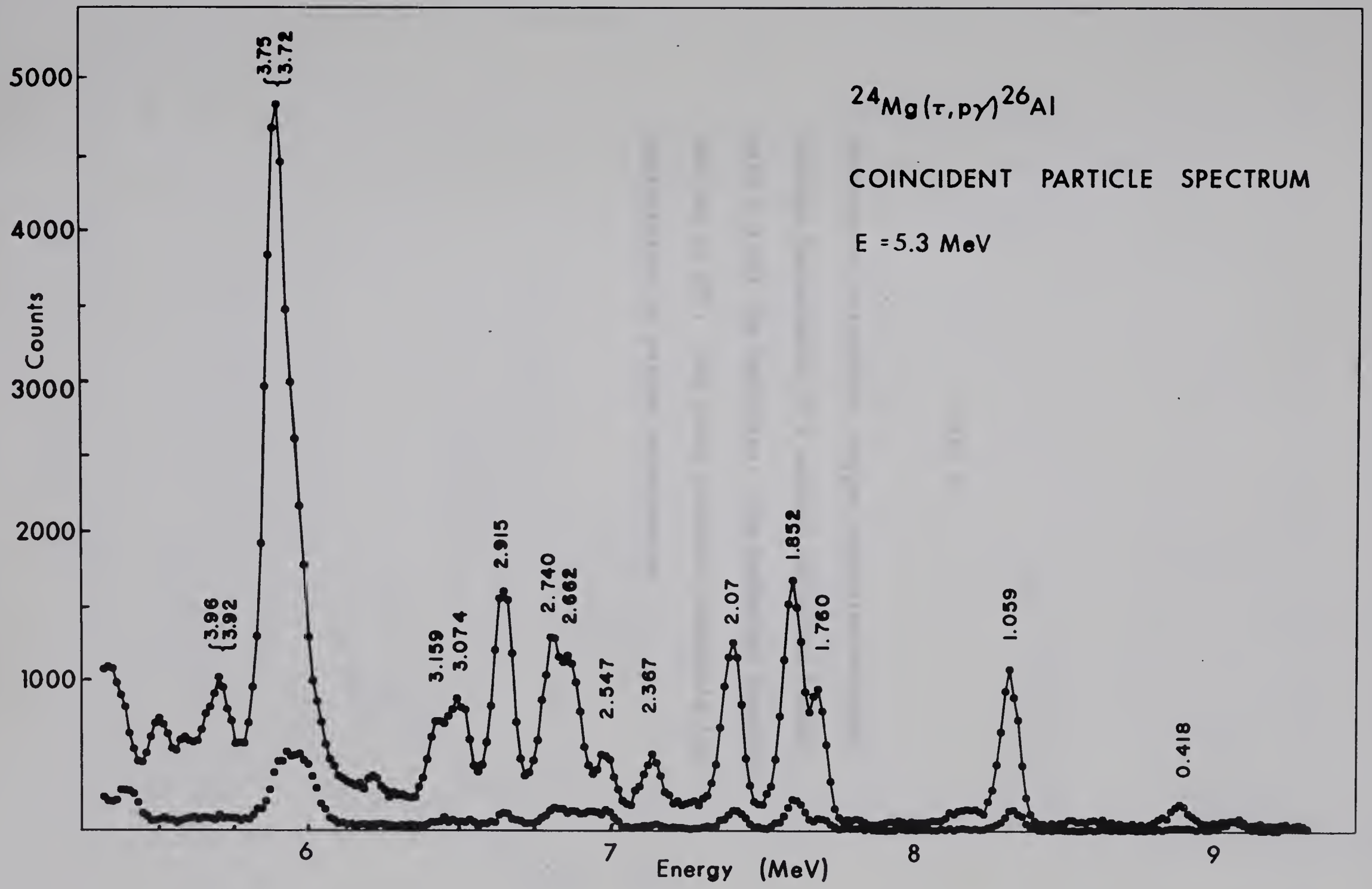
$^{24}Mg(\tau,p\gamma)^{26}Al$
COINCIDENT PARTICLE SPECTRUM
E = 5.3 MeV
Counts
Energy (MeV)
5000
4000
3000
2000
1000
6
7
8
9
3.75
3.72
3.98
3.92
3.159
3.074
2.915
2.740
2.662
2.547
2.367
2.07
1.852
1.760
1.059
0.418

Fig. 5

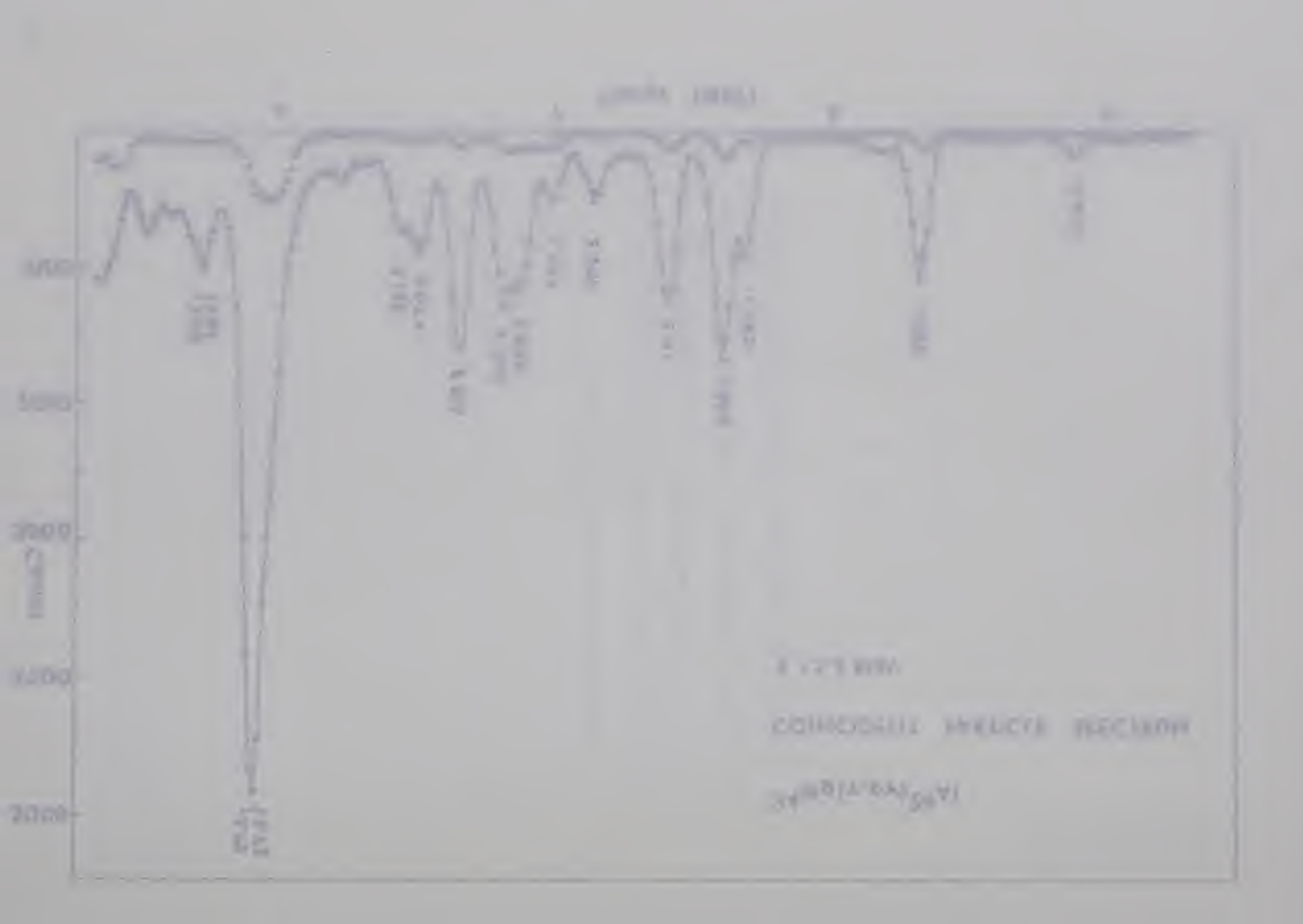

Fig. 6

Spectrum of coincident charged particles obtained through bombardment of a natural magnesium target with 6.0 MeV ^{3}He particles. The gamma-ray detector was set at 55°. The lower spectrum represents the contribution of random coincidences.

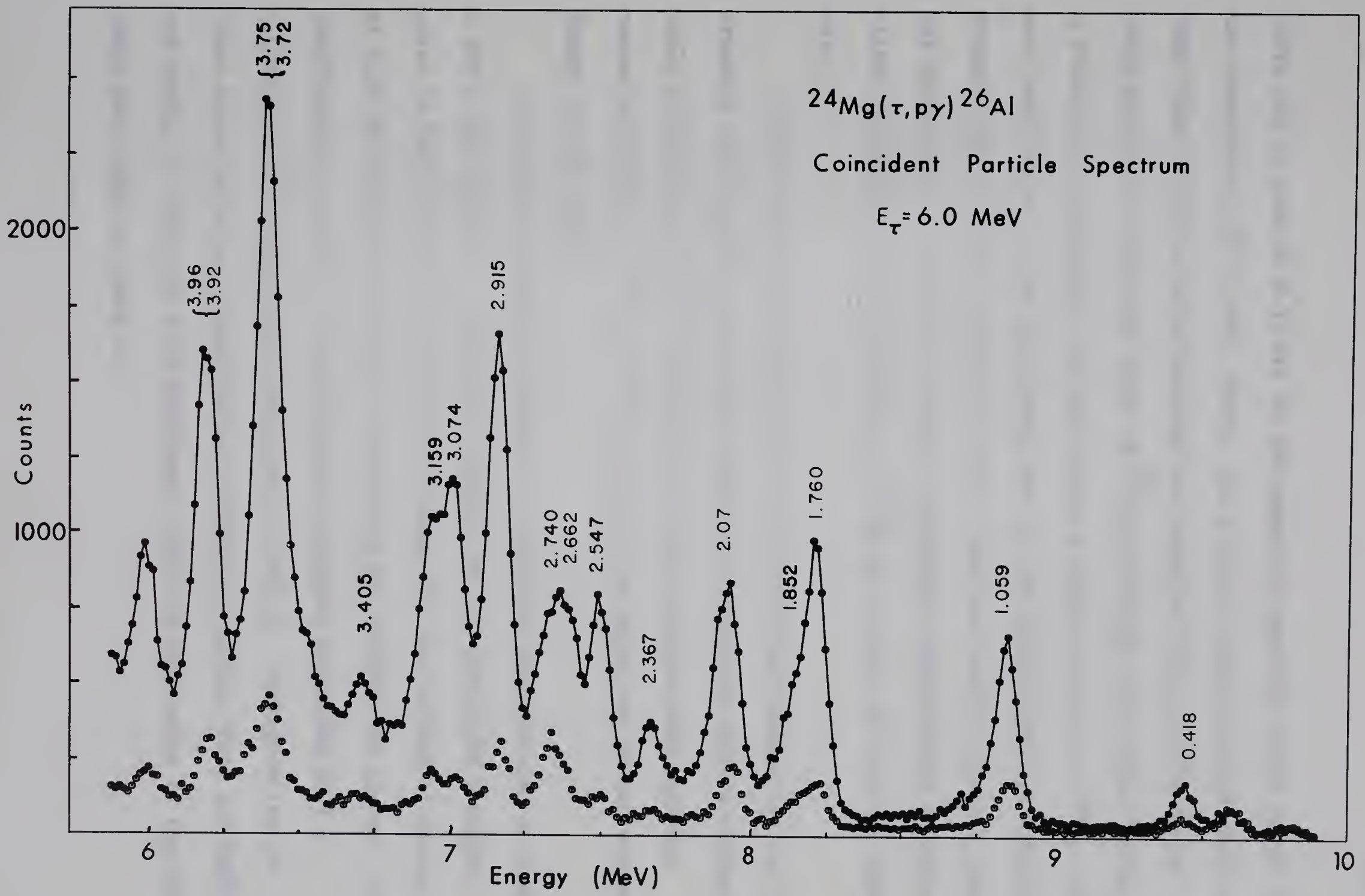
$^{24}Mg(\tau,p\gamma)^{26}Al$
Coincident Particle Spectrum
E_τ= 6.0 MeV
Counts
2000
1000
3.96
3.92
3.75
3.72
3.405
3.159
3.074
2.915
2.740
2.662
2.547
2.367
2.07
1.852
1.760
1.059
0.418
6
7
8
9
10
Energy (MeV)

Fig C

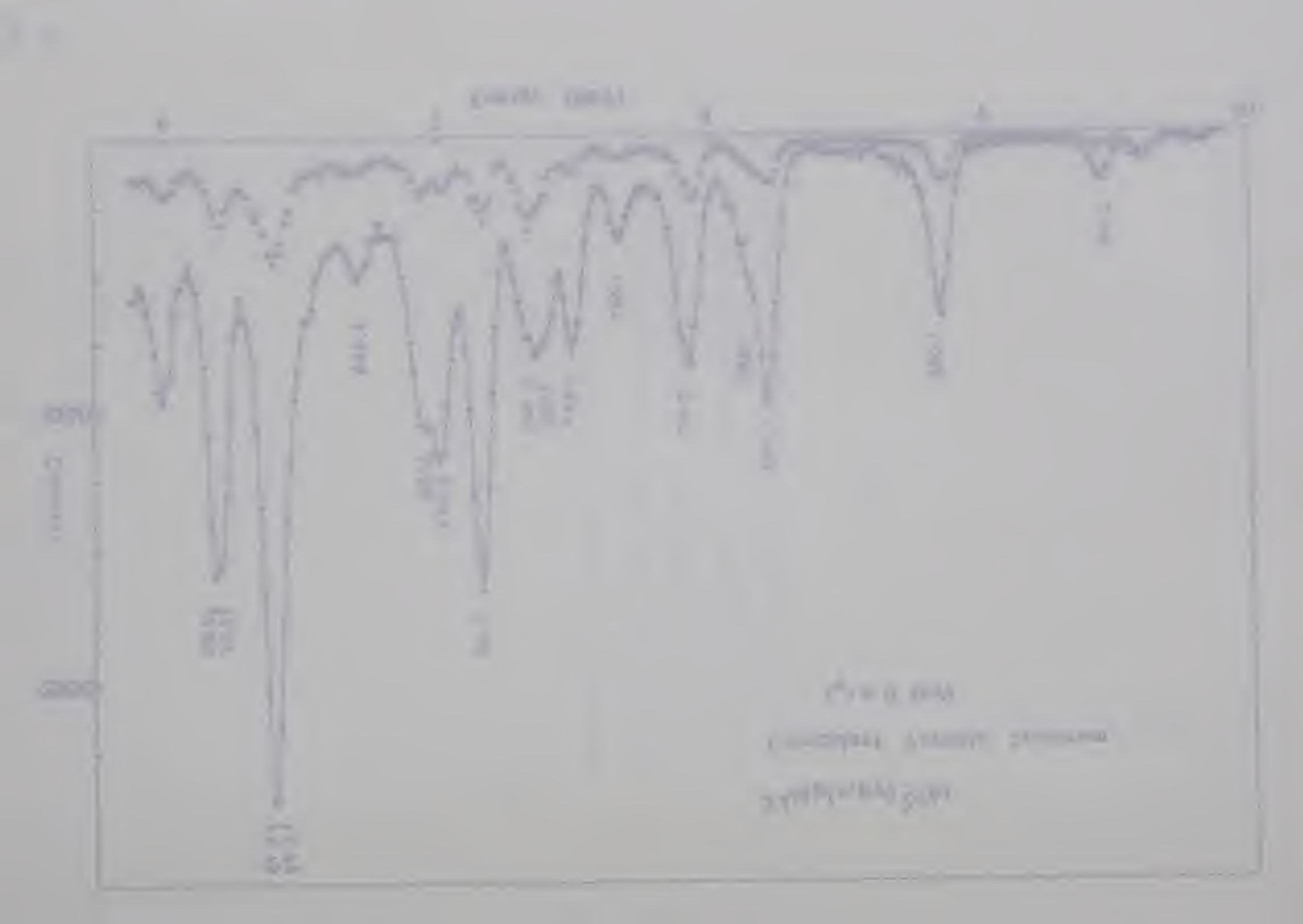

There was no peak at 0.31 MeV in the gamma-ray spectrum, which ruled out the transition 2.07→1.760. Hence, the 1.35 MeV peak was attributed to some other reaction, quite possibly the reaction $^{25}Mg(\tau,\alpha)^{24}Mg$ which could excite the 1.369 MeV state of ^{24}Mg by cascade from higher levels. A coincidence measurement was made using a target enriched in ^{24}Mg. Several small peaks at the high energy end of the charged particle spectrum, present with a natural magnesium target, were now absent. For the gamma-ray spectrum of the 2.07 MeV levels, statistical uncertainties prevented either confirmation or elimination of ^{25}Mg as a source of 1.35 MeV gamma rays.

Levels above 4 MeV excitation were not studied because (i) the increasing level density would make analysis of gamma-ray spectra increasingly difficult and (ii) ^{26}Al levels of these energies were becoming masked by levels in ^{18}F and ^{14}N resulting from oxygen and carbon contaminants on the target.

The branching ratios obtained in this work are presented in Tables 1 and 2 and Figure 4. Levels are labelled by the excitation energies given by Endt and Van der Leun (En67) except for the triplet of states at 2.07 MeV, where the values of Hausser et al. (Ha68b) are listed. Some coefficients a_2 and a_4 of the Legendre polynomial expansion $W(\theta) = a_o(1+a_2P_2(\cos\theta)+a_4P_4(\cos\theta))$ are given in Table 3. Mixing ratios for those spins which are compatible with stripping studies (Fu68 and We68) and having χ^2 below the 0.1% confidence limit for some value of the mixing ratio are listed in Table 4.

Table 1

Summary of branching ratios obtained at E_τ=6.0 MeV. Errors in branching ratios are ±10 except for bracketed values which are ±20.

Initial state(s)	Final State	E_γ (MeV)	Branching Ratio
0.418	0.	0.42	100
1.059	0.229	0.83	100
1.760	0.418	1.34	100
1.852	0.229	1.62	100
2.0687	0.	2.07	< 5
2.0695	0.229	1.84	65
2.0717	0.418	1.65	15
	1.059	1.01	20
2.367	0.418	1.95	25
	1.059	1.31	20
	2.0695	0.30	55
2.547	0.418	2.13	30
	2.0695	0.48	70
2.662	0.418	2.24	65
	1.059	1.60	25
	2.0695	0.59	10
2.740	0.229	2.51	100

Table 1 Continued

Initial state(s)	Final state	E_γ (MeV)	Branching Ratio
2.915	0.418	2.50	35
	1.059	1.86	10
	1.852	1.06	10
	2.0695	0.85	45
3.074	1.059	2.01	(20)
	2.0695	1.00	80
3.159	0.418	2.74	50
	1.059	2.10	25
	1.760	1.40	(15)
	2.0695	1.09	10
3.405	0.	3.40	(30)
	0.418	2.99	(50)
	2.0695	1.34	(20)
3.72, 3.75	0.418	3.4	(25)
	1.059	2.7	(30)
	2.0695	1.65	(30)
	3.159	0.60	(15)
3.92, 3.96	0.	3.9	10
	1.059	2.9	15
	1.852	2.1	35
	2.0695	1.9	40

Table 2

Branching ratios for unresolved groups, obtained at E_γ=5.3 MeV. See Table 1

Initial states	Final states	E_γ (MeV)	Branching Ratios
2.0687	0.	2.07	5
2.0695	0.229	1.84	55
2.0717	0.418	1.65	25
	1.059	1.01	15
3.72	0.418	3.4	10
3.75	1.059	2.7	35
	1.852	1.9	10
	2.0695	1.65	45
3.92	0.418	3.5	10
3.96	1.059	2.9	30
	1.852	2.1	20
	2.0695	1.9	40

Table 3

Coefficients of an expansion $W(\theta) = a_o[1 + a_2P_2(\cos\theta) + a_4P_4(\cos\theta)]$ of gamma-ray angular distributions at bombarding energies 5.3 and 6.0 MeV. Transitions for which the photopeak was one of an unresolved doublet are marked with a star.

Initial state(s)	Final state	E_τ = 5.3 MeV a_2	E_τ = 5.3 MeV a_4	E_τ = 6.0 MeV a_2	E_τ = 6.0 MeV a_4
0.418	0.	0.22±0.06	0.09±0.1	0.05±0.16	-0.50±0.27
1.059	0.229	-0.67±0.07	-0.03±0.13	0.14±0.09	0.08±0.12
1.760	0.418	0.15±0.05	-0.04±0.08	0.25±0.09	-0.11±0.13
1.852	0.229	-0.73±0.03	0.02±0.03	-0.36±0.12	-0.04±0.18
2.0687 2.0695 2.0717	0.	0.18±0.22	0.64±0.34		
	0.229	-0.07±0.05	-0.11±0.08	0.37±0.09	0.01±0.13
	0.418	-0.18±0.09	0.18±0.14	0.55±0.28	0.60±0.42
	1.059	-0.27±0.14	0.14±0.21	-0.23±0.18	-0.01±0.29
2.367	0.418	-0.08±0.18	0.16±0.28	-0.74±0.33	-1.0±0.55
	1.059 *	-0.20±0.19	0.56±0.31	0.31±0.34	-0.67±0.54
	2.0695			-0.42±0.16	-0.05±0.26

Table 3 Continued

Initial state(s)	Final state	E_τ = 5.3 MeV a_2	E_τ = 5.3 MeV a_4	E_τ = 6.0 MeV a_2	E_τ = 6.0 MeV a_4
2.547	0.418	-0.03±0.26	-0.32±0.42	0.56±0.21	0.20±0.30
	2.0695	-0.58±0.34	-1.01±0.51	-0.24±0.11	-0.02±0.18
2.662	0.418	-0.30±0.10	-0.17±0.18	-0.07±0.14	-0.09±0.21
	1.059 *	-0.23±0.16	0.04±0.26	-0.01±0.48	-0.25±0.74
	2.0695	0.32±0.08	-0.01±0.13	0.27±0.19	0.05±0.28
2.740	0.229	-0.06±0.04	0.04±0.06	0.07±0.16	0.03±0.26
2.915	0.418	-0.52±0.08	-0.06±0.13	-0.24±0.12	-0.03±0.19
	1.059	0.10±0.26	0.44±0.41	0.47±0.40	0.14±0.60
	1.852 *	-0.14±0.06	-0.06±0.10	-0.15±0.11	-0.01±0.18
	2.0695 *	0.03±0.04	0.01±0.07	0.11±0.08	0.08±0.12
3.074	1.059	0.10±0.23	-0.11±0.35	1.28±0.38	-0.04±0.49
	2.0695 *			-0.34±0.08	-0.15±0.12
3.159	0.418	-0.27±0.12	-0.17±0.19	0.01±0.09	-0.17±0.14
	1.059	-0.35±0.25	0.27±0.37	-0.43±0.25	0.54±0.40
	1.760 *	0.18±0.16	0.14±0.25	-0.02±0.53	-0.03±0.85
	2.0695 *			-0.35±0.20	-0.02±0.32
3.72 } 3.75 }	0.418	0.07±0.26	0.44±0.40	-0.24±0.21	0.08±0.28
	1.059	0.12±0.07	0.12±0.10	0.35±0.11	0.15±0.16

Table 3 Continued

Initial state(s)	Final state	E_τ = 5.3 MeV a_2	E_τ = 5.3 MeV a_4	E_τ = 6.0 MeV a_2	E_τ = 6.0 MeV a_4
3.92} 3.96}	0.	0.22±0.34	0.10±0.50	0.29±0.14	0.38±0.21
	1.059	-0.04±0.11	-0.07±0.16	0.27±0.11	0.04±0.18
	1.852	-0.08±0.24	-0.12±0.40	-0.10±0.13	-0.12±0.22
	2.0695	-0.21±0.10	0.12±0.16	-0.35±0.16	-0.48±0.27

Table 4

A summary of mixing ratios obtained in this work.

Energy level	Transition	Assumed Spin Sequence	Possible values of mixing ratio x	Confidence limit at χ^2_{min}
0.418	0.418→0	3→5	$0.0^{+0.27}_{-0.20}$; $1.9^{+1.2}_{-0.8}$	0.49;0.49
1.059	1.059→0.229	1→0	0	0.60
1.760	1.760→0.418	2→3	0.14 < x < 3.1	0.25
1.852	1.852→0.229	1→0	0	0.49
2.07	2.0687, 2.0717 →0.229	1→0	0	0.24
2.547	2.0695→1.059 1.059 → 0.229	2→1→0	$< -1.7; 0.1^{+0.9}_{-0.25}; > 9.2$	0.65;0.42;0.21
2.367	2.367→0.418	2→3	$< -2.5; -0.14^{+.31}_{-.37}; > 2.7$	0.02;0.04;0.03
		3→3	< -3.5; > 0.36	0.05;0.06
	2.367→1.059	2→1	< -3.7; > -1	0.14;0.61
		3→1	$0.84^{+60}_{-1.0}$	0.46
	2.367→2.0695	2→2	< -2.4; > +.05	0.21;0.88
		3→2	$< -14; 0.^{+.7}_{-.31}; 2.9^{+\infty}_{-1.9}$	.01;.87;.64
2.547	2.547→0.418	2→3	< -9.5; > -0.24	0.01;0.92
		3→3	< 1.05; > 4.7	0.89;0.01

Table 4 Continued

Energy level	Transition	Assumed Spin Sequence	Possible values of mixing ratio x	Confidence limit at χ^2_{min}
2.547	2.547→2.0695	2→2	$< -3.7;\ > 0.18$	0.25;0.46
		3→2	$< -60.; 0^{+.18}_{-.25}; 5.8^{+\infty}_{-3.4}$	.002;.17;.11
2.662	2.662→0.418	2→2	$< -2.; -0.07^{+.35}_{-.68}; > 4.$	.69;.57;.69
		3→3	$< -2.8;\ > 0.28$	0.63; 0.65
	2.662→2.0695	2→2	$-11.5 < x < 0.32$	0.99
		3→2	$-6.^{+4}_{-\infty}; -0.36^{+.17}_{-.42}; 30.$	.88;.98;.002
2.740	2.740→0.229	1→0	0	0.81
2.915	2.915→0.418	2→3	$< -0.04;\ > 8.1$	0.79; 0.36
		3→3	$1.9^{+9.6}_{-1.1}$	0.11
3.159	3.159→0.418	2→3	$< -30.; 0.^{+.37}_{-.14}; 5.7^{+\infty}_{-3.9}$	.003;.07;.17
	3.159→1.059	2→1	$< -30.;\ > 0.35$	0.005;.999

a. The ground state and states at 0.229 MeV and 1.059 MeV

The spins assigned to these states— 5^+, 0^+ (T=1), and 1^+, respectively—are based on study of beta decays $^{26}Si(\beta^+)^{26}Al$ and $^{26}Al(\beta^+)^{26}Mg$ (En67). These spin assignments were accepted in the present work.

No gamma rays were observed for a 0.229→0. transition; the 0.229 MeV level decays by β^+ emission (half-life 6.4 sec).

The angular distribution of gamma rays from the 1.059→0.229 transition was consistent with the assumption of spin sequence 1→0 and ruled out 2→0. There is, of course, no multipole mixing in a transition to a J=0 level. The fitted population parameters were $P(0) = (78\pm2)\%$ at E_τ=5.3 MeV and $P(0) = (27\pm4)\%$ at E_τ=6.0 MeV. This result is not unexpected in view of the yield curve of this level (see Figure 3), for which resonance structure appears important.

b. The 0.418 MeV level

The strong l_p=0 component in the stripping reactions (Fu68, We68) required spin 2^+ or 3^+ for this level. The absence of a transition to the 0^+ (T=1) level at 0.229 MeV makes J=2 exceedingly unlikely, in agreement with the assignment 3^+ (En67).

The half-life of the level is 1.26 nsec (En67); over this length of time the angular correlation might be perturbed by interaction with atoms of the target. However, assuming a target thickness of 0.3 microns and an energy of 0.5 MeV for the ^{26}Al nucleus, the time taken for a recoil nucleus to traverse the target is about 10^{-13} sec. The corre-

lation should not be perturbed.

Figure 7 shows χ^2 versus mixing ratio for the 0.418→0. transition, assuming spin sequence 3→5. The solution x=1.9 is extremely unlikely since E2 transitions are normally much stronger than M3 transitions, implying a mixing ratio close to zero.

c. The 1.760 MeV level

Horvat et al. (Ho63) assigned spin-parity 2^+ to the level and obtained x=0.23 or x=2.2 as the mixing ratio of the 1.760→0.418 transition. This assignment is supported by the stripping reaction studies (Fu88 and We68) which show a large l_p=0 component. The mixing ratio solutions obtained in this work (Figure 8) cannot be used to discriminate between the two solutions of Horvat et al. (Ho63). Simultaneous fitting of the 1.760→0.418 and 0.418→0. transitions did not provide any further restriction, even assuming the mixing ratio for the 0.418→0. transition was known to be 0.0.

d. The 1.852 MeV level

Horvat et al. (Ho63) stated that this level decayed to the ground state only and tentatively assigned it as J=3. A similar branching was given by Neher et al. (Ne62) and Bizot (Bi64). In this work it was found to decay 100% to the 0.229 MeV level. Only an assumed spin sequence 1→0 fitted the angular distribution, the next lowest χ^2 being 16. for 2→0. Fitted population parameters were P(0) = (82±2)% for E_τ=5.3 MeV and P(0) = (57±6)%at E_τ=6.0 MeV.

This branching ratio and spin assignment is also found by Biss-

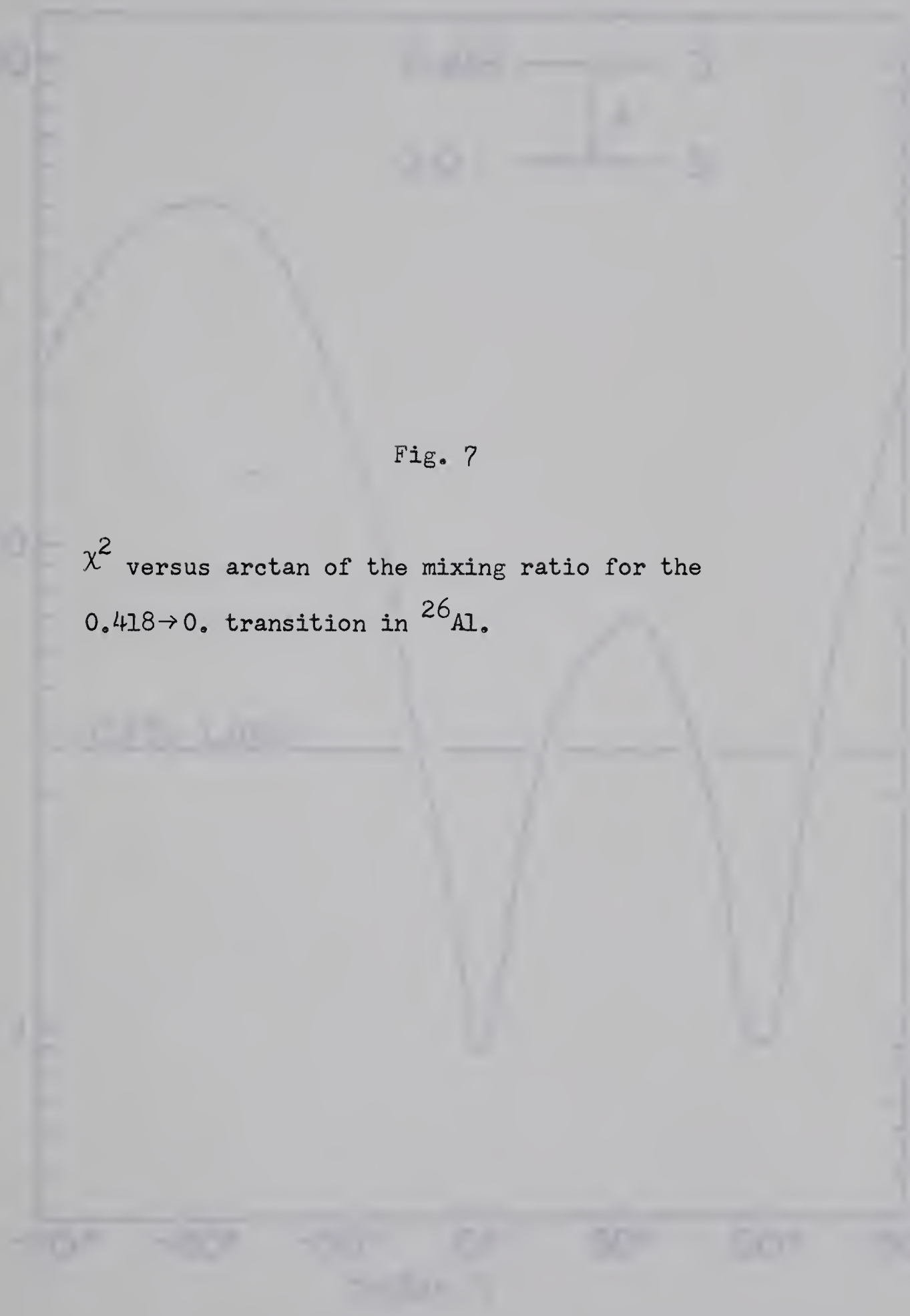

Fig. 7

χ^2 versus arctan of the mixing ratio for the 0.418→0. transition in ^{26}Al.

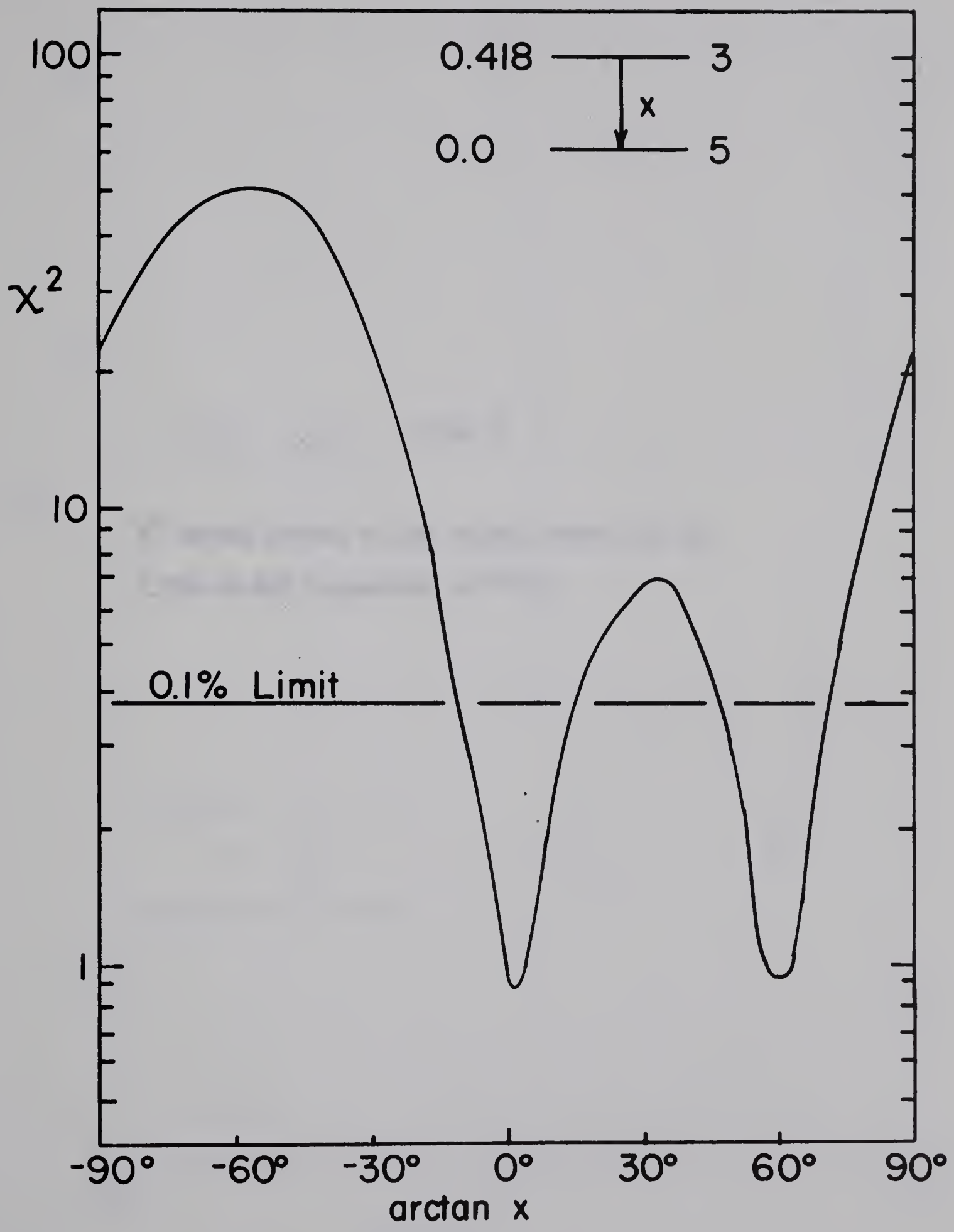
100
10
1
χ^2
0.418
3
x
0.0
5
0.1% Limit
-90°
-60°
-30°
0°
30°
60°
90°
arctan x

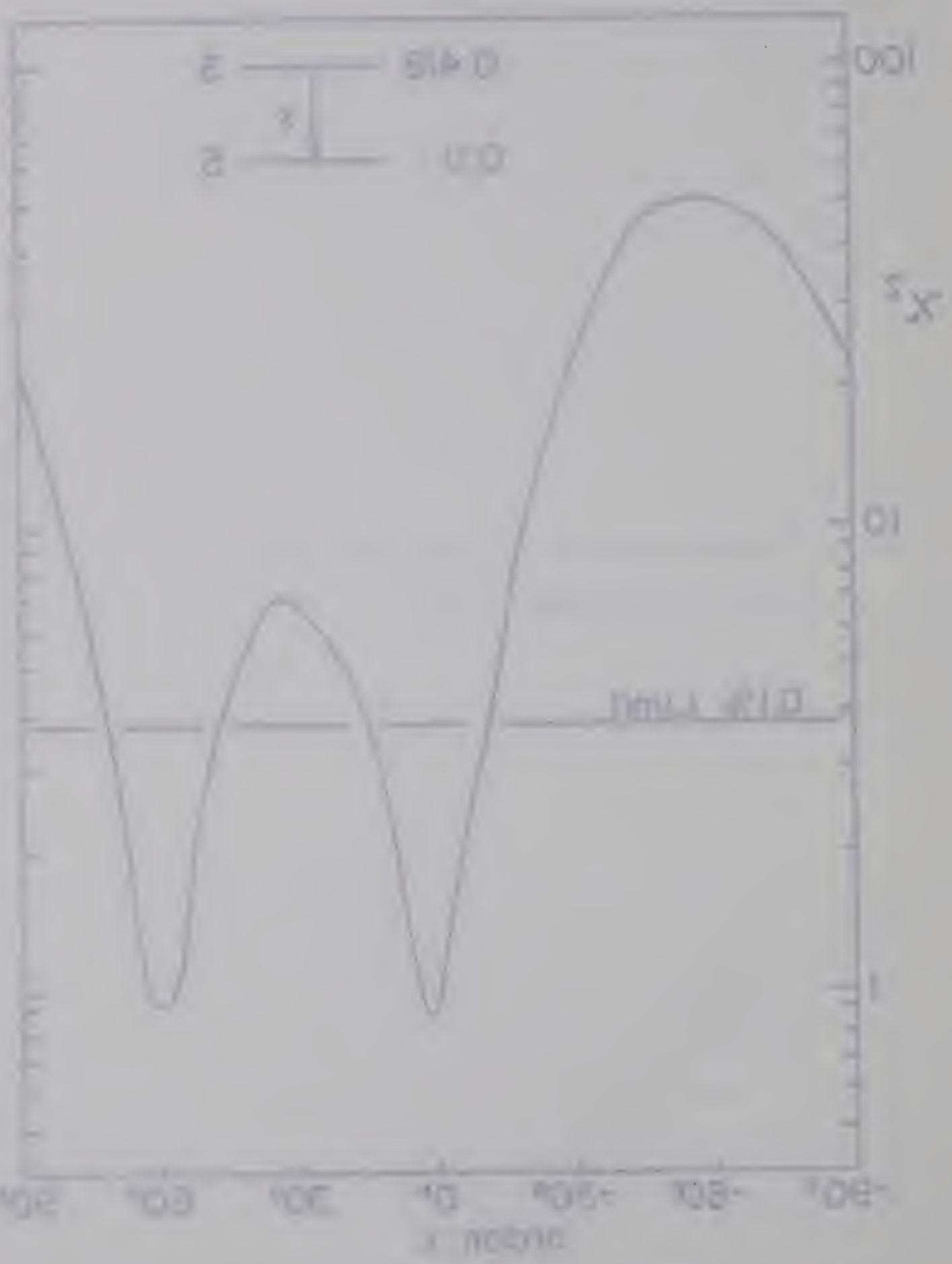

Fig. 8

χ^2 versus arctan of the mixing ratio for the 1.760→0.418 transition in ^{26}Al.

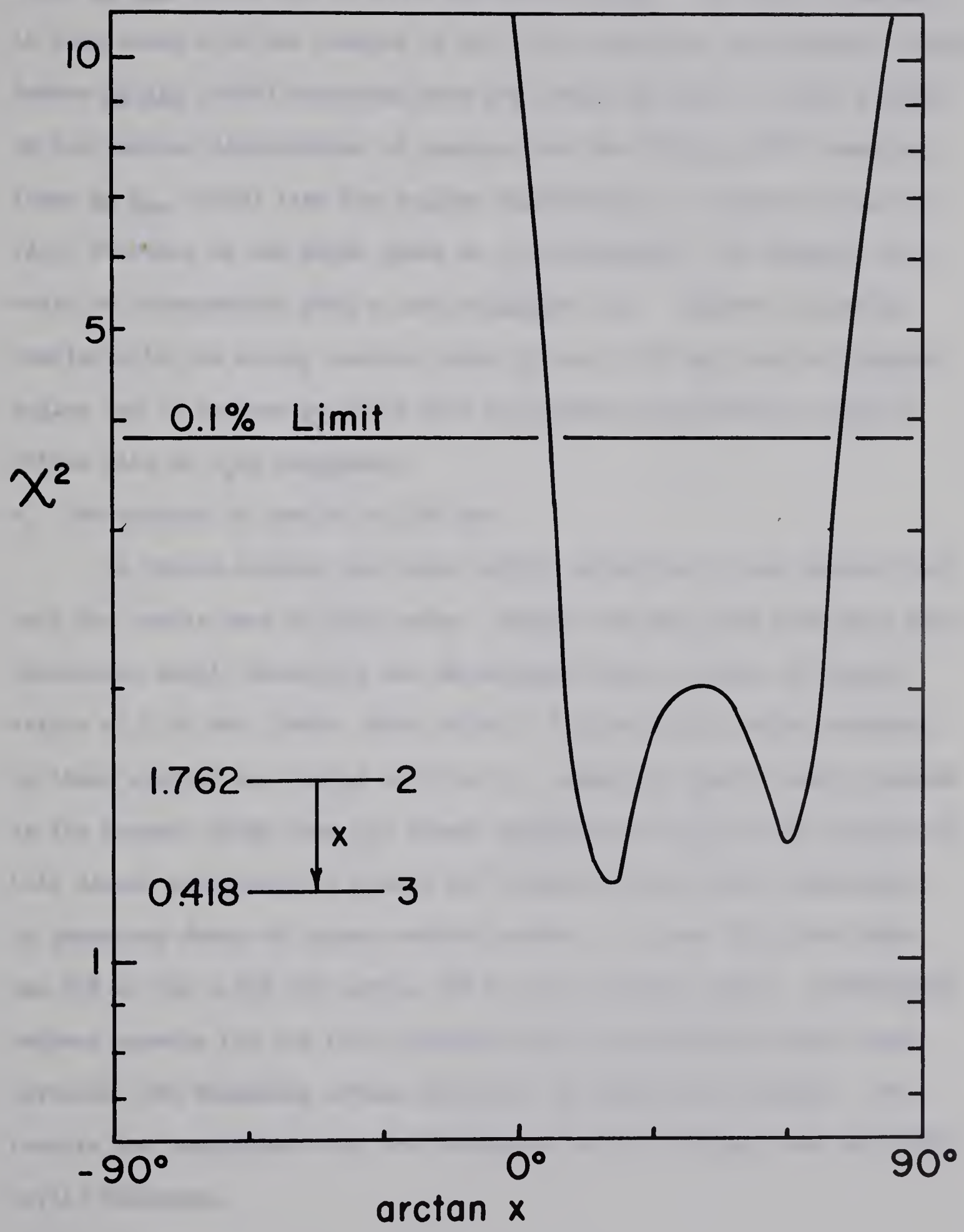
10
5
0.1% Limit
χ^2
1.762
2
x
0.418
3
1
-90°
0°
90°
arctan x

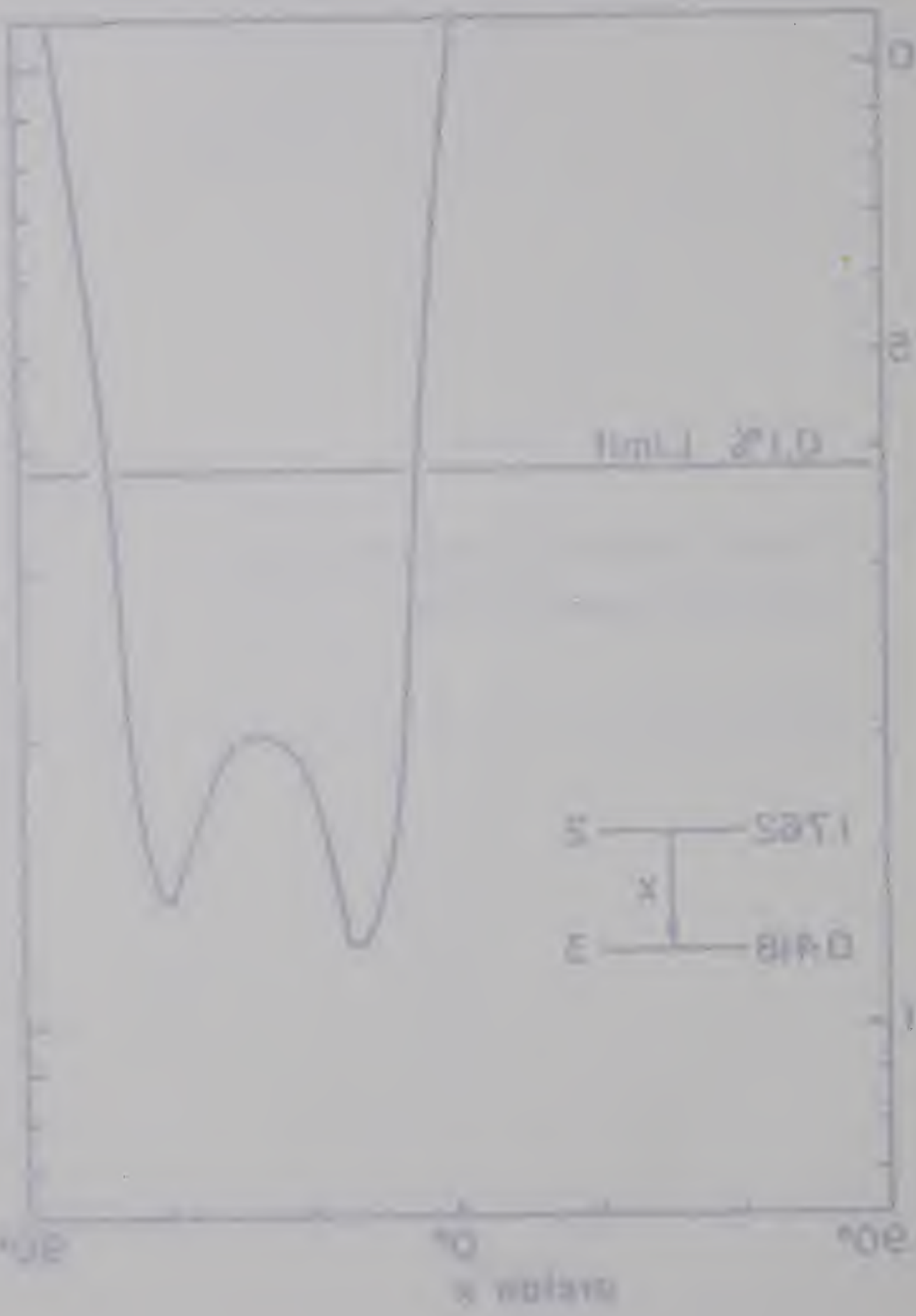

inger et al. (Bi68) and da Silva and Lisle (Si68). The spin assignment is consistent with the results of the (τ,d) stripping measurements (We68). Rosner et al. (Ro68) concluded that the level has spin 1^+ after a study of the angular distribution of protons from the $^{24}Mg(\tau,p)^{26}Al$ reaction. Fuchs et al. (Fu68) list the angular distribution of neutrons from the (d,n) reaction as one which shows an $l_p=0$ component. If correct, this would be incompatible with a spin assignment J=1. However, there is overlap with the strong neutron group of the 1.760 MeV level at forward angles and it appears possible that the angular distribution could be fitted with no $l_p=0$ component.

e. The triplet of levels at 2.07 MeV

In proton capture work with NaI(Tl) detectors it was assumed that only two levels were in this group. Within the past year work with high-resolution Ge(Li) detectors has established that a triplet of levels exists at 2.07 MeV (Ha68a, Bi68, Si68). The branching ratios obtained in these studies are listed in Table 5. Gamma-ray spectra were obtained in the present study from (i) direct excitation at $E_\tau=5.3$ MeV (Figure 9), (ii) direct excitation at $E_\tau=6.0$ MeV (Figure 10) and (iii) excitation by gamma-ray decay of higher excited states. In case (iii) the decay was 25% to the 0.418 MeV level, 75% to the 1.059 MeV level. Differences between spectra (i) and (ii) indicated that two additonal levels were involved, but branching ratios could not be determined uniquely. The results are consistent with the branching ratios obtained from work with Ge(Li) detectors.

Table 5

Branching ratios which have been obtained in other work for the triplet of levels near 2.07 MeV.

Initial state	Final state	Branching ratios obtained by Ha68a	Bi68	Si68
2.0687	0	28	29	30±3
	0.418	69	71	70±3
	1.059	3	< 3	
2.0695	0.229	5	5	
	0.418	22	22	⩽ 15
	1.059	73	73	100
2.0717	0.229	~65	> 91	100
	1.059	~35	< 9	

Fig. 9

Gamma rays seen in coincidence with protons associated with the levels at 2.07 MeV in ^{26}Al at an angle of 55° for a bombarding energy of 5.3 MeV. The lower spectrum represents the contribution of random coincidences.

^{26}Al GAMMA SPECTRUM

$E_\tau = 5.3$ MeV

$\theta_\gamma = 55°$

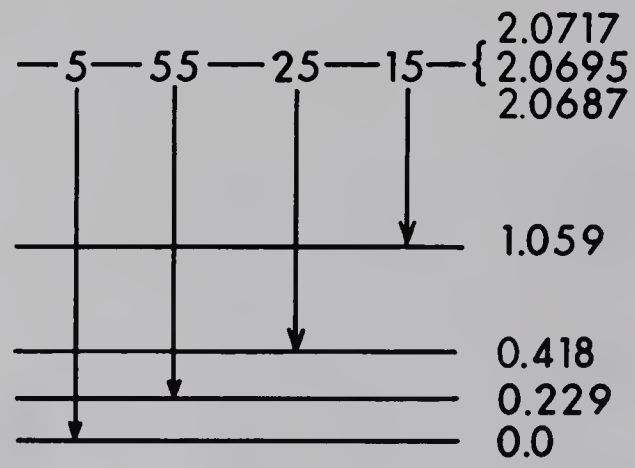

Fig 9

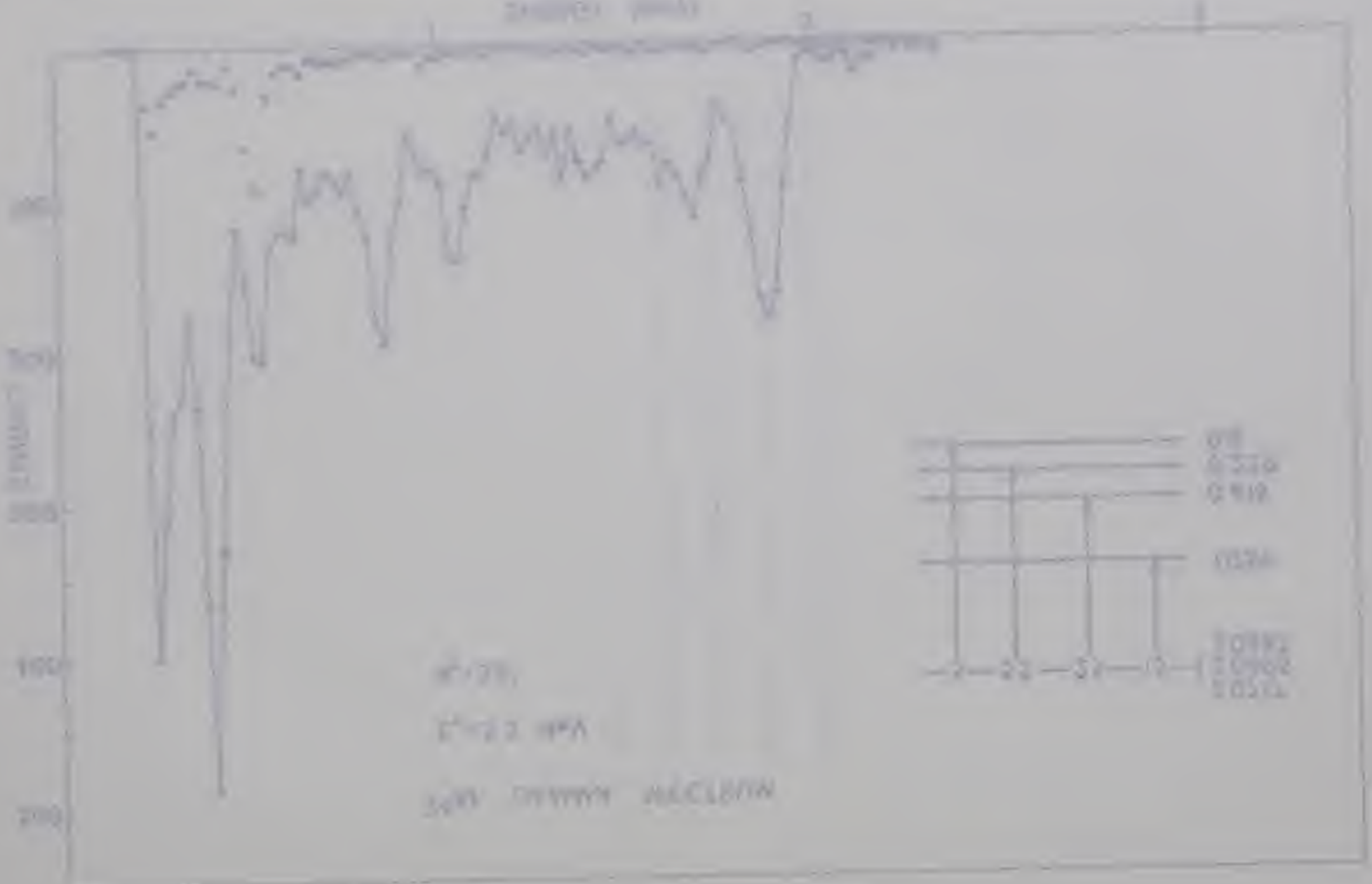

Fig. 10

Gamma rays seen in coincidence with protons associated with the levels at 2.07 MeV in ^{26}Al at an angle of 55° for a bombarding energy of 6.0 MeV. The lower spectrum represents the contribution of random coincidences.

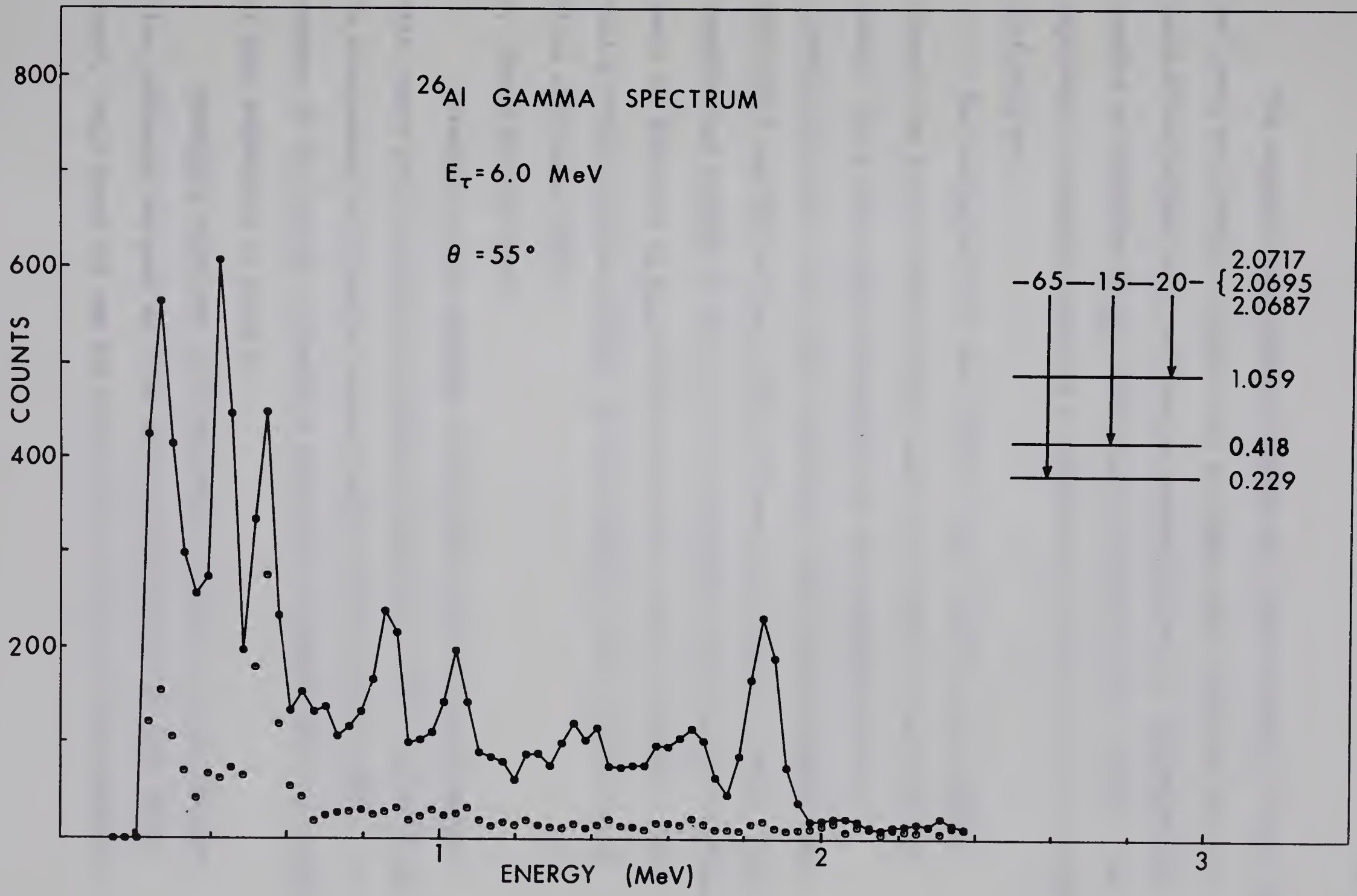
^{26}Al GAMMA SPECTRUM
E_τ = 6.0 MeV
θ = 55°
800
600
400
200
COUNTS
1
2
3
ENERGY (MeV)
-65-15-20-
2.0717
2.0695
2.0687
1.059
0.418
0.229

Fig 10

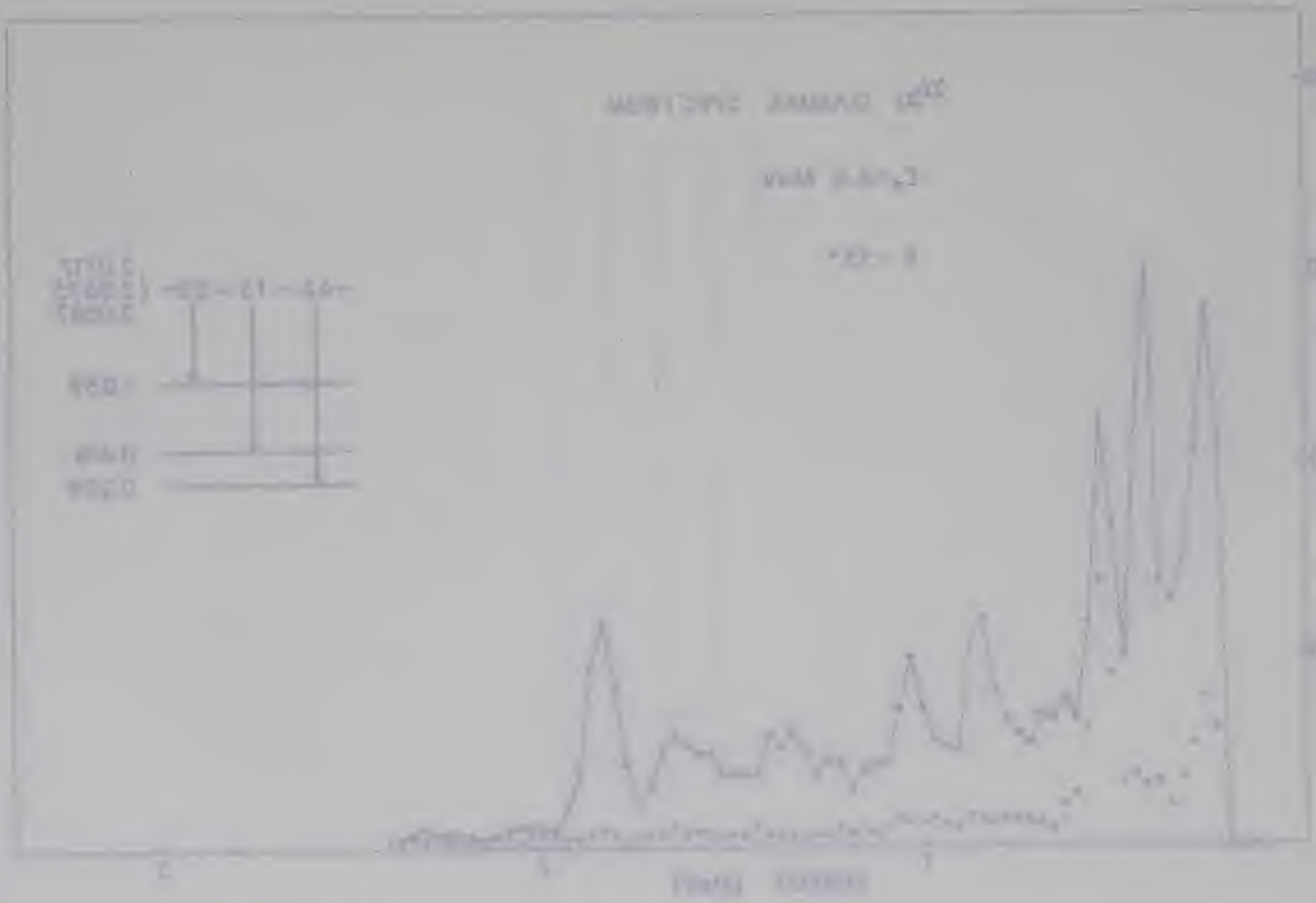

The angular distribution of gamma rays from the decay to the 0.229 MeV level was fitted, assuming that all gamma rays originated from one level of the triplet. Only J=1 gave an acceptable fit, in agreement with results of Bissinger et al. (Bi68) and da Silva and Lisle (Si68). The population parameters were P(0) = (9±5)% at E_τ=6.0 MeV and P(0) = (37±3)% at E_τ=5.3 MeV.

The mixing ratio of the 2.0695→1.059 transition was studied through the angular distributions seen in the decay of the 2.547 MeV level. The 2.547→2.0695 transition was not considered and the 2.0695→1.059 and 1.059→0.229 transitions fitted simultaneously with P(0), P(1) and P(2) of the 2.0695 MeV level all allowed to vary. Spin sequence was assumed to be 2→1→0 in accordance with the spin assignments of Bissinger et al. (Bi68) and da Silva and Lisle (Si68). The mixing ratio solutions (Figure 11) are compatible with results of da Silva and Lisle (Si68).

f. The 2.367 MeV level

Branching ratios obtained in this work were in good agreement with recent particle-gamma coincidence measurements (Bi68 and Si68) and in disagreement with proton capture results (Ne62, Ho63 and Bi64). A summary of the results of previous work may be compared with the results of this experiment in Table 6.

Stripping reactions (Fu68 and We68) indicate an l_p=0 contribution, although the peak at 0^o is not as pronounced as in many other cases. Only spins J=2 and J=3 were tried in fitting of the gamma-ray

Table 6

Comparison of branching ratios for the 2.367 MeV state found in this work and in other work.

Final state	This work	Bi68	Si68	Ha68b	Ne62	Ho63	Bi64
0.418	25	35	29	70	50	50	29
1.059	20	20	18	30	50	50	
2.0687							17
2.0695	55	45	53				54

Fig. 11

χ^2 versus arctan of the mixing ratio for the 2.0695→1.059 transition in ^{26}Al.

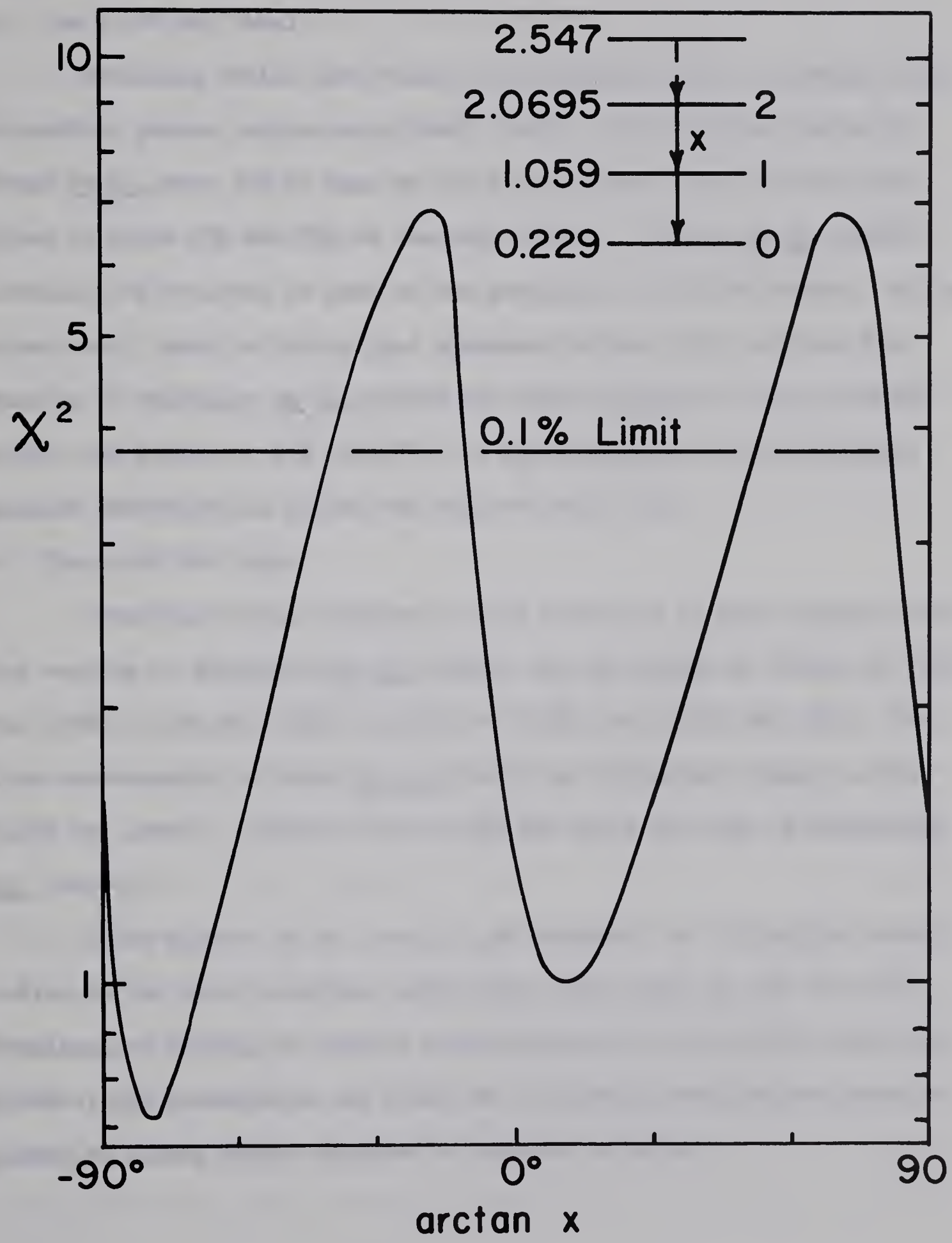

Fig. 11

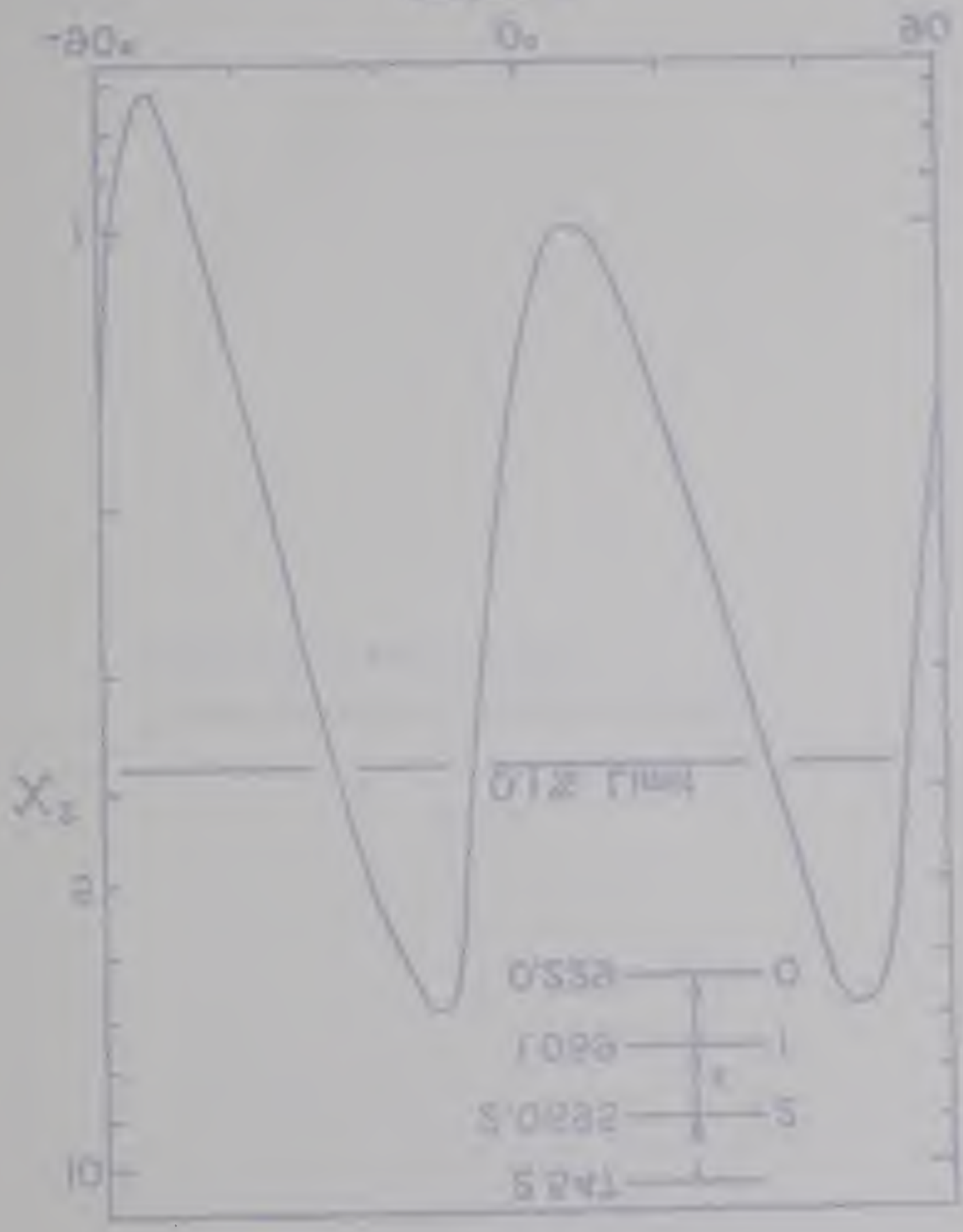
X_2

angular distributions.

g. The 2.547 MeV level

Branching ratios were found to be different from the values given by earlier proton capture work (Ne62, Bi64). The branching ratios of Neher et al. were 50% to each of the ground state and 0.418 MeV level, those of Bizot 25% and 75% to the same levels. Häusser et al. (Ha68b) obtained 50% branches to each of the ground and 1.059 MeV states. On the other hand, there is fairly good agreement between this work and the results of Bissinger et al. (Bi68) who found branches to the 0.418 and 2.0695 MeV levels of 15% and 85%. An $l_p=0$ component in the stripping angular distributions limits the spin to J=2 or J=3.

h. The 2.662 MeV level

Branching ratios obtained in this work were in good agreement with the results of Bissinger et al. (Bi68), who saw decays to levels at 0.418 MeV (70%), 1.059 MeV (15%), 2.0695 MeV (10%) and 2.0717 MeV (5%). Earlier measurements of Neher et al. (Ne62) had indicated a decay to the 1.059 MeV level. A decay to the 0.418 MeV state was seen by Häusser et al. (Ha68b).

There appears to be a small $l_p=0$ component to the angular distribution in the (d,n) reaction, which would limit spin to $J=2^+$ or $J=3^+$. Simultaneous fitting of angular distributions from the $2.662\rightarrow0.418$ and $2.662\rightarrow1.059$ transitions was tried but no further restrictions could be placed on mixing ratios obtained by separate fitting.

i. The 2.740 MeV level

This level was found to decay 100% to the 0.229 MeV state, confirming the results of Bissinger et al. (Bi68) and Häusser et al. (Ha68b). Work of Neher et al. (Ne62) had shown branching only to the 0.418 MeV level. It is not clear whether a level shown at 2.70 MeV by Bizot (Bi64) is the 2.662 MeV level or this one. The present work showed J=1 was the only spin to fit the angular distribution, also in agreement with Bissinger et al. Normalized χ^2 was 0.50 for J=1 and 33. for J=2. Population parameters were P(0) = (29±11)% at E_τ=6.0 MeV and P(0) = (38±3)% at E_τ=5.3 MeV. J=1 is consistent with the observation of a featureless, almost isotropic distribution of neutrons from the (d,n) reaction (Fu68).

j. The 2.915 MeV level

There is some disagreement among this work (Table 1), the work of Bissinger et al. (Bi 68) and that of da Silva and Lisle (Si68) concerning the weaker decay modes of the level. Bissinger et al. found a 30% branch to the 0.418 MeV level, 15% to the 2.0687 MeV level and 55% to the 2.0695 MeV state, while the results of da Silva and Lisle (Si68) showed a branch of (43±2)% to the 0.418 MeV level, < 10% to each of the 1.760 and 1.852 MeV states and (57±2)% to the 2.0695 MeV state. Häusser et al. (Ha68b) indicate decays to the 0.418 and 1.760 MeV states. The results obtained from work with a Ge(Li) detector in coincidence (Si68) should be more reliable than those taken with NaI(Tl) detectors. Branching ratios listed in this work were chosen as the ones which best

explained observed strengths of lower members of cascades in the decay of the level.

A strong $l_p=0$ component is seen in the stripping reactions (Fu68, We68) which restricts spins to $J=2^+$ or $J=3^+$. χ^2 versus mixing ratio for the 2.915→0.418 transition is presented in Figure 12. The 2.915 → 2.0695 transition was not used because it was not resolved from the subsequent 1.059→0.229 transition.

k. The 3.074 MeV level

The branching ratios of Bizot (Bi64)--40% decay to the 1.760 MeV level and 60% to the 2.07 MeV levels--are not supported by present results. Present work is in fair agreement with that of Bissinger *et al.* (Bi68), who saw a 100% branch to the 2.0695 MeV level.

Neutrons from the (d,n) reaction (Fu68) showed no stripping pattern. The unresolved doublet in the gamma-ray spectrum (from the 3.074→2.0695 and 2.0695→1.059 transitions) would have complicated χ^2 fitting of the angular distributions. Additional uncertainties introduced by partial overlap with the 3.159 MeV level (see Figures 5 and 6) made doublet fitting a pointless exercise.

l. The 3.159 MeV level

Neher *et al.* (Ne62) found a decay to the 0.418 MeV state (> 80%) and possible branches (< 20%) to the 1.059 and 2.07 MeV states. Bizot (Bi64) observed decay to the 0.418, 1.059, 1.760 and 2.07 MeV states of 55%, 26%, 12% and 7%; this is in good agreement with the results of Bissinger *et al.* (Bi68) and the results of this study.

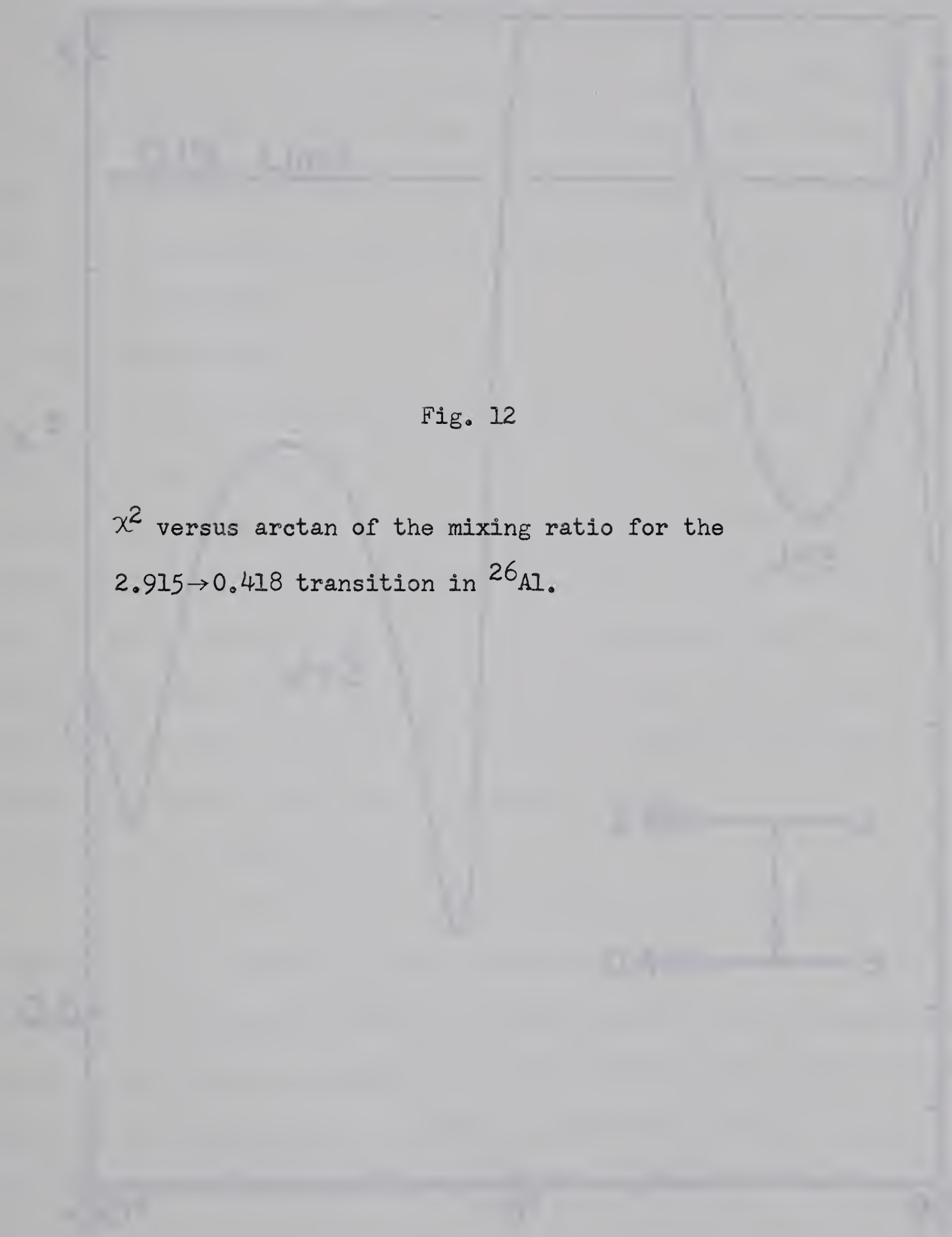

Fig. 12

χ^2 versus arctan of the mixing ratio for the 2.915→0.418 transition in ^{26}Al.

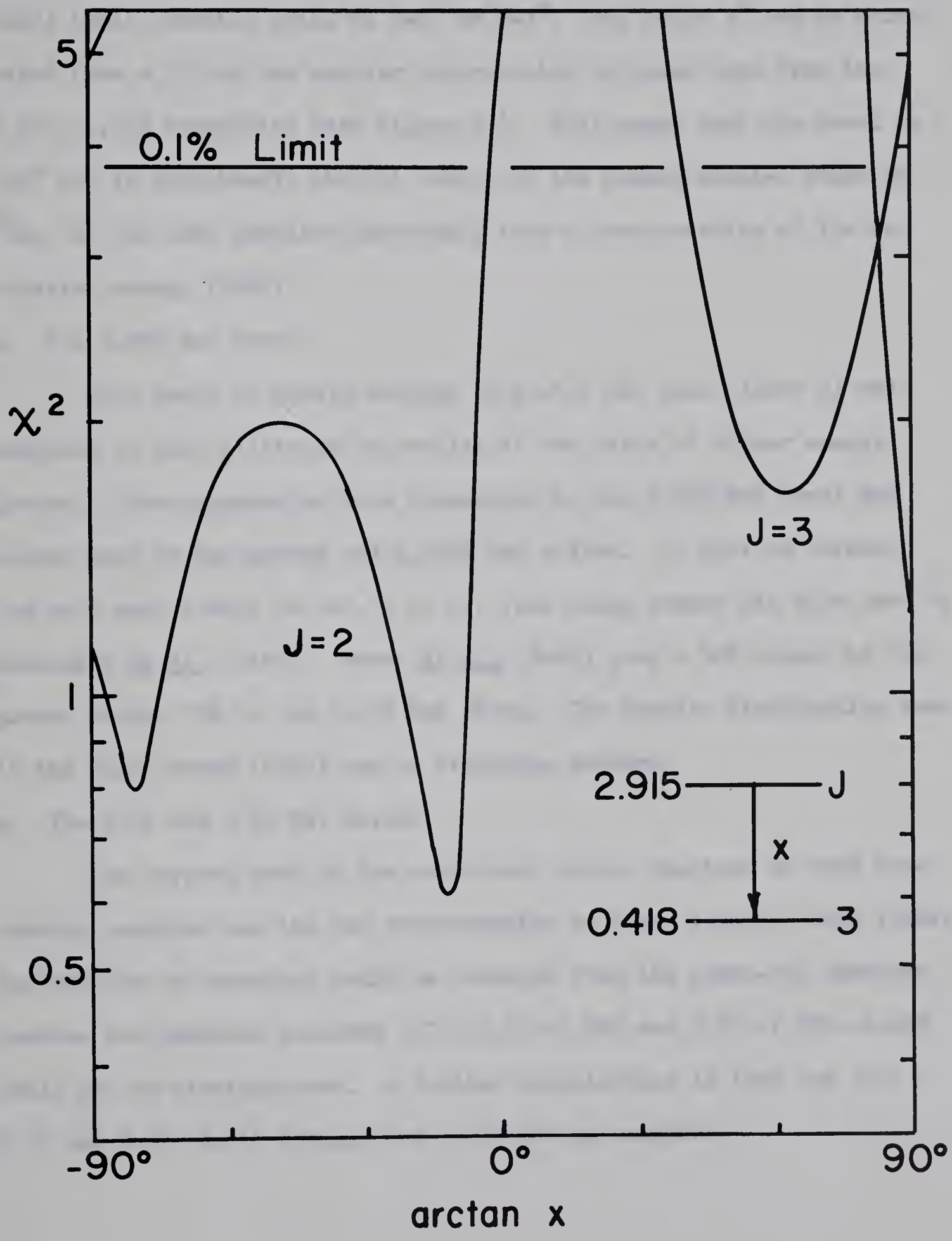

12

Results of the single-particle stripping reactions (Fu68 and We68) limit possible spins to $J=2^+$ or $J=3^+$. The value 3^+ can be eliminated from a fit of the angular distribution of gamma rays from the 3.159→1.059 transition (see Figure 13). This means that the level is $J=2^+$ and is undoubtedly the T=1 analog of the second excited state in ^{26}Mg, as had been surmised previously from a consideration of its excitation energy (En67).

m. The 3.405 MeV level

This level is weakly excited at $E_p=6.0$ MeV (see Figure 6) and analysis is made difficult by overlap of the tails of higher energy groups. There appears to be a transition to the 0.418 MeV level and weaker ones to the ground and 2.0695 MeV states. If this is correct, the spin most likely is J=3, 4 or 5. This decay scheme was also seen by Bissinger et al. (Bi68). Neher et al. (Ne62) give a 30% branch to the ground state, 70% to the 0.418 MeV state. The angular distribution seen in the (d,n) study (Fu68) has no stripping pattern.

n. The 3.72 and 3.75 MeV levels

The largest peak in the coincident proton spectrum at both bombarding energies was the one corresponding to these levels. Very little information on branching could be obtained from the gamma-ray spectrum because the possible cascades 3.72→2.07→0.229 and 3.72→1.852→0.229 could not be distinguished. A further complication is that the 3.72→2.07 and 2.07→0.418 transitions could not be resolved.

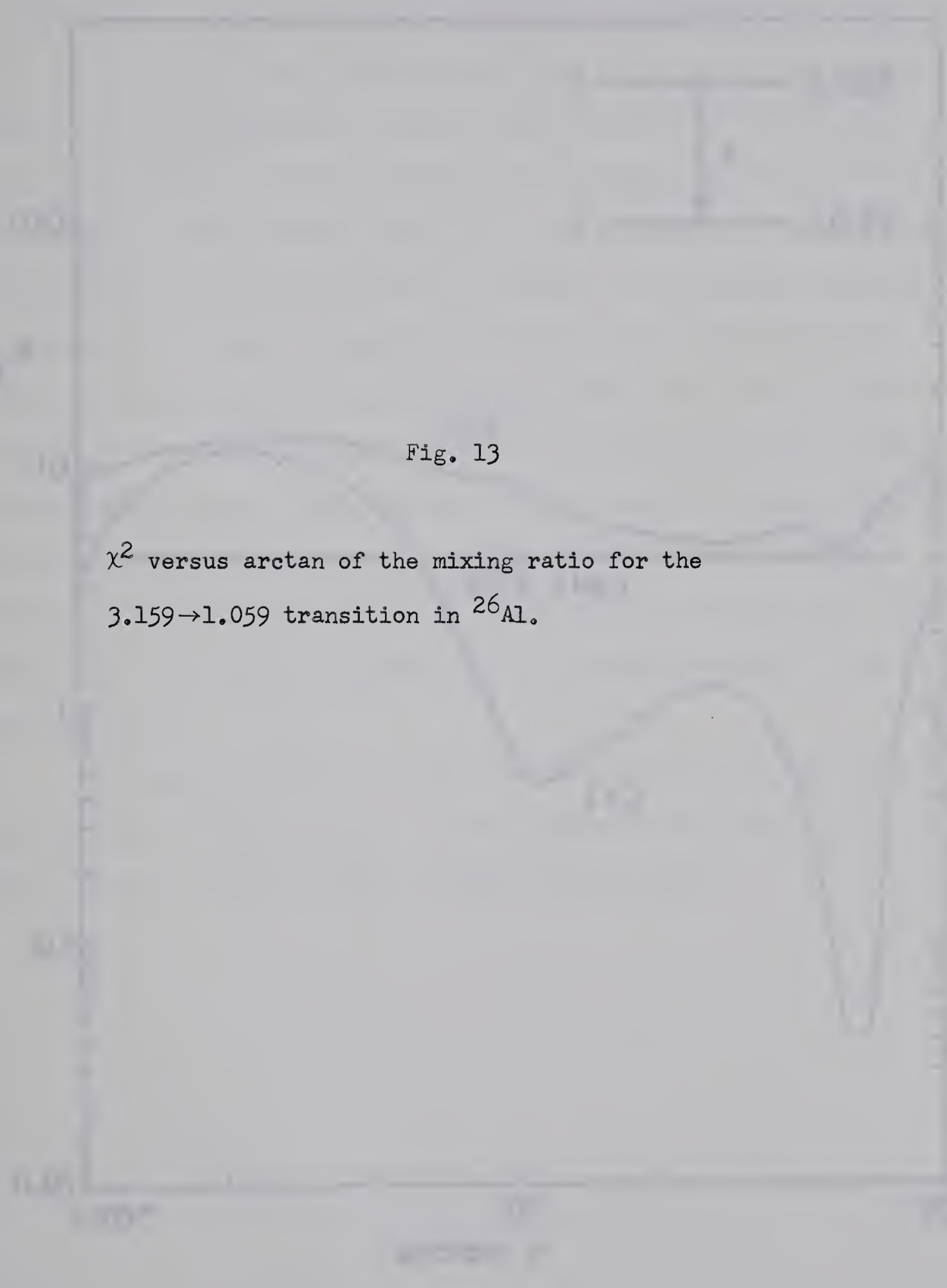

Fig. 13

χ^2 versus arctan of the mixing ratio for the 3.159→1.059 transition in ^{26}Al.

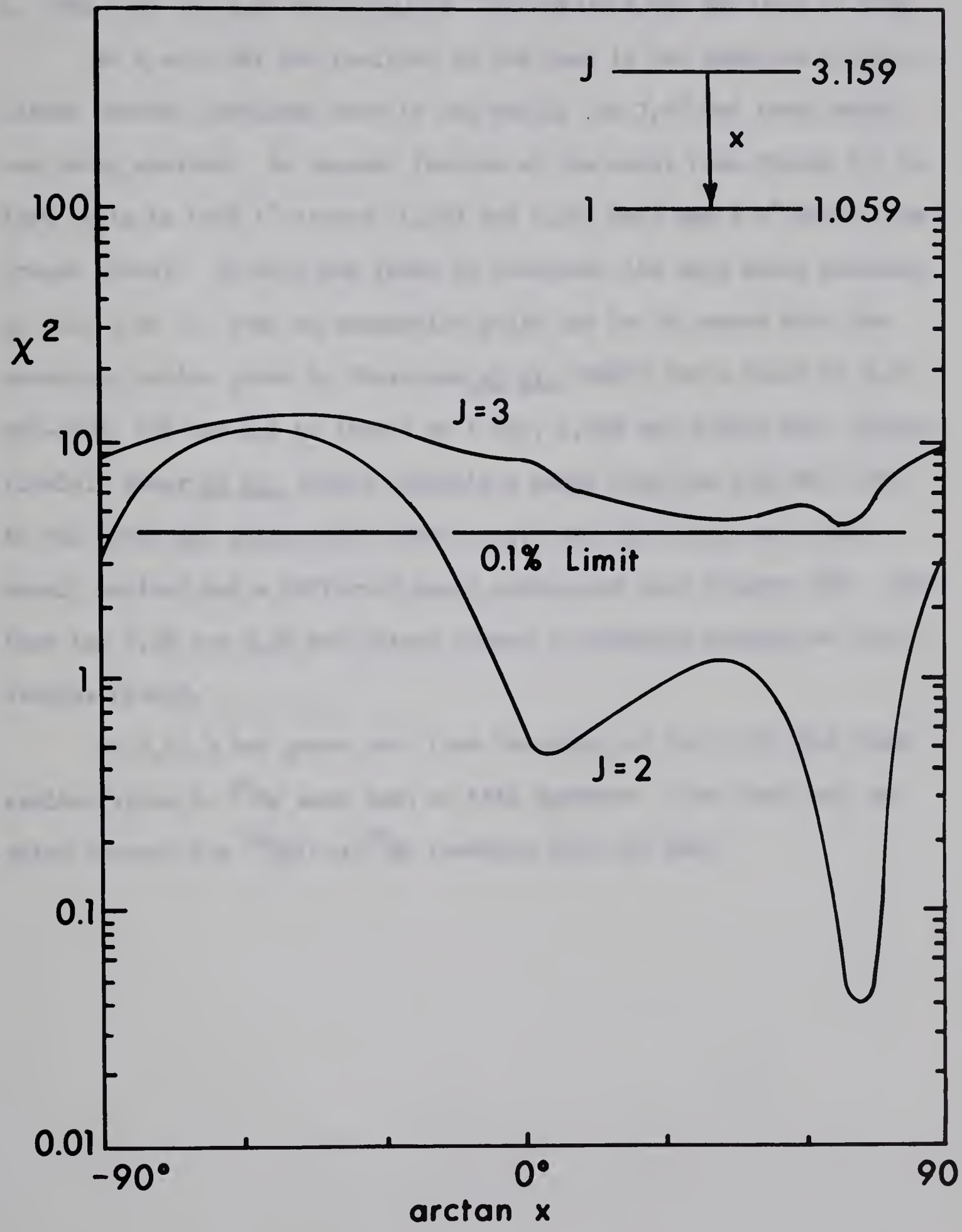
J
3.159
x
1
1.059
100
χ^2
J=3
10
0.1% Limit
1
J=2
0.1
0.01
-90°
0°
90
arctan x

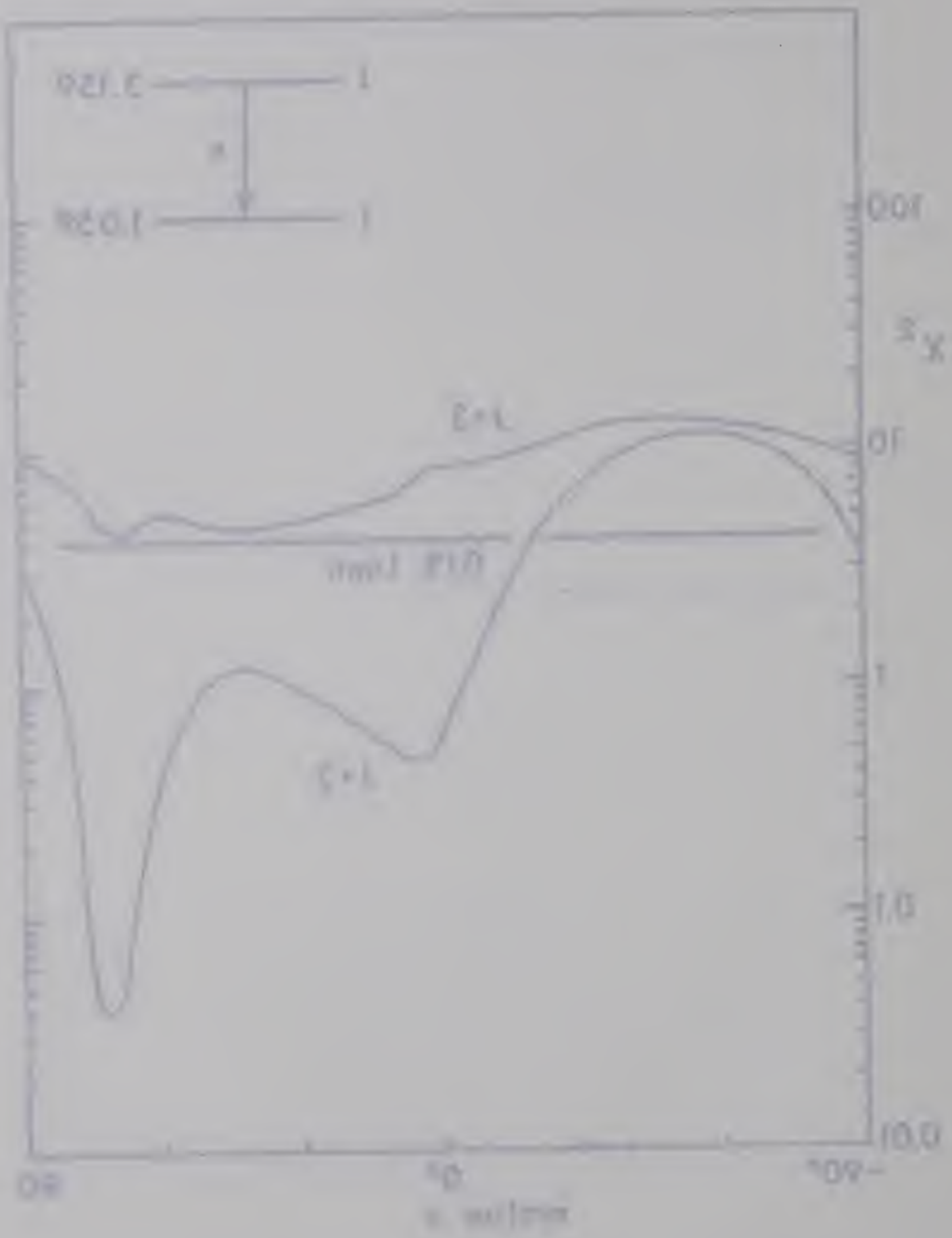

o. The 3.92 and 3.96 MeV levels of ^{26}Al and the 0.451 MeV level of ^{23}Mg

At E_τ=6.0 MeV the position of the peak in the spectrum of coincident protons indicated that it was mainly the 3.96 MeV level which was being excited. An unusual feature of the decay (see Figure 15) is that it is to both 1^+ states (1.059 and 1.852 MeV) and a 5^+ state (the ground state). If only one level is involved, its spin would probably be J=2, 3 or 4. Such an assumption would not be in accord with the branching ratios given by Bissinger et al. (Bi68) for a level at 3.96 MeV--40%, 45% and 15% to levels at 1.059, 1,852 and 2.0695 MeV, respectively. Neher et al. (Ne62) indicate a decay from the 3.96 MeV level to the 0.418 MeV state only. When E_τ=5.3 MeV the levels were more weakly excited and a different decay scheme was seen (Figure 14). Neither the 3.92 nor 3.96 MeV states showed a stripping pattern in (d,n) studies (Fu68).

At E_τ=5.3 MeV gamma rays from the decay of the 0.451 MeV first excited state in ^{23}Mg were seen in this spectrum. The level was excited through the $^{24}Mg(\tau,\alpha)^{23}Mg$ reaction (Q=4.046 MeV).

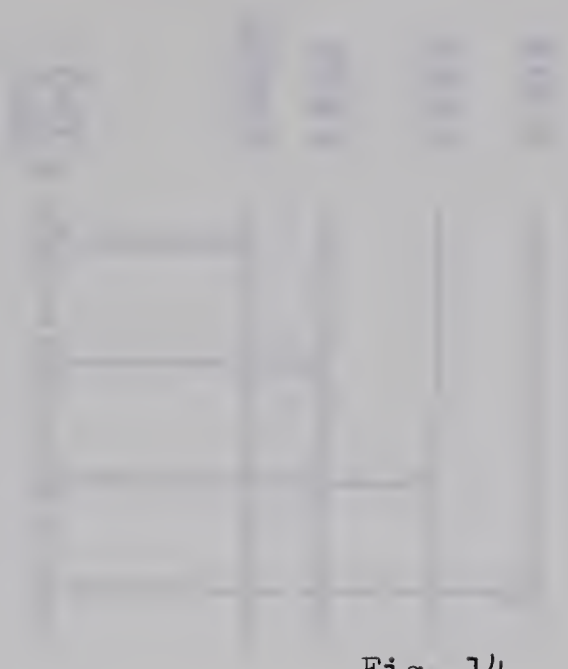

Fig. 14

Gamma rays seen in coincidence with protons associated with the levels at 3.92-3.96 MeV in ^{26}Al at an angle of 55° for bombarding energy 5.3 MeV. The lower spectrum represents the contribution of random coincidences.

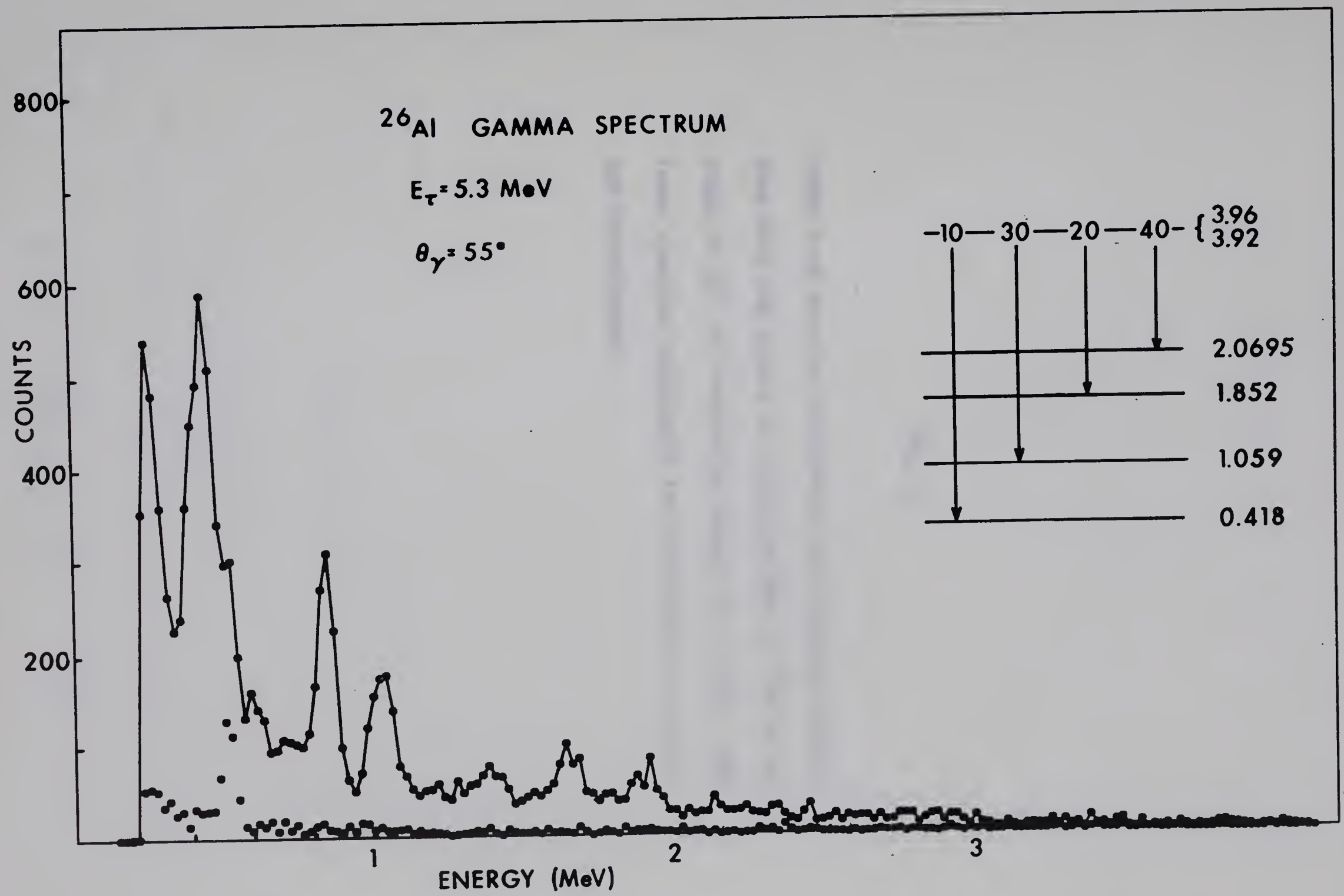
^{26}Al GAMMA SPECTRUM
E_τ = 5.3 MeV
θ_γ = 55°
800
600
400
200
COUNTS
1
2
3
ENERGY (MeV)
-1-
-0-
-2-
-4-
3.96
3.92
2.0695
1.852
1.059
0.418

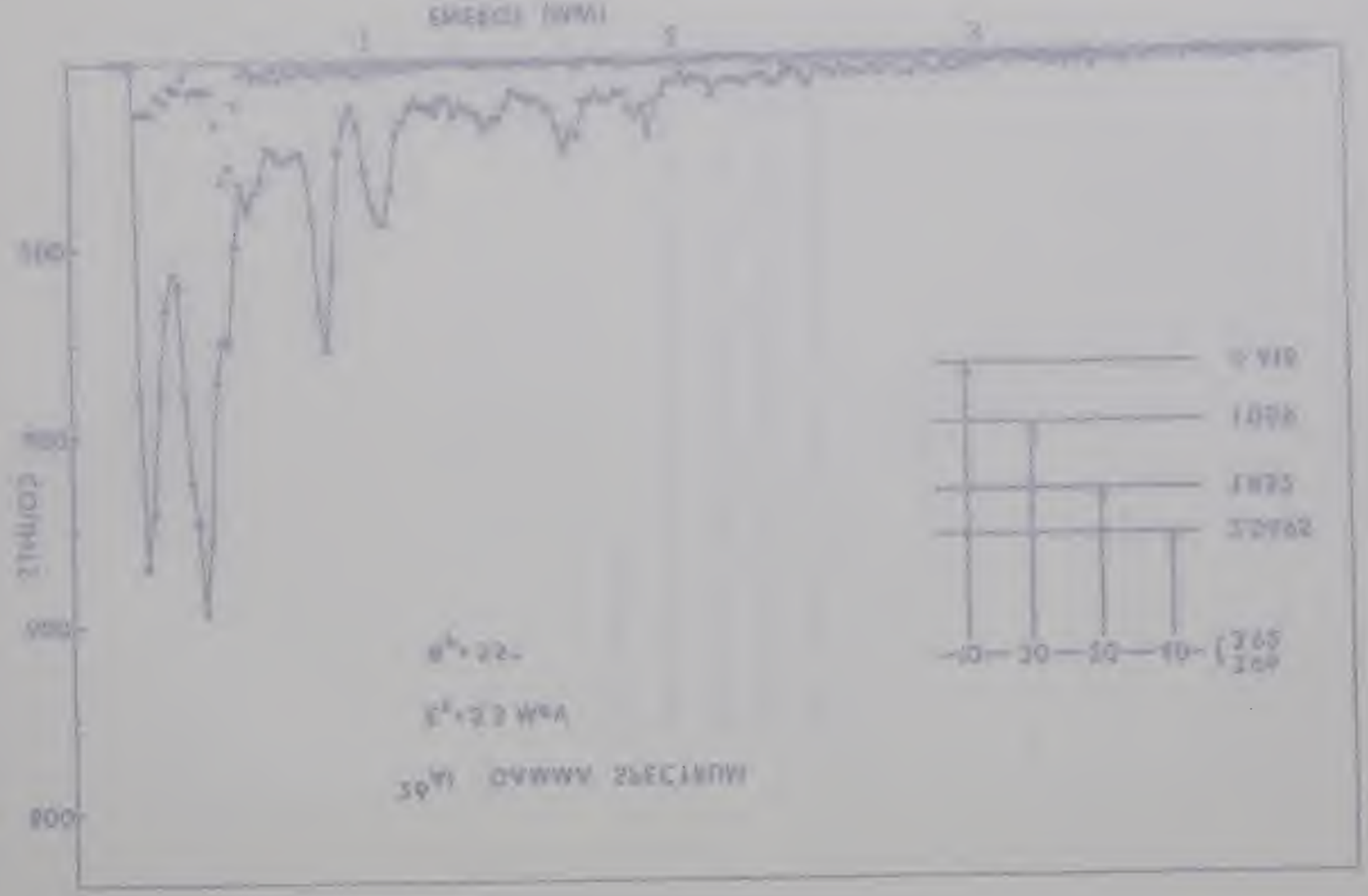

Fig. 15

Gamma rays seen in coincidence with protons associated with the levels at 3.92-3.96 MeV in ^{26}Al at an angle of 55° for bombarding energy at 6.0 MeV. The lower spectrum represents the contribution of random coincidences.

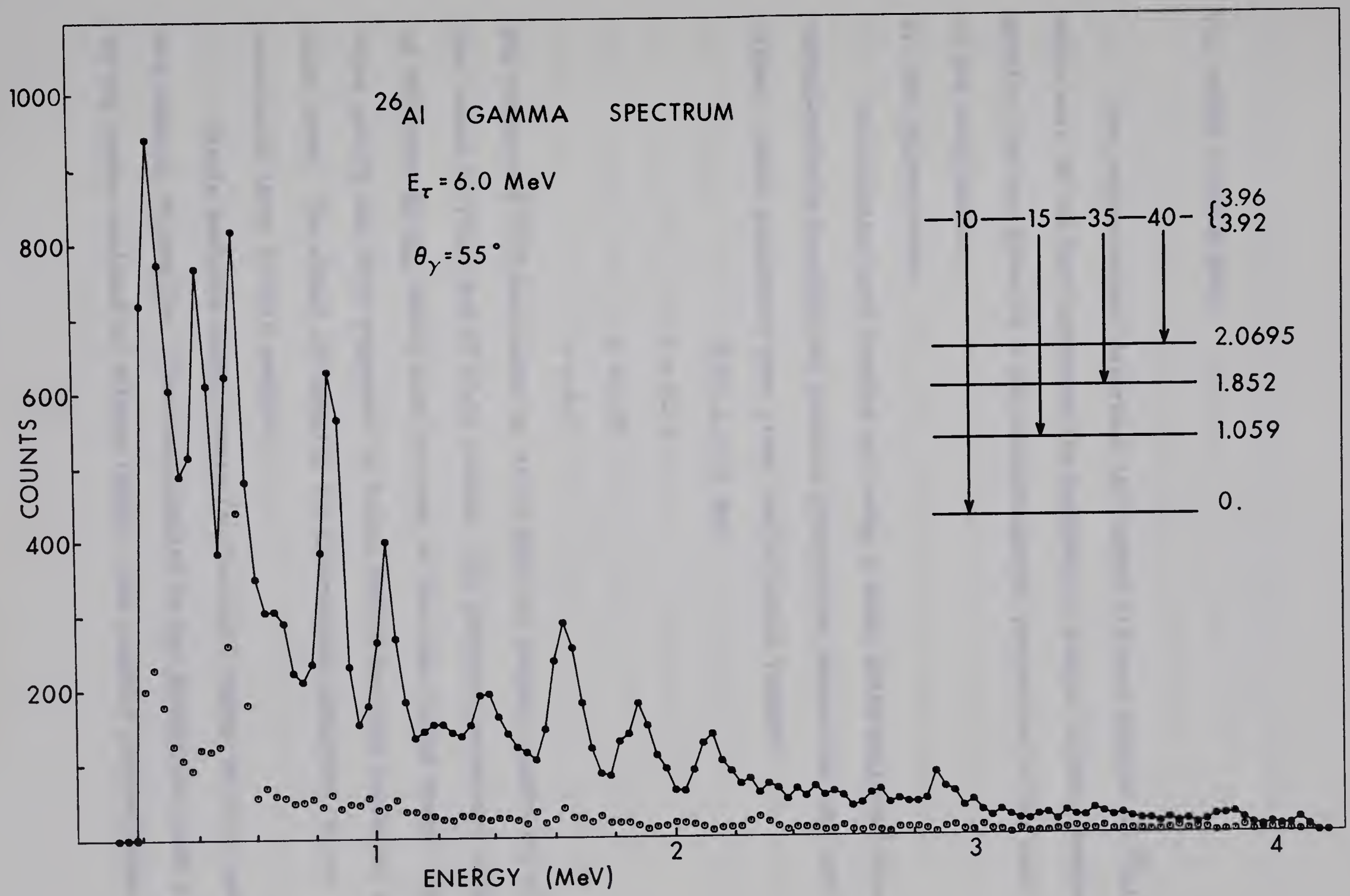
^{26}Al GAMMA SPECTRUM
E_τ = 6.0 MeV
θ_γ = 55°
1000
800
600
400
200
COUNTS
1
2
3
4
ENERGY (MeV)
10
15
35
40
3.96
3.92
2.0695
1.852
1.059
0.

Fig 15

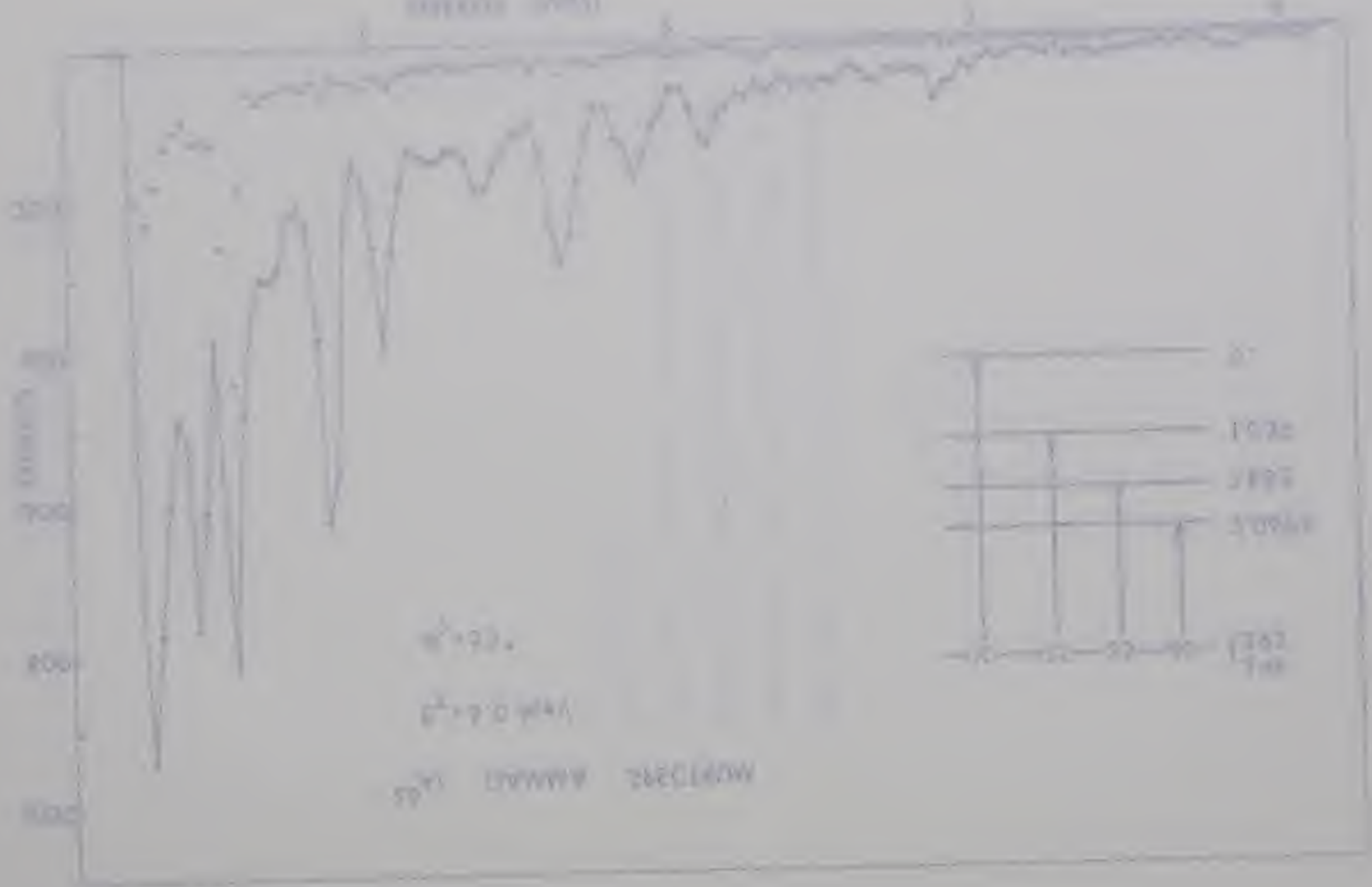

VI. MODEL CALCULATIONS

The nuclear models described in Chapter III were applied to ^{26}Al. While most of the work concerned the energies of excited states, consideration also was given to a few electromagnetic properties in the case of the shell model.

a. The Nilsson model

Calculations were carried out using a model which neglected rotational-particle coupling and residual interaction between the odd particles. Model parameters were given the following values:

$$\hbar^2/2I = 0.31 \text{ MeV}$$

$$\kappa = 0.13$$

$$\mu = 0.33$$

$$\delta = 0.2.$$

The value of $\hbar^2/2I$ was chosen so as to give the correct separation of the lowest 0^+ (T=1) and 2^+ (T=1) states. The particle parameters adopted by Weidinger *et al.* (We68) were the same as the ones listed above. The value μ=0.33 was first suggested by Bishop (Bi60) for this region of nuclear mass. The effect of changing the deformation parameter, δ, is considered later in this section.

Single particle energy levels for the above values of κ, μ, and δ are shown in Figure 16a. They are labelled by the projection Ω and also by the number assigned by Nilsson (Ni55). The computer program which

calculated the eigenvalues of the particle Hamiltonian also supplied the eigenstates in $|1\Lambda\Sigma\rangle$ representation or $|1j\Omega\rangle$ representation.

In a calculation of the total energy of the nucleus, including interaction of particles in Nilsson orbits (Pr62, page 271), an approximation for the contribution of each particle is $3/4E_p - 1/4\langle C\ \vec{l}\cdot\vec{s} + D\ \vec{l}^2\rangle$ where E_p is an eigenvalue of the Hamiltonian defined in equation (III.2). Total energy of the nucleus was taken to be the sum of rotational and particle energies where particle energies were calculated from this expression. Energy differences between different particle configurations were taken to be the differences in total energies rather than the differences in energies E_p. (It has been suggested (Ma63) that the interactions need be considered only when calculating total energies, not when determining energy differences. The principle effect is a change of energy scale and may be simulated by a suitable change of parameters K, μ and δ for levels within a shell. A change in the expression used for particle energy would increase the separation of band heads unless some adjustment was made in K.) The spectrum of states of $H_p + H_{rot}$ with excitation energy below 5 MeV appears in Figure 16b.

Several shortcomings can be seen in the spectrum so obtained. The 5^+ state is 1.5 MeV above the 0^+ (T=1) state instead of 0.2 MeV below it, there is no 3^+ state below 3.5 MeV and there are only 7 excited states below 4 MeV excitation instead of about 20. The first defect might be remedied by the inclusion of H_{res} and H_{rpc}. Kelson (Ke64) found that residual interaction should lower the J=5, K=5 state

Fig. 16

(a) Single-particle Nilsson model energies in the N=2 shell for δ=0.2, κ=0.13 and μ=0.33. (b) Energy levels in ^{26}Al as predicted by Nilsson model for odd-odd nuclei using the single particle energies in (a). Inertial parameter $\hbar^2/2\mathcal{I} \simeq 0.31$ MeV.

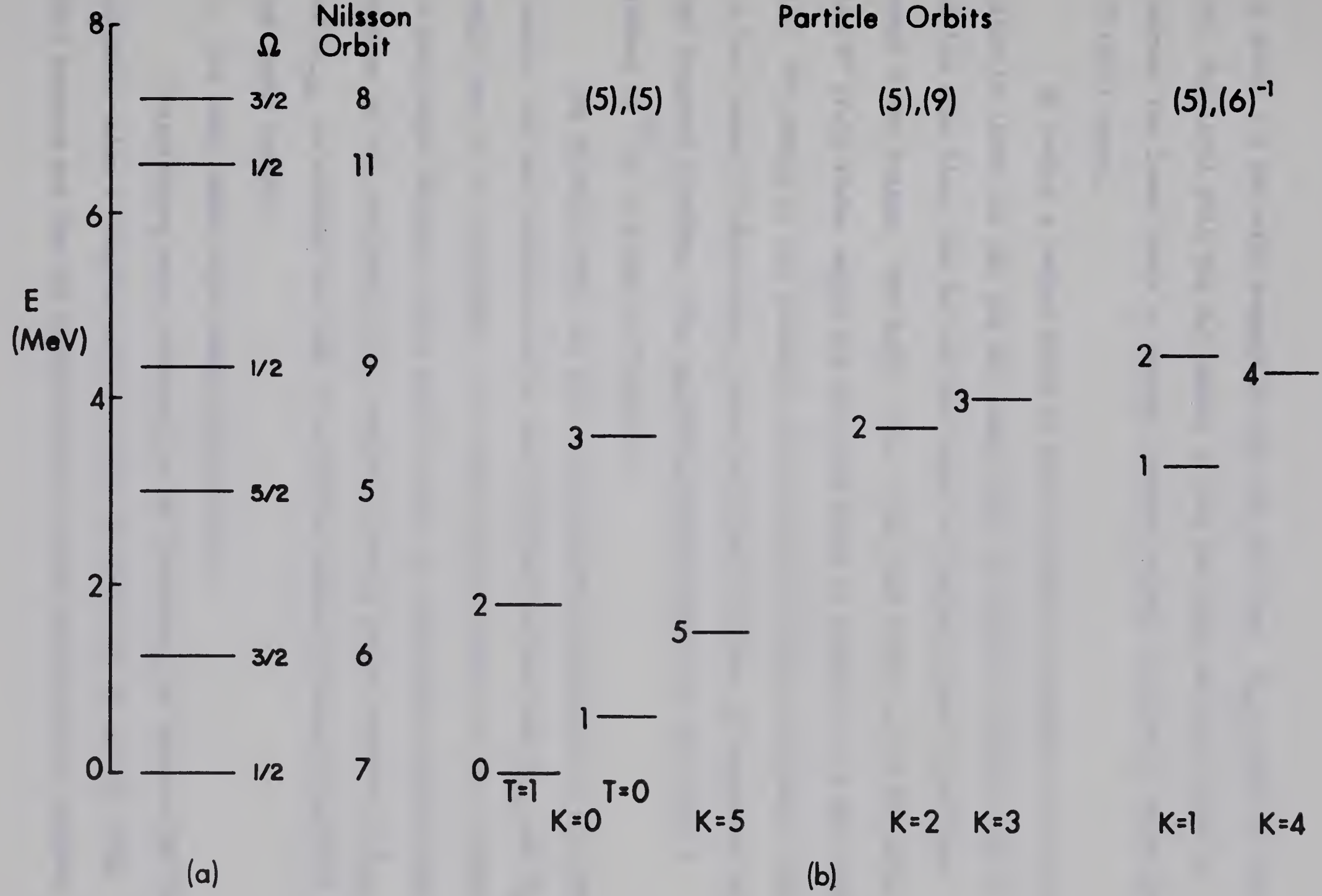
Nilsson Orbit
Ω
3/2
1/2
1/2
5/2
3/2
1/2
8
11
9
5
6
7
E (MeV)
8
6
4
2
0
(5),(5)
(5),(9)
(5),(6)⁻¹
Particle Orbits
T=1
T=0
K=0
K=5
K=2
K=3
K=1
K=4
(a)
(b)

Fig. 16

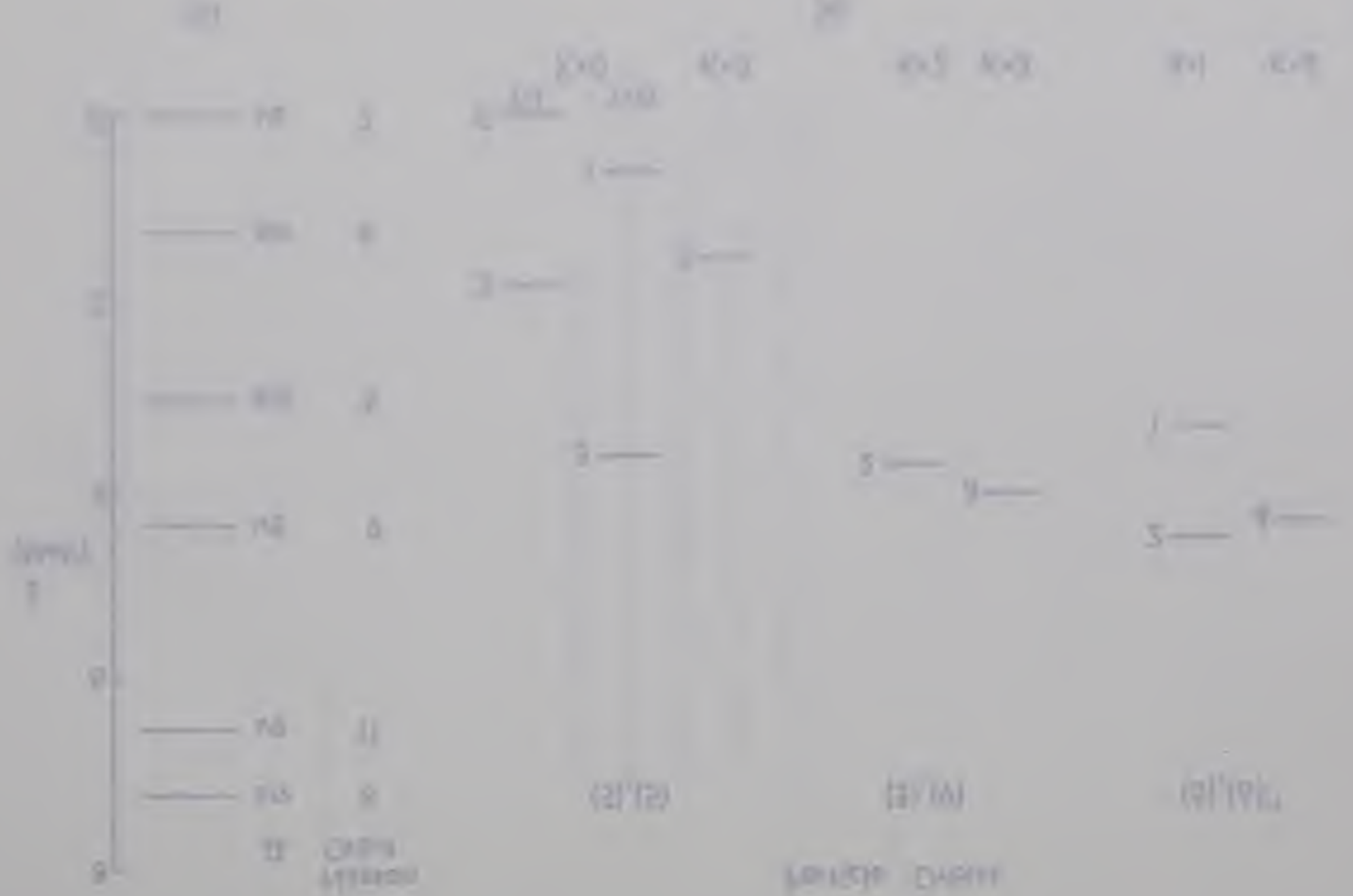

by about 1.3 MeV with respect to the J=0, K=0 one. H_{rpc} would mix the J=5, K=5 level with the J=5 member of the K=4 band and would tend to depress the lower state in energy, perhaps enough to place it below the 0^+ (T=1) state.

By taking a larger value of the deformation parameter, it is possible to lower the K=2 and K=3 bands built on particle orbits 5 and 9. At the same time, the K=1 and K=4 bands of particle orbit 5 and hole orbit 6 are raised. For δ=0.3 the J=2, K=2 level is 2.4 MeV above the 0^+ (T=1) state, while the J=1, K=1 state is raised to 4.3 MeV above it. RPC mixing of J=3 states in the K=2 and K=3 bands could well result in the lowest 3^+ state being below the first 2^+ state, in agreement with the observed spectrum. The suggested identification of the first 5 states in ^{26}Al is given in Figure 17.

The Nilsson model can give a qualitative description of the lower levels, but more precise work is very difficult since both H_{res} and H_{rpc} would have to be considered. The rather simple picture of two nucleons in particular Nilsson orbits would be lost in band-mixing calculations. Because of the complexity of a treatment taking proper account of H_{res} and H_{rpc}, no attempt was made to calculate gamma-ray decay properties of the lower levels.

b. The shell model with mixed configurations

Calculations were performed on the University of Alberta IBM 360 computer using a program which was made available by Dr. S.S.M. Wong. This program was the Oak Ridge-Rochester mixed configurations program

Fig. 17

Predictions of the odd-odd Nilsson model for $\delta=0.3$ compared to the observed spectrum.

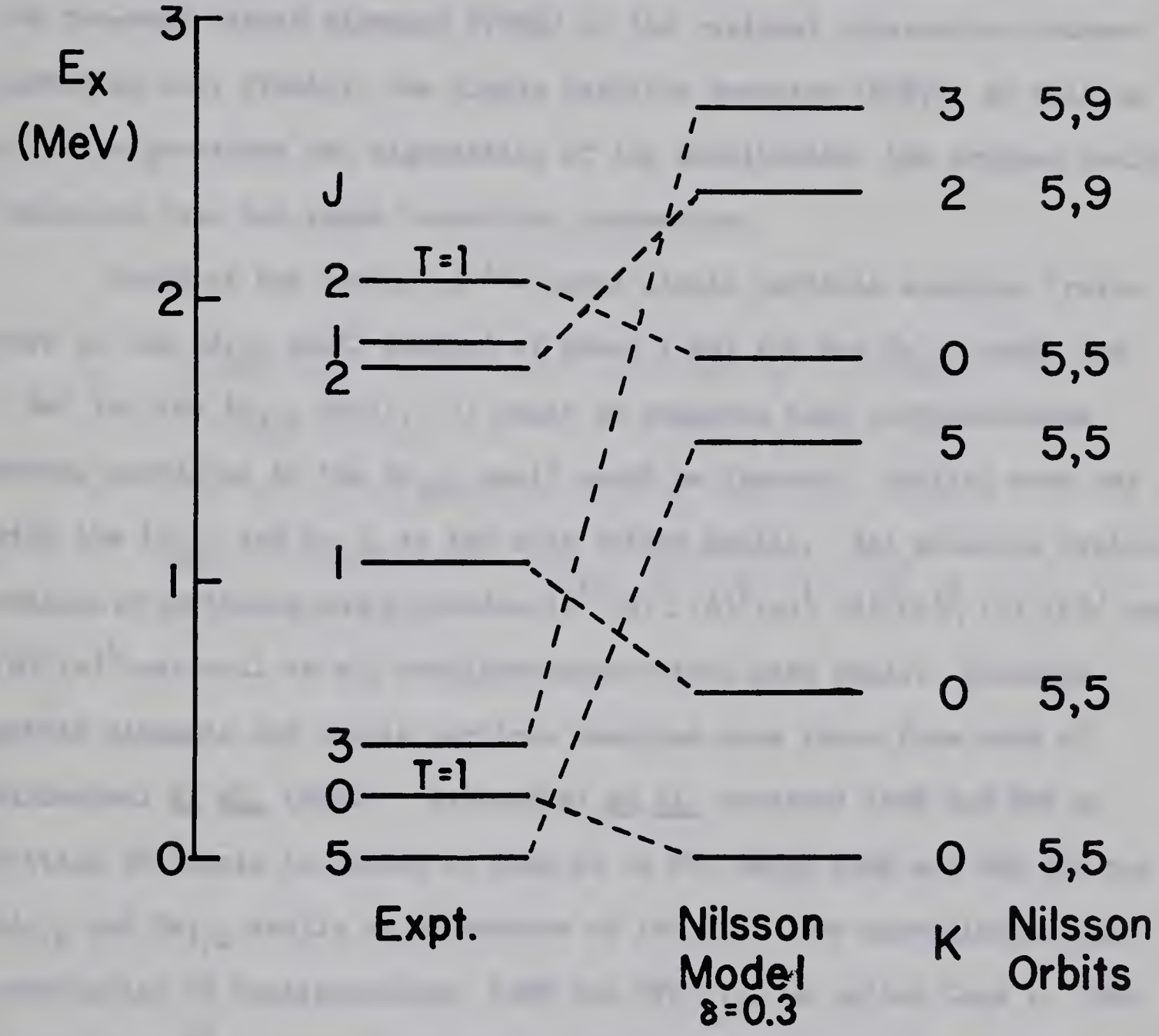
3
2
1
0
E_x
(MeV)
J
T=1
2
1
2
1
3
T=1
0
5
3
2
1
0
5
0
5,9
5,9
5,5
5,5
5,5
Expt.
Nilsson
Model
δ=0.3
K
Nilsson
Orbits

17

3
2
1
0
E*
(MeV)
4+
2+
0+
3-
2+
1-
0+

(Fr68). It could treat cases with as many as 6 active shells and diagonalize a Hamiltonian of up to 230 basis states. The user specified the distribution of particles among the active shells, the permitted configurations within a shell according to the classification of Flowers (Fl52), the two-body matrix elements (TBME) of the residual interaction between particles and, finally, the single particle energies (SPE). As well as giving eigenvalues and eigenstates of the Hamiltonian, the program could calculate beta and gamma transition properties.

Study of the levels of ^{17}O gives single particle energies (relative to the $1d_{5/2}$ shell energy) of about 1 MeV for the $2s_{1/2}$ shell and 5 MeV for the $1d_{3/2}$ shell. It might be expected that configurations having particles in the $1d_{3/2}$ shell could be ignored. Initial work was with the $1d_{5/2}$ and $2s_{1/2}$ as the only active shells. All possible distributions of particles were allowed—$(d)^{10}(s)^{0}$, $(d)^{9}(s)^{1}$, $(d)^{8}(s)^{2}$, $(d)^{7}(s)^{3}$ and $(d)^{6}(s)^{4}$—as well as all configurations within each shell. Two-body matrix elements and single particle energies were taken from work of Wildenthal *et al.* (Wi68). Wildenthal *et al.* obtained TBME and SPE by fitting 80 levels in nuclei of mass 20 to 28, using TBME and SPE for the $1d_{5/2}$ and $2s_{1/2}$ shells as parameters of the fit. For convenience, this combination of configurations, TBME and SPE will be called Case 1. The spectrum of ^{26}Al obtained by doing a mixed configuration calculation is shown in Figure 18a. This is clearly an unacceptable result, indicating the need to include the $1d_{3/2}$ shell as an active shell for calculations on this nucleus.

Fig. 18

Three cases of shell model calculations compared to the observed spectrum. (a) Single particle energies and matrix elements of Wi68, (b) S.P.E. and M.E. of Ku67 and (c) M.E. of Ku67 and adjusted S.P.E. (see text).

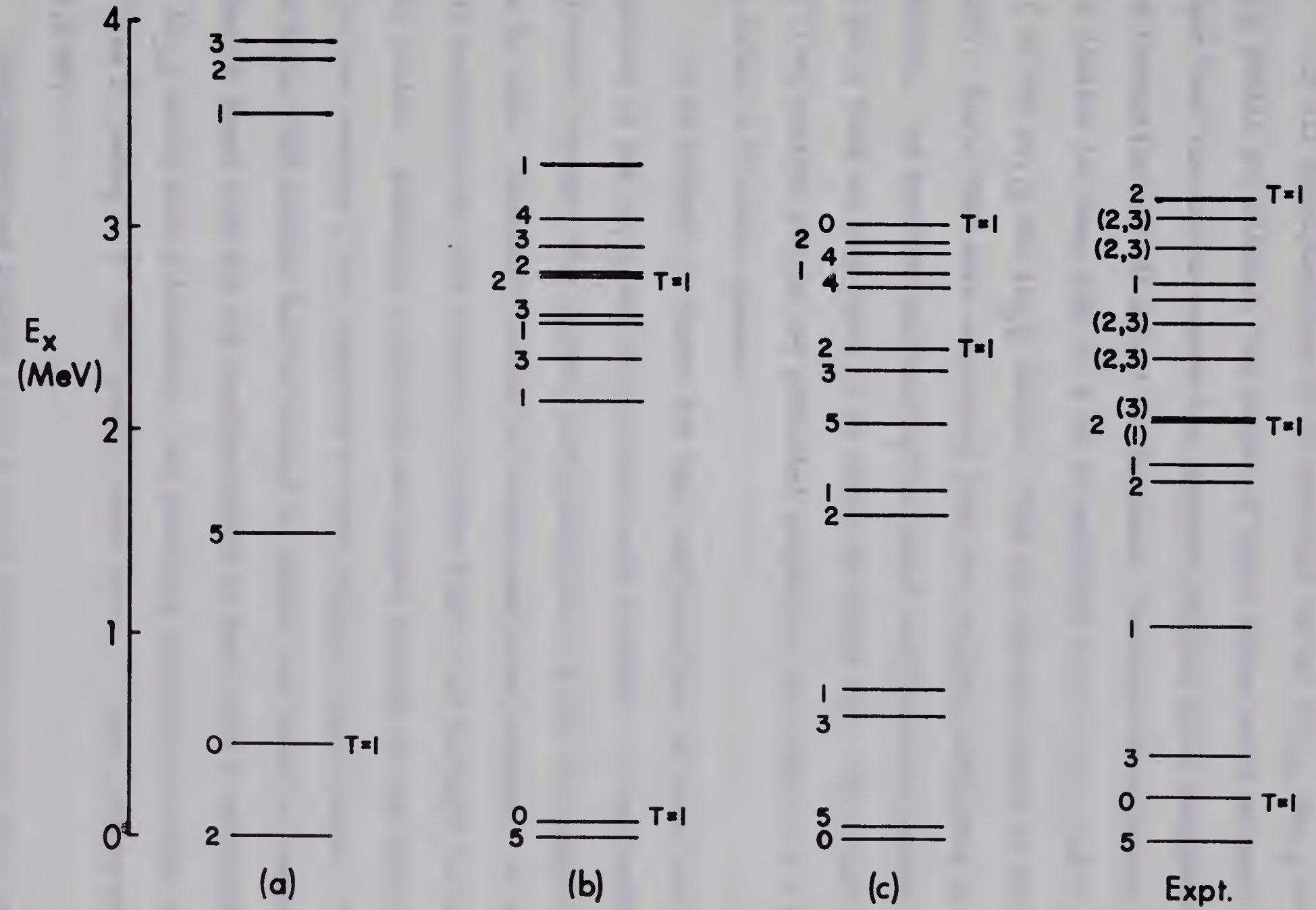
4
3
2
1
0
E_x (MeV)
3
2
1
5
0 T=1
2
(a)
1
4
3
2 T=1
3
1
3
1
0 T=1
5
(b)
2 0 T=1
4
1 4
2 T=1
3
5
1
2
1
3
5
0
(c)
2 T=1
(2,3)
(2,3)
1
(2,3)
(2,3)
2 (3) T=1
(1)
1
2
1
3
0 T=1
5
Expt.

Fig. 18

If all configurations of 10 particles in the $1d_{5/2}$, $2s_{1/2}$ and $1d_{3/2}$ shells are allowed, the number of basis states would be much larger than the maximum number the computer program could diagonalize. Some truncation procedure must be followed. Particle distributions were limited to those with 8, 9 or 10 particles in the $1d_{5/2}$ and 2, 1 or 0 in the $2s_{1/2}$ and $1d_{3/2}$ shells. TBME and SPE were those of Kuo (Ku67). Kuo's TBME were calculated from free-nucleon scattering potentials. The spectrum produced by the mixed configuration program for Kuo's TBME and SPE (Case 2) is shown in Figure 18b. The ground and first excited states are predicted correctly, but there is a 2 MeV gap before a 1^+ state appears.

In an attempt to remove the gap, configurations of more than 2 particles in the $2s_{1/2}$ and $1d_{3/2}$ shells were included. It was necessary to further truncate the allowed configurations to allow the computer program to work. Seniority truncation within shells was adopted. No single-shell configuration with seniority greater than 3 was included in the basis states. Seniority truncation was chosen because it was easy to apply, not because it was expected to have physical significance. For some spins this measure was not enough to reduce the number of basis states to fewer than 230 and configurations of more than 2 particles in the $1d_{3/2}$ shell were eliminated. The resulting spectrum was worse than for Case 2, having a 0^+ (T=1) ground state and a 5^+ first excited state at 2.6 MeV.

Configurations limited to 8, 9 or 10 particles in the $1d_{5/2}$ shell

were again considered. In order to reduce the gap between the first and second excited states, the single particle energies were varied. Kuo's SPE for the $2s_{1/2}$ and $1d_{3/2}$ shells were 0.87 and 5.08 MeV, respectively, higher than that of the $1d_{5/2}$ shell. Values of 0.25 and 2.5 MeV for SPE of the $2s_{1/2}$ and $1d_{3/2}$ shells gave the spectrum shown in Figure 18c (Case 3). All the levels below 2 MeV are predicted to within 200 keV (except the 1^+ at 1.059 MeV which is within 300 keV). Above 2 MeV the model predicts a 5^+ level which does not correspond to any known level and the third T=1 state is predicted to be J=0 rather than J=2. The density of levels is close to that which has been seen experimentally.

It is not clear how much trust should be placed in wave functions obtained with adjusted SPE. A separation of the $1d_{3/2}$ and $1d_{5/2}$ shells of only 2.5 MeV is much lower than is customarily used. Possibly the smaller spin-orbit splitting compensates for errors due to the severe truncation of basis states. If such is the case, it would be expected that different SPE would be needed for a different nucleus or for a different set of basis states. In this regard it is interesting to note that Bouten et al. (Bo67), who had only the $1d_{5/2}$ as an active shell, achieved a good fit for ^{26}Al only with an anomalously high separation of $1d_{3/2}$ and $1d_{5/2}$ states—14 MeV. The wave functions resulting from working with a truncated set of basis states may or may not adequately describe properties other than excitation energies: this must be determined for each property by doing appropriate calculations.

Some information about the composition of the wave functions of

Case 3 is given in Table 7. The strengths represent the sums of squares of coefficients of all basis states having a particular distribution of nucleons among active shells; to give coefficients for the complete set of basis states individually would have meant from 35 terms (for J=0, T=1) to 119 terms (for J=2, T=1).

The striking feature of Table 7 is that the predominant configurations have 8 nucleons in the $1d_{5/2}$ shell and 2 in the $1d_{3/2}$. It would have been expected that the (10,0,0) configuration would be more important, since the sum of SPE is 5 MeV less than for the (8,0,2) configuration. This result is not simply a consequence of adjusting SPE. For Case 2 the strength of the (10,0,0) distribution is only 0.362 for J=5 and 0.358 for J=0, (T=1).

It has been argued (Ta60b) that the spectrum of ^{18}F is an indication that the ground and first 2 excited states in ^{26}Al are well described by a configuration of 10 nucleons in the $1d_{5/2}$ shell. Such a configuration is equivalent to 2 holes in a filled $1d_{5/2}$ shell and should give states similar to those in ^{18}F, which should consist of two particles in the $1d_{5/2}$ shell. The lowest positive parity states in ^{18}F are J=1 (ground), J=3 (0.94 MeV), J=0, T=1 (1.045 MeV), J=5 (1.125 MeV) and J=1 (1.70 MeV). Talmi and Unna (Ta60b) argued that there was fairly close correspondence between the levels of spins 3, 0 and 5 in ^{26}Al and those in ^{18}F, indicating that these states in ^{26}Al were two-hole states, while the spin 1 states must have admixtures of other configurations. The wave functions obtained in Case 3 provide a counter

Table 7

Strengths of various particle distributions obtained with SPE of 0.25 MeV and 2.5 MeV, ME of Kuo. The labels give the number of particles in each of the $1d_{5/2}$, $2s_{1/2}$ and $1d_{3/2}$ shells, respectively.

J;T	E_x	Particle Distribution					
	(MeV)	10,0,0	9,0,1	9,1,0	8,0,2	8,1,1	8,2,0
0;1	0.0	0.263	0.000	0.000	0.634	0.054	0.048
5;0	0.07	0.260	0.002	0.004	0.603	0.086	0.045
3;0	0.60	0.005	0.001	0.000	0.836	0.151	0.007
1;0	0.73	0.000	0.003	0.000	0.646	0.330	0.020
2;0	1.60		0.013	0.001	0.702	0.275	0.010
1;0	1.73	0.081	0.005	0.001	0.567	0.297	0.049
2;1	2.42	0.150	0.003	0.002	0.690	0.111	0.044

example, demonstrating that it is possible to obtain the energy spectrum with other configurations.

The results summarized in Table 7 suggest that some caution is necessary if properties of excited states are inferred by comparison with the ground state. For example, spectroscopic factors were obtained for the ground state and some excited states for the reaction $^{27}Al(\tau,\alpha)^{26}Al$ (Nu68). The ratios of excited state spectroscopic factors to ground state spectroscopic factor (relative spectroscopic factors) were the same as those calculated assuming a configuration of 10 particles in the $1d_{5/2}$ shell. Present results indicate that such agreement may be accidental.

Of properties other than excitation energies, only certain electromagnetic properties were calculated using the Case 3 wave functions. In order to make use of spectroscopic factors from pickup or stripping reactions it would be necessary to do separate calculations to get a wave function for the target nucleus. The electromagnetic transition probabilities are compared with experimental results for the lower states in ^{26}Al. The output of the computer program, reduced transition probability B(M1), was converted to units of the Weisskopf estimate for single particle transition rates (see Wi60) by an expression

$$T(M1) = 0.56\ B(M1)\quad (W.u).$$

A similar expression was used for E2 transitions,

$$T(E2) = 0.22\ B(E2)\quad (W.u.),$$

in which the nuclear radius of ^{26}Al was taken to be 3.5×10^{-13} cm. The

transition rates are compared with results of lifetime measurements (Ha68b) in Table 8. An E2 transition rate of 4.4 W.u. is calculated for the 1.760→0.418 transition. Combined with the M1 rate in Table 8, this gives a calculated mixing ratio $|x|=0.23$ which may be compared with the results of Horvat *et al.* (Ho63)—$x=0.23$ or $x=2.2$. In view of the large errors in other transition rates, the agreement in mixing ratios must be considered fortuitous.

It would be interesting to determine whether the mixed configuration wave functions represent a deformed nucleus. Static quadrupole moments should give some indication about nuclear shape. Calculated quadrupole moments for some of the states in ^{26}Al are presented in Table 9. These are all small moments, equivalent to very small deformation of a uniformly charged sphere.

Table 8

Comparison of observed transition rates with rates calculated from a mixed configuration shell model.

Transition	Type	T_{exp} (W.u.) (Ha68b)	T_{calc} (w.u.)
0.418→0.	E2	17.	0.41
1.059→0.229	M1	1.6	8×10^{-3}
1.760→0.418	M1	$< 4 \times 10^{-3}$	1.7×10^{-4}
1.852→0.229	M1	8×10^{-3}	7.5×10^{-4}

Table 9

Quadrupole moments of the lowest levels predicted by a mixed configuration shell model.

Spin	Q (e^2-fm^2)
5	4.52
3	-4.35
1	-0.74

VII. CONCLUSIONS

Particle-gamma coincidence measurements proved to be a good means of determining branching ratios in the gamma-ray decay of nuclear excited states. The advantage over gamma-gamma coincidence work was that the gamma-ray spectra for different excited states could be recorded separately by sorting according to the energy of the coincident particles. The branching ratios obtained in this work were in good overall agreement with those obtained in other recent measurements of this type. Gamma-gamma coincidence work generally resulted in branching ratios which differed from those obtained in this work, particularly for levels above 2 MeV excitation.

Analysis of gamma-ray angular distributions did not provide precise definition of multipole mixing ratios. The reason was that both the M=0 and M=1 substate populations had to be treated as unknown parameters for this reaction. For a given spin there was usually a wide range of mixing ratios for which the angular distribution could be fitted. For cases of decay to a spin 0 level (with mixing ratio identically zero) the level spin could be determined by fitting the angular distribution. Spin J=1 was obtained for the level at 1.852 MeV, one of the levels at 2.07 MeV and the one at 2.740 MeV. Combined with information from stripping reaction studies, results of the present work gave $J^{\pi}=2^{+}$ for a level at 3.159 MeV. Method II (limiting magnetic substate populations

by detecting particles at 0° or 180°) would appear to be of most use in determinging mixing ratios (a) when the relative populations need not be treated as parameters or (b) when information from other work such as stripping reaction studies limits spins to one or two possibilities.

Two models, one a model with a deformed core and two extra-core particles and the other the shell model with configuration mixing were used in calculating the excitation energies of states in ^{26}Al. Model calculations do not clearly establish whether or not ^{26}Al should be regarded as a permanently deformed nucleus. Fair agreement between experiment and the deformed-core (Nilsson) model was achieved for the ground and first 4 excited states. Inclusion of terms which had been neglected in the model Hamiltonian would tend to give even better agreement. Further work with the model will be difficult if rotational-particle coupling and residual interaction terms are included. A serious disadvantage of the model is that only 8 or 9 excited states are predicted to lie below 5 MeV excitation. The shell model could predict the excitation energies of the first 5 excited states if single particle energies corresponding to a small spin-orbit potential were chosen. A surprising result of the shell model calculation was that two-hole configurations were not the dominant ones in lower levels. It would be expected that a similar result would be obtained if a larger number of basis states were used. The need for inclusion of more basis states is shown by the disagreement between calculated and observed electromagnetic transition rates. Possibly the wave functions with an expanded set of basis states

would exhibit some of the properties (for example quadrupole moment) of a deformed nucleus; this would remove the present situation that a model for a deformed nucleus and a model with very small calculated quadrupole moment both give fits to the energy spectrum of ^{26}Al.

REFERENCES

Ab64 Handbook of Mathematical Functions, M. Abramowitz and I.A. Stegun eds., U.S. Govt. Printing Office, Washington, 1964.

Bi60 G.R. Bishop, Nucl. Phys. 14(1960)376.

Bi64 J.-Cl. Bizot, Ann. Phys. (Paris) 9(1964)421

Bi68 G.A. Bissinger, P.A. Quin and P.R. Chagnon, Nucl. Phys. A116 (1968)33.

Bo67 M.C. Bouten, J.P. Elliott and J.A. Pullen, Nucl. Phys. A97 (1967)113.

Br59 C.P. Browne, Phys. Rev. 114(1959)807.

En67 P.M. Endt and C. Van der Leun, Nucl. Phys. A105(1967) 1.

Ev55 R.D. Evans, The Atomic Nucleus, McGraw-Hill Book Co., New York, 1955.

Fe65 A.J. Ferguson, Angular Correlation Methods in Gamma-ray Spectroscopy, North Holland Publishing Co., Amsterdam, 1965.

Fl52 B.H. Flowers, Proc. Roy. Soc. A212(1952)248.

Fr68 J.B. French, E.C. Halbert, J.P. McGrory and S.S.M. Wong (to be published).

Fu68 H. Fuchs, K. Grabisch, P. Kraaz and G. Röschert, Nucl. Phys. A110(1968)65.

Ga60 C.J. Gallagher, Jr., Nucl. Phys. 16(1960)215.

Gr56 L.L. Green, J.J. Singh and J.C. Willmott, Proc. Phys. Soc. (Lond.) 69A(1956)335.

Ha68a O. Häusser and N. Anyas-Weiss, Bull. Am. Phys. Soc. 13(1968)86.

Ha68b O. Häusser, T.K. Alexander and C. Broude, Can. Jour. Phys. 46 (1968)1035.

He64 R.L. Heath, AEC Research and Development Report IDO-16880, 1964

Hi59 S. Hinds and R. Middleton, Proc. Soc. 73(1959)501.

Ho63 P. Horvat, P. Kump and B. Povh, Nucl. Phys. 45(1963)341.

Hu68 D.A. Hutcheon, Internal Report, Nuclear Research Center, Univ. of Alberta, Edmonton, 1968.

Ke64 I. Kelson, Phys. Rev. 134(1964)B267.

Ku67 T.T.S. Kuo, Nucl. Phys. A103(1967)71.

Li58 A.E. Litherland, H. McManus, E.B. Paul, D.A. Bromley and H.E. Gove, Can. Jour. Phys. 36(1958)378.

Li61 A.E. Litherland and A.J. Ferguson, Can. Jour. Phys. 39(1961)788.

Ma63 E. Marshalek, L.W. Person and R.K. Sheline, Revs. Mod. Phys. 35(1963)108.

Ma64 J. Mathews and R.L. Walker, Mathematical Methods of Physics, W.A. Benjamin, Inc., New York, 1964.

Mu60 J. Muto, Jour. Phys. Soc. Japan 15(1960)17.

Ne62 D.R. Neher, F.W. Prosser, Jr., and R.W. Krone, Nucl. Phys. 31 (1962)231.

Ni55 S.G. Nilsson, Kgl. Danske Vid. Selsk. mat.-fys. Medd. 29(1955) No. 16.

Nu68 J. Nurzynski, K.H. Bray and B.A. Robson, Nucl. Phys. A107(1968) 581.

Pi65a A.-G. de Pinho and J. Picard, Report CEA-R2730, Centre D'Etudes Nucleaires, Saclay, 1965.

Pi65b J. Picard and A.-G. de Pinho, Nuovo Cimento (10) 41B(1965)239.

Pr62 M.A. Preston, Physics of the Nucleus, Addison-Wesley Publ. Co., Reading, Mass., 1962.

Ro67 H.J. Rose and D.M. Brink, Revs, Mod. Phys. 39(1967)306.

Ro68 B. Rosner, P. Neogy and L. Polsky, Phys. Lett. 27B(1968)450.

Ru59 A.R. Rutledge, Report CRP-851, Chalk River, 1959,

Si68 C.M. da Silva and J.C. Lisle, Nucl. Phys. A116(1968)452.

Sy68 D.H. Sykes and D.A. Hutcheon, Internal Report, Nuclear Research Center, Univ. of Alberta, Edmonton, 1968.

Ta60a I.J. Taylor, F. de S. Barros, P.D. Forsyth, A.A. Jaffe and S. Ramavataram, Proc. Phys. Soc. 75(1960)772.

Ta60b I. Talmi and I. Unna, Ann. Rev. Nucl. Sci. 10(1960)353.

Te66 J.W. Tepel, Nucl. Inst. and Methods 40(1966)100.

We68 A. Weidinger, R.H. Siemssen, G.C. Morrison and B. Zeidman, Nucl. Phys. A108(1968)547.

Wi60 D.H. Wilkinson in Nuclear Spectroscopy, Part B, F. Ajzenberg-Selove ed., Academic Press, New York, 1960.

Wi67 P. de Wit and A.M. Hoogenboom, Rijksuniversiteit Utrecht, private communication, 1967.

Wi68 B.H. Wildenthal, J.P. McGrory, E.C. Halbert and P.W.M. Glaudemans, Phys. Lett. 26B(1968)692.

APPENDIX A

Suppliers of apparatus used in data collection

The Van de Graaff generator was a Model CN of High Voltage Engineering Corp., Burlington, Massachusetts.

Annular detectors were purchased from Nuclear Diodes, Prairie View, Illinois. The detector used in the measurements at 5.3 MeV had an operating voltage of 100 V and a resistivity of 20,000 Ω- cm. For E_τ=6.0 MeV the detector had a resistivity of 10,000 Ω- cm and was operated at 200 V.

The NaI(Tl) detector was an Integral Line, Type 12S12/3 manufactured by Harshaw Chemical Co., Cleveland, Ohio.

Most of the electronic equipment was obtained from Oak Ridge Technical Enterprises Corp. (Ortec), Oak Ridge, Tennessee. Abbreviations listed here correspond to those used in Figure 2.

PA--Preamplifier, Ortec Model 109

SC.PA-- Scintillation preamplifier, Ortec Model 113

AMP--Linear amplifier, Ortec Model 410

S.A.F. AMP--Selectable active filter amplifier, Ortec Model 440

FZCD--Fast zero crossing discriminator, described by D.A. Gedcke and W.J. McDonald, Nucl. Inst. and Methods, 56(1967)148

TAC--Time-to-amplitude converter, Ortec Model 437

DL--Delay amplifier, Ortec Model 427

SCA—Single channel analyser, Ortec Model 406

SSCA—Strobed single channel analyser, Ortec Model 413

DG—Gate and delay generator, Ortec Model 416

MON ADC—Analog-to-digital converter (Model 217A) and memory and display unit (Model CN-1024) from Technical Measurements Corp., North Haven, Connecticut

ADCA—Analog-to-digital converter, TMC Model 217A

ADCF, ADCM—Dual analog-to-digital converter, Model ND-161F, Nuclear Data Inc., Palatine, Illinois

COMP—Digital computer (24 bit/word, 16K word memory, 8 microsecond cycle time) Model 920 of Scientific Data Systems, Santa Monica, California

The enriched-isotope magnesium targets were rolled foil supplied by the Nuclear Division of Union Carbide Corp., Oak Ridge, Tennessee.